MOISTURE SENSITIVITY OF CONTRAIL FORECAST ALGORITHMS

THESIS

Allen Christopher Rabayda

Captain, USAF

10

DEPARTMENT OF THE AIR FORCE
AIR UNIVERSITY
AIR FORCE INSTITUTE OF TECHNOLOGY

Wright-Patterson Air Force Base, Ohio

AFIT/GM/ENP/97M-08

MOISTURE SENSITIVITY OF

CONTRAIL FORECAST ALGORITHMS

THESIS

Allen Christopher Rabayda

Captain, USAF

AFIT/GM/ENP/97M-08

AFIT/GM/ENP/97M-08

MOISTURE SENSITIVITY OF CONTRAIL FORECAST ALGORITHMS

THESIS

Presented to the Faculty of the School of Engineering

of the Air Force Institute of Technology

Air University

In Partial Fulfillment of the

Requirements for the Degree of

Master of Science in Meteorology

Allen Christopher Rabayda

Captain, USAF

March 1997

The views expressed in this thesis are those of the author and do not reflect the official policy or position of the Department of Defense or the United States Government.

AFIT/GM/ENP/97M-08

MOISTURE SENSITIVITY OF CONTRAIL FORECAST ALGORITHMS

Allen Christopher Rabayda

Captain, USAF

Approved:

Michael K. Walters, Lieutenant Colonel, USAF Chairman, Advisory Committee	Date
Paul J. Wolf, Lieutenant Colonel, USAF Member, Advisory Committee	Date
Clifton E. Dungey, Major, USAF Member, Advisory Committee	Date
Daniel E. Reynolds, Professor Member, Advisory Committee	Date

Acknowledgments

First and foremost, I wish to express my heartfelt gratitude to my wife, Chrissy, for her love and support throughout my entire time at AFIT. Without her constant reassurances, occasional prodding, and general good humor, it would have been too easy to let frustration derail my desire to work hard. The indirect and direct motivation Chrissy gave me allowed me to get the most out of AFIT and enjoy the experience to the fullest.

A large portion of the credit for my performance in this research belongs to my advisor, Lieutenant Colonel Mike Walters. His guidance, insights, and willing participation were indispensable to my efforts. Lieutenant John Polander and Mr Steve Weaver of the 88th Weather Squadron were two instrumental individuals who laid the groundwork for this research project and helped me get started. Last but not least, I owe a debt of gratitude to Professor Dan Reynolds for his assistance in computer programming. His two minute shortcuts saved me countless hours. I would also like to thank Dr Richard Coleman and Dr Patrick Saatzer, who shared their unique perspectives on contrail forecasting and helped me focus my research efforts. If not for all these individuals my days would have been longer, my efforts insignificant, and my results few.

Allen C. Rabayda

Table of Contents

Page

Page

Page

Page

List of Figures

Figure Page

List of Tables

Abstract

This thesis looked at using new relative humidity (RH) climatolgies to improve the Air Force Global Weather Center's (AFGWC) contrail forecasts. To study the effect of the new RH climatolgies, the currently used empirical relative humidity (RH) profile is replaced with a more accurate climatological one, the Stratospheric And Gaseous Experiment II (SAGE II). The study begins by examining accuracy and bias of forecast contrail bases generated by the empirical and SAGE II RH profiles on 42 days. Both sets of forecast bases are shown to be statistically similar with a series of hypothesis tests. Additional RH profiles, from 0% to 100%, are then tested to gage their affect on forecast base. Again, little statistical difference in forecast bases are noted between the additional profiles. In general, a high forecast base bias is shown for contrail algorithms derived from the Appleman theory. This thesis also reveals the dependence of forecast bases on RH and lapse rate. Lapse rates ranging from 2°C/km to 9°C/km and forecast bases generated by RH values of 0% and 100% are used to show how RH variations of more than 30% may only vary forecasts by less than 1,000 feet.

The thesis demonstrated the AFGWC can not improve its contrail forecasts by using a more accurate climatological RH profile, the AFGWC contrail forecast algorithm has an inherent high forecast base bias, and the degree to which forecast bases are affected by RH greatly depends on the atmospheric lapse rate.

MOISTURE SENSITIVITY

OF

CONTRAIL FORECAST ALGORITHMS

I. Introduction

1.1 Background

1.1.1 Definition of Contrails. The long, narrow clouds of water droplets or ice crystals frequently forming behind aircraft are referred to as condensation trails (contrails). Two distinct mechanisms are responsible for these long, tubular clouds (Jiusto and Pilie, 1964; AWS, 1981). The first is a rapid pressure fall of air flowing at high speed over an airfoil. The pressure fall creates local adiabatic cooling which raises the relative humidity (RH) of the affected environment to saturation. This type of contrail is referred to as a "aerodynamic trail". These rarely occur, are of short duration and form in nearly saturated layers of the atmosphere during extreme flight maneuvers such as sharp "pull-outs" or high speed dives. The second mechanism which causes contrails to form is fuel combustion within the aircraft engine. During combustion, the engine produces water vapor, which saturates the environment in the wake of the aircraft. This type of contrail is referred to as the "engine-exhaust trail". The study only addresses contrails formed by the second mechanism, therefore, any references to contrails hereafter are to engine-exhaust trails.

1.1.2 Rationale for Contrail Study. Contrails are a form of military intelligence during combat. These sky signatures have played a key role in offensive and defensive military air operations since WWII, revealing an aircraft's location to enemy ground and air forces. Often air operations require aircraft to fly at altitudes just below contrail-prone areas, thus the forecasted base of contrail layers becomes essential for mission planning. Military Weather Forecasters are charged with the continuing mission to improve their contrail base forecast accuracy to better support the Armed Forces.

1.1.3 Air Force Global Weather Center (AFGWC) Contrail Forecast Procedure. Currently, AFGWC produces daily contrail forecasts for three general classes of aircraft engines: high-bypass, low-bypass, and non-bypass. AFGWC uses a high speed processor and complicated algorithm to forecast contrail bases and tops for gridded locations throughout the northern hemisphere.

The algorithm uses current data analyses and forecasts of temperature, pressure, tropopause height, and RH values. These variables are provided at 500-, 400-, 300-, 250-, 200-, 150-, 100-, 50-, and 30-mb pressure levels. Temperature and pressure values are derived from the Navy Operational Global Atmospheric Prediction System (NOGAPS) forecast model. Another AFGWC program then predicts tropopause height and assigns RH values of 70% to pressure altitudes within 300 m of the tropopause height, 40% 300 m and below this height, and 10% 300 m and above it (AWS,1981).

For each pressure level, beginning with 500 mb, a critical temperature, needed for contrail forecasting, is computed using a method first described by Appleman (1953) and

updated by Schrader (1994). The critical and ambient temperatures are compared until the ambient temperature falls below the critical temperature. The pressure altitude where this occurs is designated the contrail base. The comparison continues until the ambient temperature rises above the critical temperature. The pressure altitude where the ambient temperature becomes warmer again is designated the contrail top. Contrail layers less than 2,000 feet thick are discarded, and layers less than 1200 feet apart are consolidated.

1.2 Problem

The RH values used in the AFGWC algorithm are empirical estimates dating back to 1953 (Appleman, 1953). Today, more accurate climatological RH profiles are available. (Larsen et al., 1993; Chu et al., 1993; Rind et al., 1993; McCormick and Chiou, 1994). Will a more accurate climatological RH profile increase the AFGWC contrail base forecasts, and to what degree are these forecasts affected by different RH values?

1.3 Approach

1.3.1 Scope. To assess the impact of RH on the AFGWC algorithm's forecast bases, two series of tests were conducted: RH Profile Tests and Lapse Rate Tests. The RH Profile Tests compared the forecast bases generated by the AFGWC algorithm using the different RH profiles. There were seven different RH profiles used to produce seven sets of forecast bases (see Table 1). All seven profiles were then tested with a second contrail forecast algorithm, the Saatzer algorithm. This algorithm is based on a series of General

Electric equations used in a recent contrail test by the Northrop Grumman Corporation (Saatzer, 1995). The Saatzer algorithm provided seven sets of reference forecasts for comparison with the AFGWC algorithm's forecasts.

A second series of tests was used to measure the impacts of RH on the AFGWC algorithm's forecast base under different lapse rate conditions. Average lapse rates from 2 ^{o}C km^{-1} to 9 ^{o}C km^{-1} were used in the AFGWC algorithm with RH values of 0%, 50%, and 100% to produce forecasts. Each lapse rate was used to generate a set of three forecast bases. The difference in altitudes between each set of forecast bases was then compared.

Each forecasted base was treated as a continuous quantity. Just as high temperature forecasts are measured against the day's observed maximum temperature, the forecasted bases were measured against reported aircraft contrail bases. This measure of accuracy has not been used in previous validation studies of contrail forecast algorithms. Appleman (1957), Miller (1990), Bjornson (1992), Peters (1993), and Speltz (1995) each used contrail occurrence/non-occurrence contingency tables to assess an algorithm's accuracy in predicting a contrail. The accuracy measurements made herein, however, were based on how close the forecast base came to the reported base.

1.3.2 Data Set. The data base consisted of 42 cases where aircraft contrail base altitudes were reported (or estimated) and corresponding atmospheric measurements taken. The 42 cases spanned all four seasons and ranged in latitude from 35 - 40^{o}N. The atmospheric measurements were collected from the surface to about 68 kft. Aircraft engine types were either non-bypass or high bypass.

1.3.3 Organization of Thesis. The following four chapters of the thesis provide technical background, a detailed description of the methodology, test results and analysis, and conclusions and recommendations. Chapter II, Technical Background, presents the principles of contrail formation and explains contrail prediction methods. It also provides a synopsis of the AFGWC algorithm and the SAGE II profile. The chapter concludes with some recent studies validating the Appleman Theory. Chapter III, Methodology, describes the assumptions made, data used, and procedures taken in this study. In addition, this chapter discusses the numerical solution of the non-linear equations used in the AFGWC contrail forecast algorithm and the sensitivity of the resulting forecast to the solution method. Chapter IV, Results and Analysis, gives an explanation of the results and summary. The last chapter, Findings and Conclusion, addresses the research questions, offers AFGWC some short-term contrail forecast suggestions, and shows several areas requiring further investigation.

II. Technical Background

2.1 Principles of Contrail Formation

Combustion of hydrocarbon fuels by jet engines, injects both water vapor and heat into an aircraft's wake (Appleman, 1953). The added water vapor raises the wake's RH, bringing it closer to saturation and contrail formation, while the added heat lowers RH and opposes formation. At the same time exhaust vapor and heat are injected into the wake, environmental air is entrained into it. The mixture of exhaust and environmental air must reach saturation in the wake for a contrail to form. Therefore, the saturation process within the wake is dependent on the amount of heat and water vapor contained in the exhaust, the initial temperature, pressure, and RH of the environment, and the ratio of entrained environmental air to exhaust gas in the wake.

The ratio of moisture to heat added by combustion is referred to as the contrail factor (Appleman, 1953). Different engine types produce different amounts of moisture and heat (Jiusto and Pilie, 1964; Peters, 1993; Saatzer, 1995). Based on an engine's level-flight characteristics, they are placed into one of three general classes: turbojet or non-bypass, low-bypass turbofan, and high-bypass turbofan (Peters, 1993). The contrail factors associated with each class are 0.030 g kg^{-1} $^{o}C^{-1}$, 0.034 g kg^{-1} $^{o}C^{-1}$, and 0.039 g kg^{-1} $^{o}C^{-1}$, respectively (Schrader, 1994).

2.2 Early Prediction Methods

2.2.1 Appleman Theory of Contrail Formation. Appleman (1953) introduced the basic contrail forecast method, currently used by AFGWC today. He described contrail formation in terms of ambient pressure, temperature, and RH, and the heat and water vapor produced by the combustion of the fuel. He then related these variables through the mixing cloud which forms when two parcels (representative "blocks") of air become saturated with respect to water when mixed. After saturation is reached, liquid drops form then immediately freeze. A visible and prolonged contrail may be seen depending on the excess water content available in the trail. Appleman (1953) summed the contrail formation with three key points:

(1) the aircraft wake must reach saturation with respect to water

(2) after water droplets form, they immediately freeze and excess vapor in the trail will deposit onto the ice crystals until the RH in the trail falls to 100% with respect to ice.

(3) an ice crystal content of 0.004 g m^{-3} is needed for a faint trail and 0.01 g m^{-3} for a visible trail

Appleman (1953) graphically represented the critical temperatures needed for contrail formation with a set of four contrail curves drawn on a pressure-temperature graph. This graph, shown in Fig. 1, is referred to as the Appleman nomogram. The curves in this figure represent critical temperatures at RH values of 0%, 60%, 90%, and

100%. To determine if a contrail will form at a flight level in a standard atmosphere, enter the nomogram at the flight's pressure altitude and temperature. Compare this point to the contrail curves. If the point lies to the right of the 100% contrail curve, a contrail will never form because the air is too warm to become saturated with respect to water. If the aircraft conditions are to the left of the 0% contrail curve, a contrail will always form, regardless of the ambient RH. And if the point is between 0 and 100%, contrail formation will depend on whether the ambient RH equals or exceeds the indicated RH value on the curve.

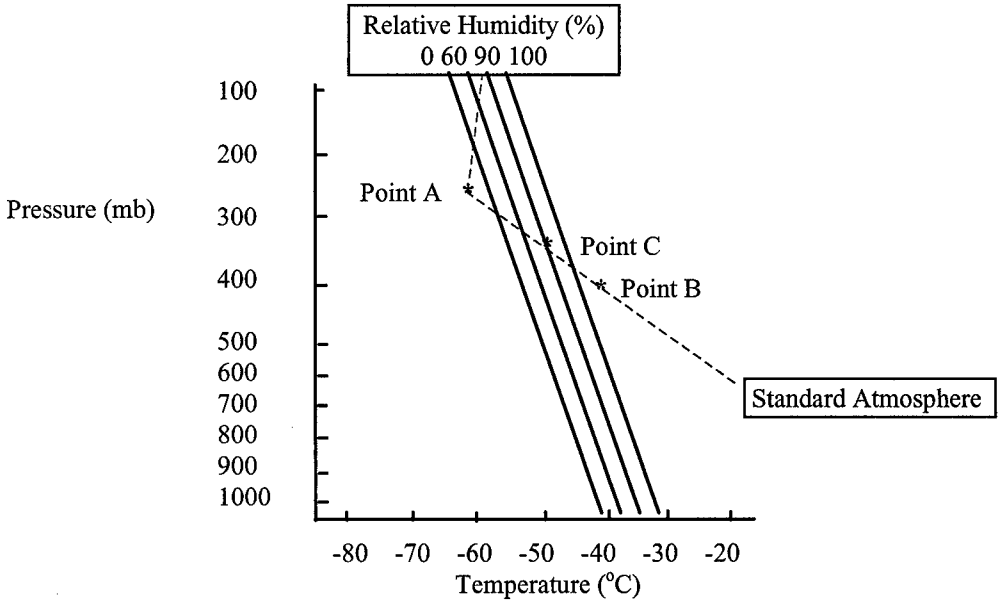

FIG. 1: Appleman Contrail Forecast Nomogram

For example, if an aircraft is flying in a standard atmosphere at a pressure altitude of 250 mb (Point A), then the aircraft will be to the left of the 0% contrail curve and a contrail would form irrespective of the ambient RH. If the same aircraft was flying at a

pressure altitude of 400 mb in a standard atmosphere (Point B), it would then lie to the right of 100% contrail curve and a contrail would never form. Finally, if the aircraft flew at 350 mb (Point C), an ambient RH of at least 90% would be needed for contrail formation.

Appleman (1953) derived the theoretical ratio of moisture and heat added to an aircraft wake by a pure turbojet engine. He reasoned for each gram of fuel burned, 12 grams of exhaust gas, 1.4 grams of water vapor, and 10 000 heat calories would be added to the wake. Each gram of exhaust gas would mix in the wake with N grams of surrounding air causing a mixing ratio (Δw) and temperature (ΔT) increase. The ratio ($\Delta w/\Delta T$) became:

$$\frac{\Delta w}{\Delta T} = \frac{\dfrac{\text{water vapor} \cdot (\text{mixing ratio conversion})}{\text{exhaust gas} \cdot (\text{surrounding air})}}{\dfrac{\text{heat calories}}{\text{exhaut gas} \cdot (\text{surrounding air}) \cdot c_p}}$$

$$= \frac{\left[\dfrac{1.4\text{g} \cdot \left(1000\dfrac{\text{g}}{\text{kg}}\right)}{12 \cdot \text{g} \cdot (\text{N})}\right]}{\left[\dfrac{10{,}000 \cdot \text{cal} \cdot \left(4.186 \cdot \dfrac{\text{J}}{\text{cal}}\right)}{12 \cdot \text{g} \cdot \left(1004\dfrac{\text{J}}{^{\circ}C \cdot \text{kg}}\right) \cdot \left(\dfrac{\text{kg}}{1000\text{g}}\right)}\right]} = 0.0336\frac{\text{g}}{\text{kg} \cdot ^{\circ} C}, \quad (1)$$

where vapor c_p is the specific heat of dry air at constant pressure and 1 000 g kg^{-1} is used to convert water vapor and exhaust masses into standard mixing ratio units of g kg^{-1}. Using these values, Appleman (1953) derived a contrail factor of 0.0336 g kg^{-1} $^{o}C^{-1}$. He assumed all the heat of combustion would be added to the wake so contrail factor was a constant. He also believed the heat and moisture liberated by the combustion process was constant for all fuel types. Thus, he assumed the contrail factor and contrail curves were universally applicable to all engine types.

Appleman (1957) also laid the groundwork for the empirically based RH profile used by the AFGWC algorithm today. He observed mean RH values of 40% in the troposphere (upper-tropical) and 70% in the stratosphere (near the tropopause, in the lower polar-stratosphere) for data collected in Project Cloud Trail. Project Cloud Trail was an Air Force experiment which collected near 1000 pilot reports of visible contrails.

2.2.2 Jiusto (Pilie) Alternate Approach to Contrail Formation. The work of Jiusto and Pilie (1958) challenged Appleman's use of a generic contrail factor for all engines. They introduced temperature diffusion in calculating contrail factor. This diffusion took into account radiant heat and mechanical heat losses by propeller engines, which decreased the heat added by the aircraft to the wake. This temperature decrease effectively increased the RH inside the wake, increasing the probability of contrail formation.

In addition, Jiusto (1961) provided an alternate means of calculating and representing contrail formation. This new method provides insight into the cloud physics of contrails. By using a phase diagram with the saturation mixing ratio curve drawn, the original air-

exhaust mixture could be compared to the curve (see Fig. 2 below). If the mixture lies to the left of the curve, the mixture exceeds saturation and a contrail forms (line extending from point C). An indication of the density of the contrail is given by the degree to which the mixture exceeds saturation, and may therefore indicate the persistence of a contrail. This process is analogous to formation of a mixing cloud, where two distinct parcels of air reach saturation and form visible moisture when mixed, depending on their initial temperatures and moisture contents.

The air-exhaust mixing process can be visualized on the phase diagram (Fig. 2 below) by drawing two points to represent the initial conditions of the surrounding environmental air (point A) and the air exiting from the exhaust (point B). Since the mixing between the engine exhaust and environment is assumed to be linear and isobaric, a line connecting points A and B will indicate the wake conditions during mixing. The slope of this line indicates the change of moisture (Δw) and temperature (ΔT) the environment has undergone in the wake and is referred to as the contrail factor. If the line were tangent to the saturation mixing ratio curve, as the solid line in Fig. 2, then the mixture will just reach saturation at that point. The temperature corresponding to the tangent is referred to as the critical temperature (T_c) at 100% RH, since the saturation mixing ratio curve represents RH values of 100%. T_c for Fig. 2 is about -48 °C. Critical temperatures for subsaturated RH values are then found by the intersection of the tangent line with the respective RH curves drawn on the phase diagram. The temperature corresponding to the intersection of the tangent line and the abscissa or 0% RH is the critical temperature(T_d) for 0% RH. Jiusto (1961) describes T_c as the warmest

temperature which will permit contrail formation in a saturated atmosphere, and T_d as the warmest temperature which will permit contrail formation in a perfectly dry atmosphere.

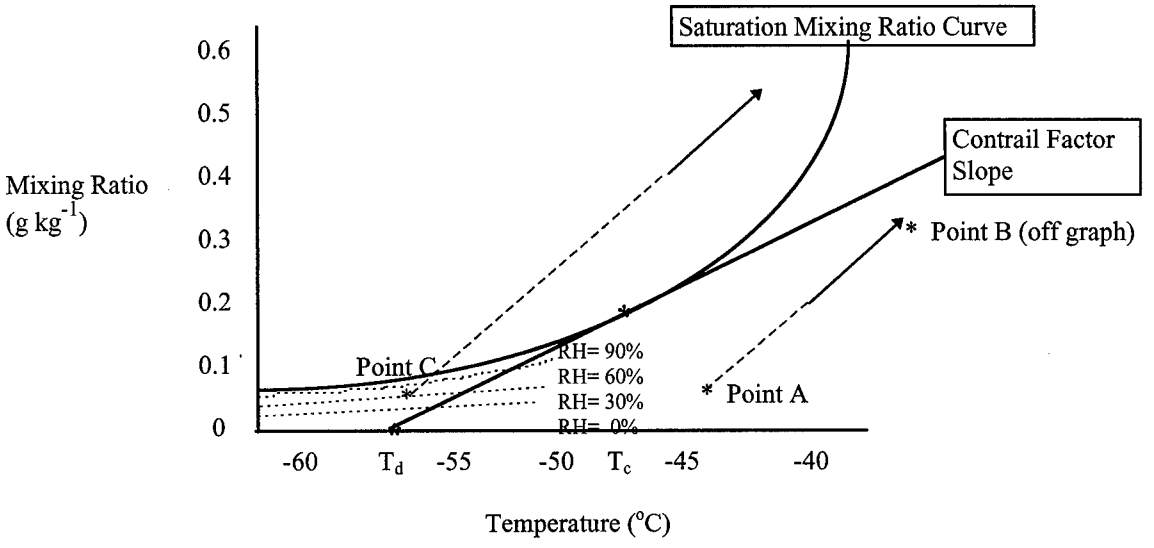

FIG 2: 300 mb Phase Diagram

Jiusto and Pilie (1964) used their research to develop several contrail forecast procedures. In the complete absence of observations, they suggested using a RH profile of 40% in the upper troposphere and 0% in the stratosphere. They caveat this with a suggestion of using 60% in the upper troposphere if the air flow is moist and 0% if the air is dry. Both of these suggestions are similar to Appleman's (1957) empirical values of 40% in the upper troposphere and 70% in the stratosphere, near the tropopause.

2.3 SAGE II Reports

2.3.1 Introduction to SAGE II Data. The SAGE II sensor and measurement technique is described by McCormick (1987). This sensor collects atmospheric water vapor profiles from the Earth Radiation Budget Satellite with a downward looking, sun-scanning radiometer which measures water vapor (i.e. RH) to the surface or cloud tops. Therefore, it provides only clear air (cloud free) RH profiles. SAGE II makes 15 spacecraft sunrise and 15 spacecraft sunset measurements each day, separated by 24.5° longitude, near the same latitude. The SAGE II measurements move spirally in latitude, from 80° N to 80° S, every 4 -5 weeks. The vertical resolution between each measurement is approximately 1-3 km (3-9 kft).

2.3.2 Comparison of SAGE II Water Vapor to Rawinsonde Measurements. Larsen et al. (1993) compared SAGE II measurements against 1987 rawinsonde climatology and the Global Atmospheric Circulation Statistics (GACS) (1963-1973). The SAGE II data were collected over a period of 4 years, from 1986-1989. The data are divided into 20 degree latitudinal bands, separated vertically by 1 km increments from 6.5 - 16.5 km, and grouped by season. Although Larsen et al. (1993) noted a significant moisture profile departure in the upper troposphere (15-24 kft), he attributed this to a moist bias of about 25% for the radiosonde measurements. Because the radiosondes can' t consistently

provide observations in the dry upper troposphere, they produce a moist climatology relative to the true climatology. Radiosonde moisture profiles made with a new thin film type hygrometer, the Vaisala

Humicap, agreed nicely with SAGE II data further substantiating the moist bias of typical radiosonde data bases (Larsen et al., 1993).

Rind et al. (1993) stressed the dry RH bias of cloud-free measurements made by SAGE with the moist RH bias in the 1987 and GACS climatologies. He then demonstrated SAGE II moisture data were more accurate and exhibited a smaller systematic bias than either the 1987 database or GACS when compared to in-situ measurements. This was due, in part, to the sparse and inconsistent measurements of the 1987 and GACS databases.

Finally, a SAGE II instrumentation error analysis was shown by Chu et al. (1993) to exhibit an 18% random error for individual RH profile measurements. The error was reduced to near 10% when zonally averaged in the 4 year SAGE II database.

2.3.3 Summary of SAGE II Water Vapor. McCormick and Chiou (1994) listed advantages of the SAGE II water vapor profiles as: (1) high accuracy and vertical resolution; (2) near continuous middle and upper tropospheric and stratospheric coverage; and (3) a global coverage over a four year period. The key disadvantage discussed was the limit of the SAGE II data to include only cloud-free measurements.

2.4 Contrail Forecast Validation Studies

2.4.1 Peters' Engine Types. Peters (1993) ran extensive analysis on different engine types and their effect on contrail formation. He made three distinct categories of engine contrail factors: non-bypass, low-bypass, and high-bypass and then derived contrail factors of 0.036 g kg^{-1} $°C^{-1}$, 0.040 g kg^{-1} $°C^{-1}$, and 0.049 g kg^{-1} $°C^{-1}$. The contrail factors for each class were based engine characteristics such as tailpipe moisture and temperature for a wide range of power settings, Mach numbers, and flight levels. For each contrail factor, he developed a set of nomograms similar to Appleman's (1953) nomogram which uses a constant contrail factor of 0.0336 g kg^{-1} $°C^{-1}$. The new nomograms indicated higher critical temperatures. Peters (1993) concluded by showing improved forecast accuracy with the new contrail factors.

2.4.2 Schrader's Interpolation for Critical Temperatures. Schrader (1994) extended Peters' (1993) work. He made two corrections to Peters' (1993) derivations for critical temperatures. First, he recalculated saturation vapor pressures with respect to water rather than ice to again be consistent with Appleman's point (1) above: "the aircraft wake must reach saturation with respect to water for contrail formation". Schrader (1994) then derives a way to estimate critical temperatures at relative humidity values from 0 to 100%. Peters (1993) originally used a simple linear interpolation, which Schrader (1994) states is unreasonable due to the non-linear behavior of vapor pressure as a function of RH. Schrader (1994) developed a physically more meaningful, non-linear method for iteratively calculating critical temperatures at relative humidities between 0 and 100%.

Additionally, he updated the Peters' nomogram with his newly derived water saturation and non-linear interpolation equations. He used recently developed contrail factors of 0.030 g kg^{-1} $^{o}C^{-1}$, 0.034 g kg^{-1} $^{o}C^{-1}$, and 0.039 g kg^{-1} $^{o}C^{-1}$ for non, low and high-bypass engines.

2.4.3 Saatzer Validation of the Appleman Theory Using Curve Fit Equations. Saatzer (1995) conducted detailed flight tests and analyzed over 800 contrail observations spanning seven months. These tests conclusively showed contrails never occurred at temperatures warmer than the critical temperature contrail curve for 100% relative humidity. This clearly established that ice saturation is not a criteria for contrail occurrence. Furthermore, the tests demonstrated that contrails will not form unless the exhaust plume mixing causes the liquid saturation boundary to be exceeded. This is in full agreement with Appleman's (1953) first key point above: "aircraft wake must reach saturation with respect to water before a contrail can form".

Saatzer (1995) also developed an engineering approach to contrail factors, which helped him explain the different contrail factors produced by his single turbojet (T33) aircraft over the 800 observations. This approach (Fig. 3) can be understood by assuming the exhaust plume is a control volume. The work and heat transfer across the volume's boundaries are assumed to be zero. Ambient air entrainment is assumed to cease beyond the downstream boundary, so the mixing volume temperature and ambient temperature are equal. As the temperatures and vapor pressure gradients approach one another through mixing, the contrail becomes more dilute, and eventually evaporates.

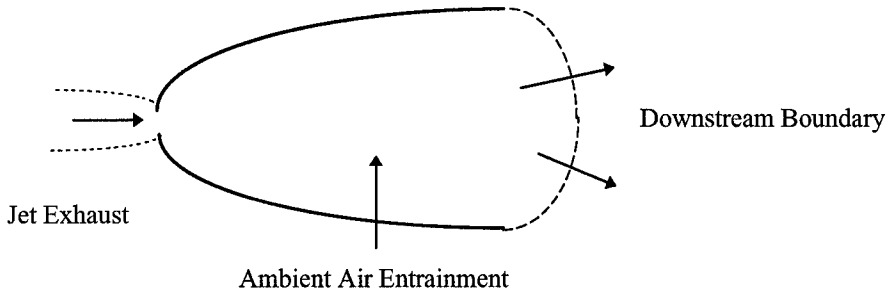

FIG 3. Control Volume Moving with Aircraft

The mixing volume can then be related to engine characteristics and ambient conditions in the contrail factor equation:

$$\textit{Contrail}\ \text{Factor} = \text{CF} = \frac{1.3 \cdot M_F}{M_a \cdot (T_E - T_a)}, \tag{2}$$

where CF is the contrail factor, M_F is the engine fuel mass flow, M_a is the engine air mass flow, and T_E and T_a are the engine and ambient temperatures.

During the tests, Saatzer directly measured the engine's volumetric flow and fuel temperature to derive the fuel mass. Air mass flow was derived from engine speed, inlet total pressure, ambient air temperature, and the engine manufacturer calibration curves. The exhaust gas temperature was measured directly, as was the ambient air temperature.

After calculating different contrail factors for each flight test and comparing them to the their flight profiles, Saatzer noted slight departures for different profiles on same day flights. During the 32 flight days, he noted contrail factors ranged from 0.020 to 0.040 g kg^{-1} $^{o}C^{-1}$. He attributed the slight departures on the same days to banks, throttle settings, and climb maneuvers. These departures, however, were not statistically significant as a typical test may have varied from 0.022 to 0.025 g kg^{-1} $^{o}C^{-1}$. This agreed with Appleman's (1957) results in Project Cloud Trail, where variations in power setting from 85-98% were found to have little effect on contrails and the contrail factor of an F-84. Saatzer then compared the contrail factor for different groups of flights. The cumulative results indicated a bimodal distribution, with the most frequently occurring contrail factors at 0.031 and 0.025 g kg^{-1} $^{o}C^{-1}$. He concluded a contrail factor of 0.030 g kg^{-1} $^{o}C^{-1}$ was appropriate for his non-bypass (T33) test aircraft.

To analyze the tests fully, Saatzer used a numerical procedure developed by General Electric for calculating critical temperatures. The procedure uses two separate sets of curve fit equations for RH values at and below 90% and above 90%. The first set of equations relies on the fact that the difference between the critical temperature at some RH and the critical temperature at 0% RH is a function of RH alone. Both sets of equations are curve fit to empirical results for pressure altitudes from 25 - 50 kft and contrail factors from 0.025 - 0.040 g kg^{-1} $^{o}C^{-1}$. The theory behind these equations is based on the Appleman nomograms, which rely on an integration of the Clausius-Claperyon equation, and on empirical results to compute critical temperatures. An empirically based equation used to form the curve fit equations is presented by Buck (1981).

2.4.4 1995 - Speltz Validation of Appleman Contrail Forecasting Scheme. Speltz (1995) analyzed a set of new contrail observations to validate the accuracy of the Appleman contrail forecasting technique. He used the updated contrail factors and equations presented by Schrader (1994) and the same RH assumptions used in the AFGWC algorithm (see section 2.4 for full explanation). The results indicated the updated and consequently lower contrail factors of 0.030, 0.034 and 0.039 g kg^{-1} $^{o}C^{-1}$ performed more poorly than the Peters' values of 0.036, 0.040 and 0.049 g kg^{-1} $^{o}C^{-1}$. The results also indicated the updated contrail algorithm made the most accurate forecasts for stratospheric contrails. Overall, the tropospheric critical temperatures were forecast too cold, frequently by more than 10°C and as much as 34°C.

Speltz (1995) attributes a portion of the cold critical temperatures to poor RH assumptions and the updated contrail factors. However, he explained that poor RH assumptions and lower contrail factors could only account for a 10°C critical temperature difference and suggested the remainder of the difference can be attributed to incorrect contrail observations or faulty ambient observed temperatures. He also noted the assumption of a constant RH in the stratosphere is acceptable because the changes in low RH values have a smaller effect on critical temperature than do changes in high RH values. He summarized by suggesting improvements in forecasting high humidity levels are needed to improve contrail algorithm accuracy.

2.4.5 1996 - Coleman's Contrail Forecast Technique. Coleman (1996) derived an analytical equation to compute critical temperature for contrail formation in terms of water vapor mixing ratio and pressure, rather than in terms of RH and pressure. He

claims the new approach reduces the sensitivity of critical temperature to errors in relative humidity, thus providing a more accurate contrail forecast.

2.5 AFGWC Algorithm Synopsis

The AFGWC algorithm is based on the Appleman (1953) nomogram. In order to apply the nomogram, a critical temperature is computed at each discriminate pressure altitude then compared to the ambient temperature at that same pressure. A contrail is forecast if the ambient temperature is less than the critical temperature as described by Appleman (1953) and Jiusto (1961).

First, the critical temperature for 100% RH ($T_{c.100}$) must be found. This will be the warmest critical temperature and it is used to find critical temperatures at RH values less than 100%. To find $T_{c.100}$, the slope of the saturation curve is set equal to the contrail factor and solved for temperature. The contrail factor or ratio of moisture to heat added by the exhaust, is often referred to as the "critical slope". To calculate the critical slope, the contrail factor is converted from grams per kilogram (mixing ratio units) per degree Celsius to millibars (vapor pressure units) per degree Celsius. This conversion is required since the saturation curve is described by a form of the Clasius-Claperyon equation. For the range of temperatures observed in the earth's atmosphere, a simple relationship is used to convert mixing ratio to vapor pressure (Wallace and Hobbs, 1977):

$$e_S \cong p \cdot \frac{w_S}{0.622}, \qquad (3a)$$

where e_S is the saturation vapor pressure in millibars, p is the pressure in millibars and w_S is the mixing ratio in grams per kilogram.

Critical slope is calculated from

$$CritSlope = p \cdot \frac{CF}{0.622}\ , \tag{3b}$$

where CritSlope is the critical slope in millibars per degree Celsius, CF is the contrail factor in grams per kilogram per degree Celsius and p is the pressure in millibars .

The Clausius-Clapeyron equation is used to derive a formula which shows the dependence of saturation vapor pressure on temperature. A general form of the Clausius-Claperyon equation is (Fleagle and Businger, 1980):

$$\frac{dp_S}{dT} = \frac{L}{T\left(\alpha_2 - \alpha_1\right)}, \tag{4}$$

where the left hand side represents the change in saturation vapor pressure with respect to temperature, T, during phase change, and α_2 - α_1 represents the change in specific volume. L is the latent heat of condensation.

When applied to water vapor, Eq. 4 is modified. Under normal atmospheric conditions, α_2 is assumed much greater than α_1, and water vapor is assumed to behave closely to an ideal gas. Therefore Eq. 4 is reduced to (Fleagle and Businger, 1980):

$$\frac{de_S}{dT} = \frac{L \cdot e_S}{R \cdot T^2}, \tag{5}$$

where e_S is the saturation vapor pressure for water, L is the heat of condensation and R is the specific gas constant for water vapor.

In 1947, the Goff-Gratch Formula was adopted by the World Meteorological Association (WMO) to use as an empirical estimate for the integration of Eq. 5 over a range of temperatures observed in the atmosphere (List, 1984). The Goff-Gratch Formula was validated with experimental data for temperatures from 0°C to 100°C and extrapolated from -50°C to 0°C. The Goff-Gratch formula and its derivative, as used in the AFGWC algorithm today, are as follows:

$$e_S = 10^{(A-B-C+D-E)}, \tag{6}$$

$$\frac{de_S}{dT} = 10^{(A-B-C+D-E)} \cdot \ln(10) \cdot (-B + F + G + H), \tag{7}$$

where

$$A = 23.832241 \qquad E = \frac{2949.076}{T}$$

$$B = 5.02808\left(\frac{\ln(T)}{\ln(10)}\right) \qquad F = 4.20004 \cdot 10^{-9} \cdot 10^{11.334 - 0.0303998 \cdot T} \cdot \ln(10)$$

$$C = 1.3816 \cdot 10^{-7} \cdot 10^{11.334 - 0.03039 \cdot T} \qquad G = \frac{10.596098 \cdot 10^{3.4919 - \frac{1302.844}{T}}}{T^2} \cdot \ln(10)$$

$$D = 8.128 \cdot 10^{-3} \cdot 10^{3.4919 - \frac{1302.844}{T}} \qquad H = \frac{2949.076}{T^2}$$

where e_S is in mb and T in Kelvin.

Next, Eq. 3b is set equal to Eq. 7 and solved for $T_{c.100}$, the critical temperature for 100% RH. This solution is equivalent to finding the zero of $f(T_{c.100})$ given by

$$f(T_{C.100}) = \frac{de_S(T_{C.100})}{dT} - CritSlope(T_{C.100}), \tag{8}$$

where $de_S(T_{c.100})/dT$ is the Goff-Gratch derivative.

If the ambient RH is 100%, $T_{c.100}$ is compared to the ambient temperature (T) to determine if ambient temperature is cold enough to produce a contrail. If the ambient RH is less than 100%, an additional computation must be made. This computation uses Eqs. 6, 7, and 8 with the ambient RH (RH) to solve for a critical temperature at RH values less than 100% (T_c). The solution, as described by Schrader (1994), is given by the zero of $f(T_c)$, given by

$$f(T_C) = \frac{e_S(T_{C.100}) - (T_{C.100} - T_C) \cdot \dfrac{de_S(T_{C.100})}{dT}}{e_S(T_C)} \cdot 100 - RH, \tag{9}$$

where $e_S(T_{c.100})$ is the saturation vapor pressure at $T_{c.100}$, $e_S(T_c)$ is the saturation vapor pressure at T_c and $de_S(T_{c.100})/dT$ is the Goff-Gratch derivative at $T_{c.100}$.

Once each level's critical temperature is found, the method of predicting a contrail is as described in chapter one: "For each pressure level, beginning with 500 mb, the critical

and ambient temperatures are compared until the ambient temperature falls below the critical temperature. The pressure altitude where this occurs is designated the contrail base. The comparison continues until the ambient temperature rises above the critical temperature where the altitude is then designated as the contrail top."

2.6 Summary of Technical Background

Generally, contrails occur at altitudes where the temperature is below 32 °F, so saturation can occur over ice or supercooled water. Only saturation pressures over supercooled water, however, are used since contrails form first by liquid phase condensation, not by direct ice nucleation, which is a relatively slow process (Appleman, 1953, Saatzer, 1995). The critical saturation temperature is the warmest temperature at which a contrail may form (Appleman, 1953). The critical temperature is a function of pressure altitude, contrail factor, and ambient RH. Only when the atmosphere reaches or drops below this temperature does a contrail form.

As RH increases, the critical temperature increases and contrails form at warmer ambient temperatures. These warmer temperatures generally occur at lower altitudes. Similarly, for warmer ambient temperature profiles, contrails will occur at lower altitudes. Lastly, by increasing the contrail factor, contrails will form at lower altitudes.

Common practice in contrail prediction algorithms use a simpler form of the Goff-Gratch equation such as Teten's formula (Duffield, 1984). These simpler forms may be curve fit for a series of specific altitudes and contrail factors, as described by Saatzer (1995).

III. Methodology

3.1 Chapter Overview

This chapter presents the procedures and programs used to test the contrail forecast algorithms. Before discussing the actual tests, key assumptions and a detailed description of the data are given. The last section provides an in-depth look at the numerical solution of the Goff-Gratch equation.

3.2 Assumptions

(1) *Constant Contrail Factor:* The contrail factor was assumed constant and defined as 0.030 g kg^{-1} $^{o}C^{-1}$ or 0.039 g kg^{-1} $^{o}C^{-1}$ for the aircraft's non- bypass or high-bypass engine classification respectively (Schrader, 1994).

(2) *Standard Atmosphere for All Reported and Forecast Altitudes.* Altitude calculations assumed a standard atmosphere, because aircraft altimeters are calibrated for a standard atmosphere when flying at altitudes greater than 18 000 feet. All reported aircraft contrail bases and forecasts were well above 18 000 feet.

(3) *WMO Tropopause Designation.* The tropopause height was calculated based on attaining a minimum lapse rate of 2 g kg^{-1} $^{o}C^{-1}$ for at least a 2 km depth as recommended

by the WMO and outlined in Air Weather Service Technical Report AWS/TR-79/006 (AWS, 1979).

(4) *Saturation Vapor Pressure Only for Water.* Only saturation vapor pressures over supercooled water were used since contrails first form by liquid phase condensation not by direct ice nucleation, which is a relatively slow process (Saatzer, 1995).

(5) *Excess Water Vapor Required for Visible Contrails.* After saturation is reached, 0.004 g m^{-3} of excess water vapor is needed to condense and form a visible cloud or contrail (Appleman, 1953). Since droplets immediately freeze after condensation, the mixture is supersaturated with respect to ice and automatically exceeds the 0.004 g m^{-3} criteria (Appleman, 1953). Therefore, initial excess water vapor was required in this study to forecast a contrail base.

(6) *Contrail Non-Persistence Designation.* All contrail forecasts are made for non-persistent contrails. Since the study focuses on the altitude and instant when a contrail is first reported, contrail persistence is not considered.

(7) *Statistical Distribution.* The joint distribution of forecast and observed contrail bases is assumed to be a bivariate normal (parametric) distribution (Wilks, 1995).

3.3 Data Description

3.3.1 Meteorological Measuring Equipment. Two types of rawinsondes, Aerospace Instrument Recorder (AIR) and Vaisala, were used to collect in-situ temperature, pressure, and relative humidity. The Vaisala rawinsonde accurately measures (Vaisala, 1996):

(1) Pressure - within 0.5 mb (15 ft pressure altitude)

(2) RH - within 3%

(3) Temperature - within 0.2 °C

The AIR rawinsonde specifications show a slightly less accurate instrument which measures (Aerospace, 1996):

(1) Pressure - within 1 mb (30 ft pressure altitude)

(2) RH - within 3%

(3) Temperature - within 0.3 °C

Vertical resolution of rawinsonde measurements differed between data sets and cases. These vertical resolutions varied between 10 ft and 60 ft.

3.3.2 Data Sets. Three sets of data were used to compile a data base of 42 contrail cases. They include data collected from experiments by the Air Force, NASA, and Northrop Grumman Corporation.

The first data set was collected by Air Force's 88th Weather Squadron at Wright Patterson AFB between 6 June 1996 and 17 October 1996 (Weaver, 1996). AIR or Vaisala rawinsondes were launched on 24 days within this period between 1500 to 1800 UTC to collect meteorological data. On 12 of the 24 days, visual confirmation of contrails and their persistence was recorded by a surface observer. The remaining 12 days consisted of only meteorological data. During the rawinsonde launches, a surface observer with 25x power binoculars or a 50x power telescope would identify contrailing and non-contrailing aircraft type and commercial affiliation. The ground observer would then record the time he observed each aircraft. These times were matched to Federal Aviation and Administration (FAA) flight logs and planned flight corridors to determine aircraft altitude. A contrail base was identified when a second aircraft, of the same type as the recorded contrailing aircraft, was observed not contrailing. The second aircraft had to be observed flying 2 kft (or less) below the contrailing aircraft and within 20 minutes of the contrailing aircraft to verify a contrail base. Aircraft which were climbing, descending, or could not be positively identified were not used. A midway point between the contrailing and non-contrailing aircraft was estimated as the contrail base altitude. If the contrailing aircraft was seen to begin contrailing overhead by the ground observer, then the contrailing aircraft's altitude was reported as the contrail base. Only 8 of the 12 contrail days could be positively identified for contrail bases. The other four days lacked non-contrailing aircraft within the 2 kft criteria. Observed aircraft used in this data set included Boeing 727's, 737's, 757's, and 767's, McDonnell Douglas MD-80's, and DC-9's. All of these are aircraft use high-bypass engines. Since only a limited number of cases were produced by this data set, two other data sets were also used.

The second data set contains data from a series of flight tests performed by NASA aircraft over Oklahoma and Kansas from 13 April 1996 - 4 May 96 (NASA, 1996). During this time, a total of 12 flights were flown. Six of the 12 flights were flown to observe and record contrails of which only four recorded the contrail base altitude. All four cases from this data set were flown near the Clouds And Radiation Testbed (CART) Site. Visual confirmation of a contrail and the aircraft's altitude were recorded by an observer in a trailing aircraft or by the pilot in the contrailing aircraft, since the flight pattern often permitted the pilot full view of his most recent track. All the contrails used in this data set were produced by a DC-9 with a high-bypass engine. Flights took place between 1500 and 1900 UTC, and meteorological measurements were taken with Vaisala rawinsondes launched between 1730 and 2030 UTC from site B1 near the CART site and within the test area.

The third data set was collected by the Northrop Grumman Corporation over southern California's eastern Sierra Nevada Mountains and Owens Valley from 3 September 1992 to 4 March 1993 (Saatzer, 1995). A total of 32 flights were flown during this test, 30 of which produced usable contrail bases. As in data set two, visual confirmation of a contrail and the aircraft's altitude were recorded by an observer in a trailing aircraft and by the pilot in the contrailing aircraft. Flights took place between 0400 and 2200 UTC. Each contrail in this set was produced by a T-33 jet trainer with a low-bypass engine. Meteorological measurements were taken with AIR rawinsondes launched between 1000-2000Z from Edwards AFB, about 70 miles southwest of the test site.

All three data sets combined produced 42 recorded contrail base cases with matching meteorological data collected by the rawinsondes.

3.4 Procedures

3.4.1 Overview. In order to assess the impact of RH on the accuracy of the forecast contrail bases by the AFGWC algorithm and determine whether the SAGE II RH values (profile 4) produce more accurate bases than the empirical RH values (profile 3), the RH profile was varied for each case while maintaining the in-situ temperature and pressure measurements. Each RH profile was used to generate a set of forecast bases for each of the 42 cases. Overall, seven RH profiles (see Table 2) were tested on both the AFGWC and Saatzer algorithms (described in Section 3.5), generating 14 sets of forecast bases. All 14 sets of bases were then statistically compared to the reported aircraft base altitudes. The Forecast Bases matrix was organized as shown in Fig. 4.

Case #	**AFGWC Algorithm**							**Saatzer Algorithm**							**Reported Aircraft Base**
	RH Profiles							**RH Profiles**							
	1A	**1B**	**2A**	**2B**	**2C**	**3**	**4**	**1A**	**1B**	**2A**	**2B**	**2C**	**3**	**4**	
1 2 3 to 42															

FIG 4: Example of Forecast Bases Matrix for the RH Profile Tests

A second series of tests was developed to observe the impact of RH for different temperature profiles or lapse rates. Artificial lapse rates were constructed from a reference altitude and used with profile 1B (0% RH) to observe how lapse rate affected the forecast base altitude. Each lapse rate provided a set of unique forecast bases so the distance between the reference point and forecast bases provided altitude differences or depths. This depth demonstrated a range of bases possible for all RH values. As the depth or difference became smaller the range of possible bases was shown to decrease.

3.4.2 RH Profile Tests. First, the set of bases generated by the Profile 2A (In-Situ), 3 (Empirical), and 4 (SAGE II) were compared (see Fig. 5a). By making this comparison, the bases generated by Profile 4 could be directly compared to the bases by profile 3 with profile 2A's bases used as a control group.

The bases generated by Profile 2A was selected as a control or "ground truth" set. This profile was expected to produce the most accurate forecasts since it contains RH values that most closely resemble the flying conditions encountered by the aircraft during contrail formation. Profile 3 was selected to emulate the AFGWC forecast method (AWS, 1981). Initially, this profile was expected to produce the most inaccurate forecasts (Appleman, 1953; Jiusto and Pilie, 1964) since it is only a very rough approximation and simplification of actual atmospheric RH. Profile 4 was next used since it is one of the most accurate climatological tables for upper atmospheric RH data (McCormick, 1987; Chiou, 1996). Its accuracy was expected to fall between the results of profiles 2A and 4. Below is an extract from the meteorological measurements (Profile

2A) taken from a Success rawinsonde on 16 Apr 96 at 1700Z, along with the profiles' 3 and 4 values at each level of rawinsonde data.

Table 1: Comparison of RH values for Profiles 2A, 3, and 4. Vertical profile of RH values extracted from rawinsonde data and RH profile computations.

Profile 2A (%)	Profile 3 (%)	Profile 4 (%)	Altitude (kft)
11	40	32.5	30.07
16	40	32.5	30.76
17	40	28.6	31.83
18	40	28.6	31.90
19	40	28.6	31.97
20	40	28.6	32.04
20	40	28.6	32.11
14	40	28.6	33.40
12	40	28.6	34.19
12	40	20.8	35.04

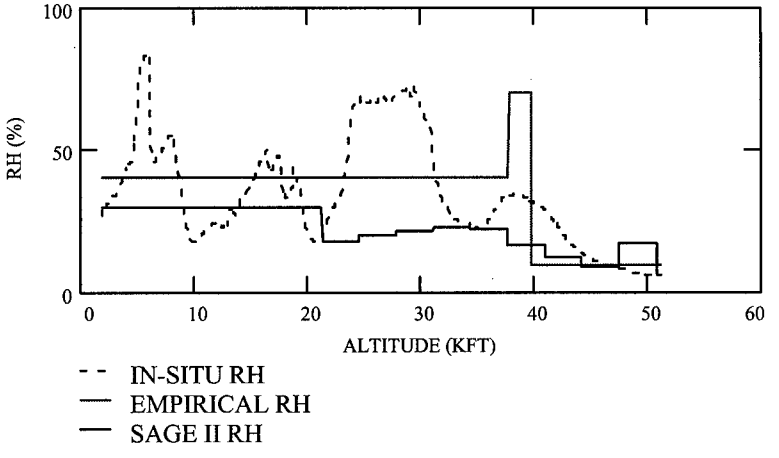

FIG 5A: Example of RH values for Profiles 2A, 3, and 4.

When comparing the three sets of forecast bases produced by profiles 2A, 3, and 4, they showed little or no variation for each case and overall. Therefore, additional RH profiles were constructed and compared.

The next series of RH profile comparisons involved modifying profile 2A to exhibit a moist and dry bias. Since individual SAGE RH measurements may exhibit up to an 18% random error (Chu et al., 1993), and Saatzer (1995) indicated a 15% RH uncertainty in the Northrop data set, a bias of 20% was selected In order to modify profile 2A with a moist bias, each of its levels had 20% of its initial value added to it. This new profile was the Modified +20% (2B). Similarly, to make a dry bias, each level of profile 2A had 20% of its initial value subtracted from it. This new profile was Modified -20% (2C). The modifications were not allowed to exceed RH values of 100% or fall below 0%. These modifications were made for each of the 42 cases (see Fig. 4). Once modified profiles were built, forecast bases were generated and compared to each other. Again, the bases generated by Profile 2A were used as a control group, so a total of three sets of bases were used in the comparison.

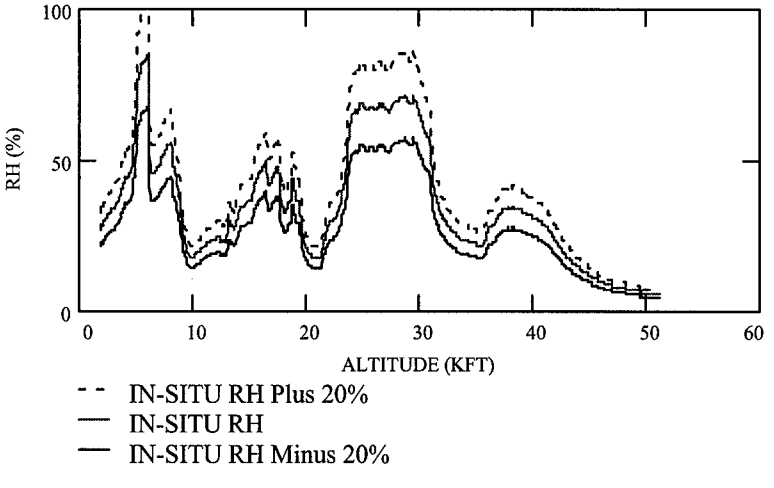

FIG 5B: Example of RH values for Profiles 2A, 2B, and 2C.

The bases produced by these profiles also exhibited remarkable similarity. As a result, it was decided to observe the maximum difference in bases possible by constructing two extreme RH profiles: a 100% and 0% RH profile.

RH profiles of 100% (1A) and 0% (1B) were then built for the entire depth of the rawinsonde. These profiles were tested to observe the possible range of bases generated by any RH value. A range such as this could be computed since profile 1A always generates the warmest critical temperature or lowest base altitude, while profile 1B generates the coldest critical temperatures or highest base altitudes (Appleman, 1953).

3.4.3 Lapse Rate Tests. The first part of these tests compared how contrail bases, generated by profile 1B and a 50% RH profile (referred to as profile 1C), vary with different lapse rates. The comparison shows the impact of RH on a forecast bases for different lapse rates. A reference altitude of 30 kft was chosen. This altitude represents a typical forecast base, using profile 1A, for the 42 cases. The different lapse rates and the forecast bases generated by them were then visualized on a Skew-T, Log-P diagram (AWS, 1979). Figure 6 shows the same Appleman nomogram from Fig. 1, on a Skew-T, Log-P diagram.

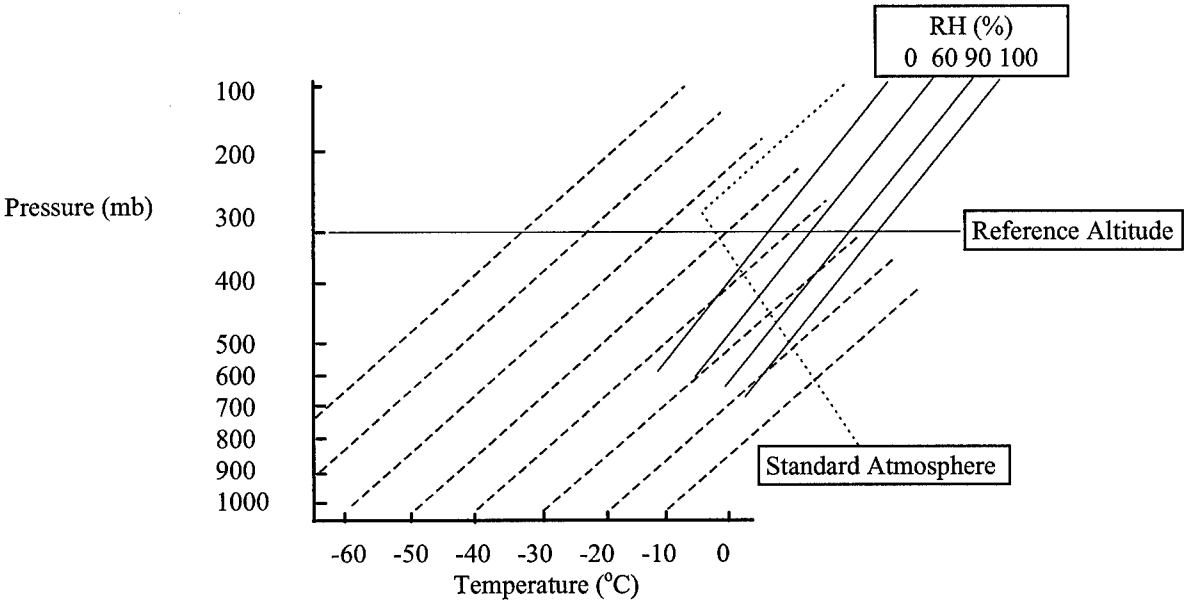

FIG 6: Skew-T, Log-P Diagram with Appleman Nomogram

Next, four lapse rates, 2, 3, 6, 9 g kg^{-1} $^{o}C^{-1}$ were built upward from the reference altitude. Figure 7 shows each of these lapse rates on a Log-P, Skew-T Diagram. They were assumed constant and penetrated the standard tropopause altitude of 36 kft (226 mb). The standard tropopause height (226 mb or 36 kft), however, was used to compute forecast base altitudes since aircraft compute pressure altitudes similarly and report contrail base altitudes with these standard atmospheric assumptions.

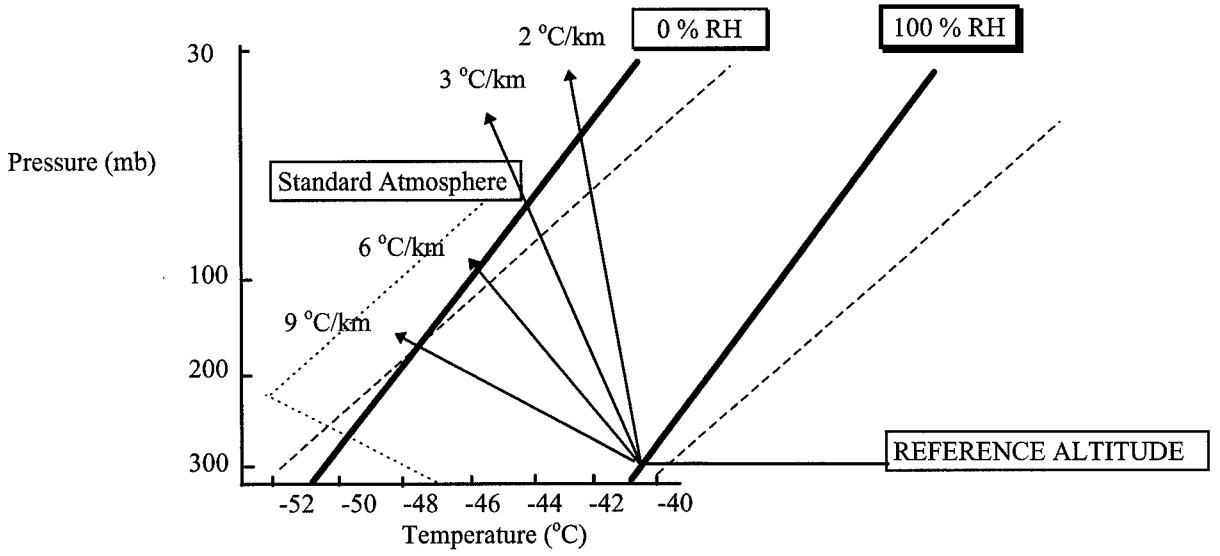

FIG 7: Lapse Rates on Skew-T, Log-P Diagram

There was both an upper and lower limit to which lapse rates could be tested. An average lapse rate of 1.5 °C km^{-1} for the AFGWC Contrail Curves (see Fig. 14) provided a lower limit of 2 °C km^{-1} (smallest whole number). It is also interesting to note from Fig. 6, as the tested lapse rate approaches 1.5 °C km^{-1}, the forecast base for profile 1B approaches the top of the atmosphere. An upper lapse rate of 9 °C km^{-1} was used since atmospheric conditions do not normally exceed the dry adiabatic lapse rate of 9.8 °C km^{-1} (Wallace and Hobbs, 1977). Therefore, 2 °C km^{-1} was tested as the shallowest lapse rate and 9 °C km^{-1} as the steepest. Additionally, two intermediate lapse rates of 3 °C km^{-1} and 6 °C km^{-1} were arbitrarily selected and tested to demonstrate intermediate changes.

The reference altitude shown in Fig. 6 is shown to coincide with the 100% contrail curve. This was done to compare how lapse rate affects forecast bases generated with RH values from 100% to 0%. Additionally, forecast bases for each lapse rate were generated using a 50% RH profile. These bases provided a midway RH value to compare the effects of RH at different lapse rates

Next, the difference between the reference point and forecast base generated by profile 1B was taken for each lapse rate. The difference demonstrated a depth, or range of possible contrail bases. Then the depths generated by the four lapse rates were compared to each other. This relative comparison demonstrated how the environmental lapse rate could affect the range of possible forecast bases for different RH values.

Finally, lapse rates and depths for each of the 42 cases and their overall averages were computed.

3.5 Computer Programs

3.5.1 RH Profile Program. The RH Profile program is primarily concerned with implementing the series of tests described above. A Flow Chart of the RH Profile program (Appendix A) illustrates the 3 main steps of this program. The first step initializes the program by reading in data from the rawinsondes, converting pressures to pressure altitudes, defining tropopause heights, and building RH profiles. The second step processes the initialization data through the AFGWC and Saatzer Algorithms to produce critical temperatures and contrail base forecasts for each profile type and case. Finally, the third step produces graphical displays of the forecast bases to allow the

overall comparison between different profiles on all the days. All three steps are performed as array operations from the surface to the highest altitude measured by the rawinsonde, which ranged from 50 - 75 kft. Math Soft Applications Software, MATHCAD Professional 6.0, was used to perform all forecast base analysis and calculations. For a detailed description of the MATHCAD program code, refer to Appendix B

3.5.1.1 Step 1 - During step 1, two programs were developed to convert rawinsonde pressures into pressure altitudes and define tropopause levels for placing the empirical RH values. After the altitudes and levels were defined, several RH profiles were constructed for later testing.

(1) *Pressure Altitude Conversion Procedure* - First, the rawinsonde pressure levels were converted to pressure altitudes. Since rawinsondes provided pressure in millibars and the reported contrail altitudes (by aircraft) were in thousands of feet, a standard conversion was necessary to compare the algorithms' forecasts to the reported aircraft contrail observations. These conversions (List, 1984), listed below, are derived from the ideal gas law and Hypsometric equations and assume a linear decrease of temperature with height up to the tropopause and an isothermal layer above (i.e. Standard Atmosphere).

At or below 11,000 m (226.19 mb), the standard conversion equation was:

$$\frac{p_S}{1013.25mb} = \left(\frac{288K - 0.065 \cdot Z}{288K}\right)^{5.25}, \qquad (10)$$

Above 11,000 m:

$$\frac{Z - 11{,}000m}{14{,}600m} = \log\left(\frac{226.19mb}{p_S}\right), \qquad (11)$$

Since aircraft fly on a constant pressure surfaces above 18,000 feet (FAA, 1996) and are programmed to provide cockpit altitudes with these same conversion equations, the pressure altitude conversions are consistent with the reported aircraft bases.

(2) *Tropopause Designation* - The location of the tropopause is required for profile 4, since the profile's 70% RH layer is defined as 300 m above and below the tropopause altitude, 40% is defined below the 70% layer, and 10% is defined above the 70% layer. Few rawinsonde measurements provided a derived tropopause height, therefore a method was developed for calculating this height based on lapse rate. This method computes a lapse rate over a 2 km depth. Typical lapse rates below the tropopause are 4 °C km^{-1} to 6 °C km^{-1} and 2 °C km^{-1} to 0 °C km^{-1} just above the tropopause (Wallace and Hobbs, 1977). To eliminate low-level inversions (steep lapse rates) from being misidentified as the tropopause, the program starting analyzing data at 350 mb. Lapse rates were computed for each incremental 2 km depth from 350 mb to the top of the rawinsonde data. When the lapse rate decreased to 2 °C km^{-1} for a 2 km depth, the base of that increment was designated as the "conventional tropopause" altitude. This

criteria is defined by the World Meteorological Organization (WMO) and outlined in an AWS technical reference report, AWS/TR-79/001 (AWS, 1979).

(3) *RH Profiles* - In order to compare the effect of RH on the AFGWC and Saatzer (1995) algorithm's forecast bases, profile 2A (rawinsonde RH profile) was evaluated with six constructed profiles making a total of seven RH profiles evaluated (Table 5).

Table 2: Relative Humidity (RH) Profile Descriptions

RH Profile	Name	Description
1A	100%	RH values of 100% designated at all levels
1B	0%	RH values of 0% designated at all levels.
2A	In-Situ	RH values for each level are taken from meteorological measurements.
2B	Modified +20%	Each level of profile 2A is given a high bias by 20% of its original value.
2C	Modified -20%	Each level of profile 2A is given a low bias by 20% of its original value.
3	Empirical	RH values are designated by AFGWC method
4	SAGE II	RH values based on recently derived satellite climatology.

Although seven different RH profiles were used during the tests, only pressures and temperatures measured by the rawinsonde were used. Profile 2A was simply the rawinsonde's measured RH values. The first RH profile built, profile 3, was made by replacing profile 2A values within 300 m of the tropopause with 70% RH, below that layer with 40%, and above that layer with 10%. Profile 4 was built similarly. The SAGE

II tables (McCormick, 1994) provide RH averages in layers every 1 km (3 280 feet) from 6.5 km (21 000 ft) to 16.5 km (54 000 ft). Profile 4 was built by replacing profile 2A values at and above corresponding rawinsonde levels with SAGE II table values. Additionally, profile 2A values were replaced with 30% RH below the table boundary of 6.5 km and 5% RH above its boundary of 16.5 km. These replaced values were representative of typical rawinsonde values tested for those levels. These replaced values proved inconsequential as post analysis indicated no 100% RH bases occurred below 6.5 km or 0% bases above 16.5 km. The next two profiles, 2B and 2C, were modifications of profile 2A. At each level of profile 2A, 20% of its value was computed and added to it to make a high biased RH profile, profile 2B. Similarly, profile 2A was modified with a 20% low bias to produce profile 2C. An example of profile 2A, 2B, and 2C is provided in Fig. 5a. The sixth constructed profile, profile 1A, was created by replacing profile 2A values at each level with 100% RH. This provided the maximum amount of moisture a profile could have and gave the warmest critical temperature and lowest forecast base for a moist atmosphere. The last profile (profile 1B) replaced profile 2A values with 0% to provide the warmest critical temperature and highest contrail base in a perfectly dry atmosphere.

(4) *Substitution* - To decrease the processing time in computing Eq. 9 (critical temperatures), Eq. 3b (critical slope) was substituted for Eq. 7 (Goff-Gratch derivative).

$$f(T_C) = \frac{e_S(T_{C.100}) - (T_{C.100} - T_c) \cdot CritSlope(T_{C.100})}{e_S(T_C)} \cdot 100 - RH \ , \qquad (12)$$

This was easily done since Eq. 3b and Eq. 7 are equal at $T_{c.100}$. Post analysis of these two quantities indicates a maximum difference on the order of 10^{-4} between them. This difference altered critical temperature by less than 0.01 °C, which did not affect the forecast contrail base altitude. An extract of a case from the Wright Patterson data set is provided (Table 3a) to show the difference between the critical slope and Goff-Gratch derivative for a series of 10 rawinsonde levels.

Table 3a: Example of computed Critical Slopes and Goff-Gratch derivative values (evaluated at 100% RH) for 10 rawinsonde levels.

Critical Slope	Goff-Gratch Derivative	Difference
0.0031	0.0032	0.0000
0.0063	0.0063	0.0000
0.0125	0.0126	0.0000
0.0188	0.0189	0.0001
0.0251	0.0251	0.0000
0.0314	0.0314	0.0000
0.0376	0.0376	0.0000
0.0439	0.0440	0.0001
0.0502	0.0502	0.0001
0.0627	0.0627	0.0000

3.5.1.2 Step 2 - The process of computing critical temperatures and forecasting bases for the AFGWC algorithm has been described in Chapter II. Therefore, only the Saatzer (1995) algorithm process is discussed in this section.

The Saatzer (1995) algorithm uses a series of General Electric curve fit equations designed for contrail factors between 0.020 - 0.039 g kg^{-1} $°C^{-1}$ and pressure altitudes from

25 - 50 kft. Since all cases analyzed assumed contrail factors of 0.030 or 0.039 g kg^{-1} $^{o}C^{-1}$ and the bases approximated the altitude range of 25 - 50 kft, no variations to the Saatzer algorithm were needed. The procedure for curve fitting the equations relies on the fact that the difference between the T_C at some value of RH and T_C at 0% (T_d) for all combinations of altitude is only a function of RH up to values of 90% (Saatzer, 1995). The Saatzer algorithm therefore uses different equations to calculate critical temperatures for RH values > 90% and ≤ 90%.

The first set of equations computes critical temperatures when RH is greater than 90%. The critical temperature, T_{C40}, in this set of equations was developed by curve fitting the variations in critical temperature at an altitude of 40 kft. Next, the variation in ΔT_{C40} was curve fitted versus Δaltitude. (Saatzer, 1995).

$$\Delta altitude = 40kft - altitude \quad , \tag{13}$$

$$\Delta T_{C40} = 0.032 + 0.4711 \cdot \Delta altitude + 0.00019286(\Delta altitude)^2 \quad , \tag{14}$$

$$T_{C40} = 61.27 + 581.1 \cdot CF - 4500 \cdot CF^2 \quad , \tag{15}$$

$$T_C = T_{C40} + \Delta T_{C40} , \tag{16}$$

where Δaltitude is in kft, ΔT_{C40} and T_{C40} are in °C, and contrail factor, CF, is in grams per kilogram per degree Celsius.

The second set of equations computes critical temperatures for RH values less than or equal to 90%. A curve fit for T_d (ΔT_{RH}) was developed for each contrail factor at altitudes between 25 - 50 kft (Saatzer, 1995).

$$A_0 = 117.445 + 6487.20 \cdot CF - 182454 \cdot CF^2 + 1772719 \cdot CF^3 , \quad (17)$$

$$A_1 = 0.332437 + 60.6166 \cdot CF + 1552.4 \cdot CF^2 - 13265.5 \cdot CF^3 , \quad (18)$$

$$A_2 = 0.0055724 + 0.42889 \cdot CF - 10.1451 \cdot CF^2 + 76.2117 \cdot CF^3 , \quad (19)$$

$$T_d = A_0 + A_1 \cdot altitude + A_2 (altitude)^2 , \quad (20)$$

$$\Delta T_{RH} = 0.04466 \cdot RH - 0.0003944 \cdot RH^2 + 0.0000064815 \cdot RH^3 , \quad (21)$$

$$T_{RH} = T_{d,alt} + \Delta T_{RH} , \quad (22)$$

where A_0, A_1, A_2 are empirically derived coefficients which account for contrail factor. T_d, ΔT_{RH}, and T_{RH} are in °C.

Once each level's critical temperature is calculated, the contrail bases are computed similarly to the AFGWC algorithm procedure.

3.5.1.3 Step 3 - The forecast bases for each case were displayed by case number/date and RH profile type, as Fig. 4 illustrates. In order to display all 630 bases in this fashion, each case was processed with the seven sets of RH profiles, in both algorithms, to generate a set of 14 critical temperatures at each rawinsonde level. Next, each set of critical temperatures were subtracted from the ambient temperatures to make 14 sets of ΔT's. The 14 sets of ΔT's were then analyzed for the first level where ΔT became negative above 350 mb. When this occurred, a base was forecast at that altitude. This process produced 14 sets of forecast bases for each case. The entire method was

performed for all 42 cases, providing 588 forecast bases. Additionally, the set of 42 reported aircraft bases were added to the matrix to provide a total of 630 bases for comparison. Therefore the example matrix, Fig. 4, had 630 contrail base entries.

3.5.2 Lapse Rate Program. This program consisted of three short sections. In the first section, preliminary analysis was performed on the AFGWC curves. First critical temperatures for the AFGWC algorithm were computed at the 1000-, 800-, 700-, 600-, 500-, 400-, 300-, 200-, 100-, and 50-mb pressure levels, in a similar fashion to the RH Profile Tests Program. Next, an average lapse rate for these curves between 500 - 50 mb was computed by dividing the difference of temperatures at the 500 and 50 mb level by their difference in pressure altitudes. Although this was a simplified approach at computing an average rate, sample lapse rates along the curve show the slope doesn't change by more than 0.01 $^{\circ}C\ km^{-1}$ between any two pressure levels.

The second section of this program computed four sets of contrail depths for lapse rates described in section 3.4.3 for a high-bypass and non-bypass contrail factor. To compute the depths, four lapse rates were constructed from 30-100 kft at vertical intervals of 100 m. Next, critical temperatures were computed for each level at RH values of 0% and 50% (profiles 1A and 1C). Contrail bases were identified by defining the level where the temperature profile value dropped below the critical temperature. The forecast bases using profiles 1A and 1C were then compared by plotting the forecast base against its corresponding lapse rate. The lapse rates were averages through the entire layer and often penetrated the standard atmospheric tropopause at 226.19 mb. However, since aircraft measure altitude against a standard tropopause height, the AFGWC algorithm and

the newly constructed lapse rates maintained this standard so appropriate forecast bases could be produced and compared to reported bases. The depth was then computed by subtracting the altitude of the forecast base generated by profile 1A from 1B. A plot of bases against lapse rate is referred to as a Depth Chart, Fig. 8.

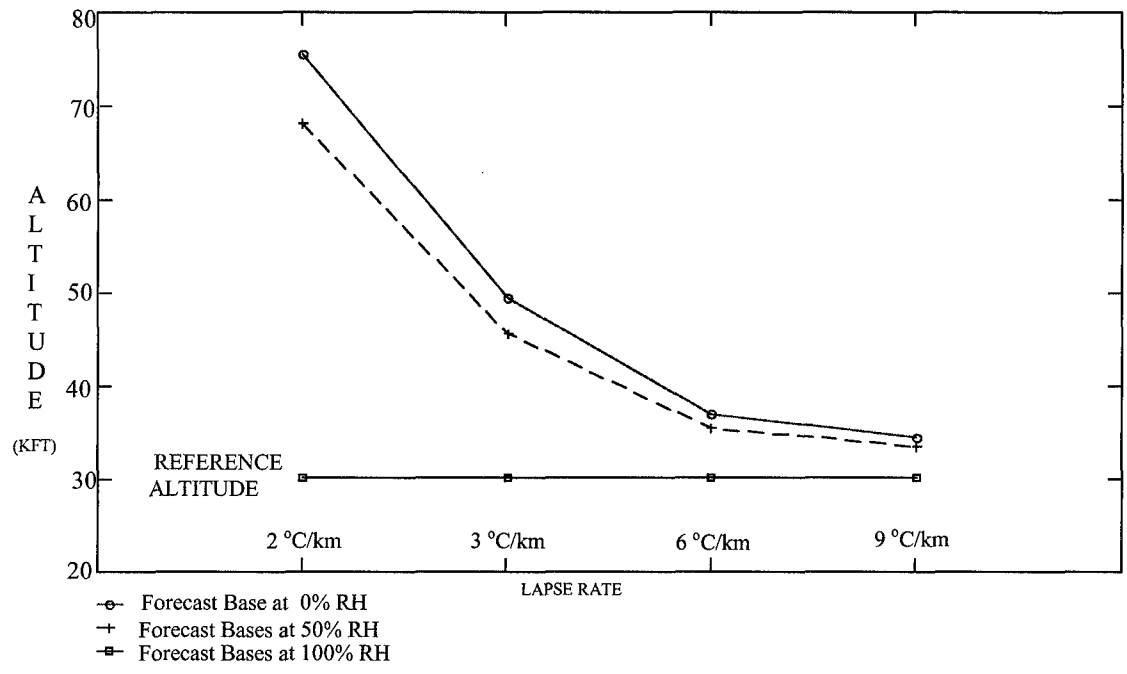

FIG 8: Depth Chart for Four Constructed Lapse Rates. Each curve shows how the relative depth of forecast base changes for a specific RH as a function of lapse rate.

The last section of this program assesses the lapse rates and depths of each case. The depth again was computed by subtracting the altitude of the forecast base generated by profile 1A from 1B. Next, the lapse rate was computed by determining the ambient temperature difference of the same two levels then dividing the difference by the depth.

These results were then separated by data set. Average depths and lapse rates were then computed for each data set and overall.

3.6 Non-Linear Root Functions

3.6.1 Overview. This section describes several important characteristics of the equations and methods used to compute critical temperatures by the AFGWC algorithm. It begins by reviewing the Secant convergence method used to find the zero of Eqs. 8 and 9, describes the non-linear response of these equations, and then outlines steps used to chose between multiple roots found in the solution of Eq. 9.

3.6.2 Secant Method. Since Eqs. 8 and 9 are non-linear quadratic functions, a convergence technique was used to solve for the zero root of each equation (T_C). The Secant method was selected. This method approximates the root, within a user defined tolerance. Once the tolerance is set, a reasonable initial guess is chosen for the root solution. Selection of both tolerance and initial guess affects the critical temperature solution.

3.6.3 Non-Linear Response. When computing critical temperatures on an array of rawinsonde pressure levels, different critical temperatures were produced when repeating the same computations. At first, this was done accidentally by varying the tolerance in Eq. 8 and making a different initial guess of critical temperature in Eq. 9. To explain these results, both functions were plotted to observe how they change as a function of

temperature and to observe their behavior near the critical temperatures. Both Eqs. 8 and 9 were tested at altitudes of 2, 10, 20, 35, and 85 kft and a high-bypass contrail factor. Additionally, Eq. 9 was provided an RH value of 30% at each pressure altitude. Figures 9 and 10 shows how Eqs. 8 and 9 change with temperature for several selected pressure altitudes. The point where each trace crosses the zero ordinate indicates the critical temperature for that pressure altitude. Both figures were plotted over the range of temperatures normally observed in the atmosphere.

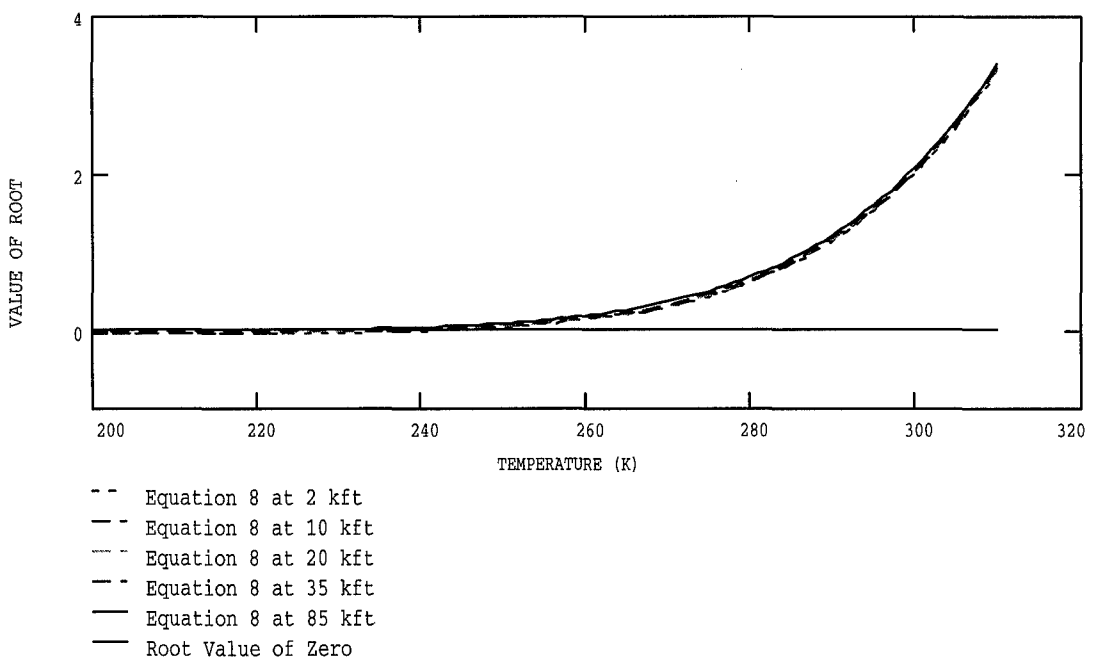

FIG 9: Non-Linear Behavior of Eq. 8 Plotted as a Function of Temperature and Altitude.

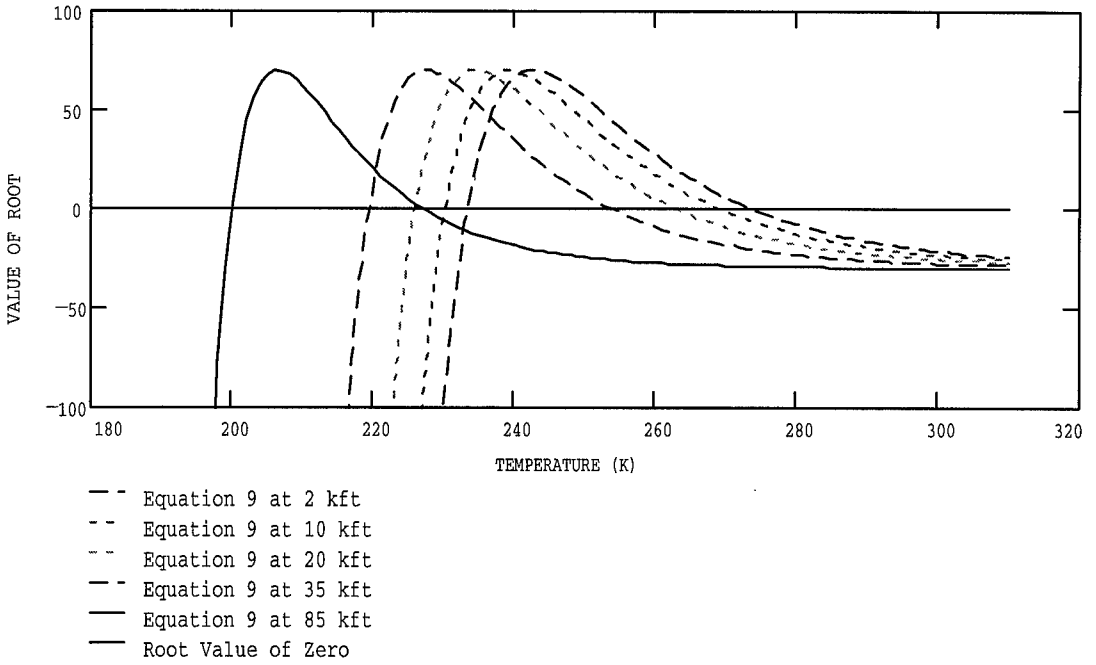

FIG 10: Non-Linear Behavior of Eq. 9 Plotted as a Function of Temperature and Altitude.

From Fig. 9, Eq. 8 is shown to decrease exponentially as temperature decreases from 300 K. Each trace or pressure altitude behaves similarly. The altitude traces approach the zero ordinate asymptotically and most even cross over it. Since critical temperature is found by an approximation to the zero root, and the slope of this function near the zero root is very small, small tolerance selection is crucial to an accurate solution. For example, if the tolerance for Eq. 8's 35 kft trace was decreased from 10^{-12} to 10^{-1}, the

critical temperature changes from 223 K to 251 K. This will effectively change the forecast base from 27.72 kft to 29.16 kft. From the figure, error is shown to be generally biased toward warmer critical temperatures for large tolerances.

Figure 10 shows the dramatically different behavior of Eq. 9. Here Eq. 9 is shown to have two roots for each altitude over the range of temperatures tested. These multiple roots are explained in the next section. Tolerance, however, does not play a significant role for the lower-valued roots of these traces. This insignificance is again the result of the function's slope, where Eq. 9 is now steeply sloped as its lower-valued root approaches zero.

Since the RH profiles included RH values from 0 to 100%, Eq. 9's response to different RH values was plotted as a function of temperature. Figure 11 shows how this function varies at 85 kft for RH values of 0, 25, 75, and 100%.

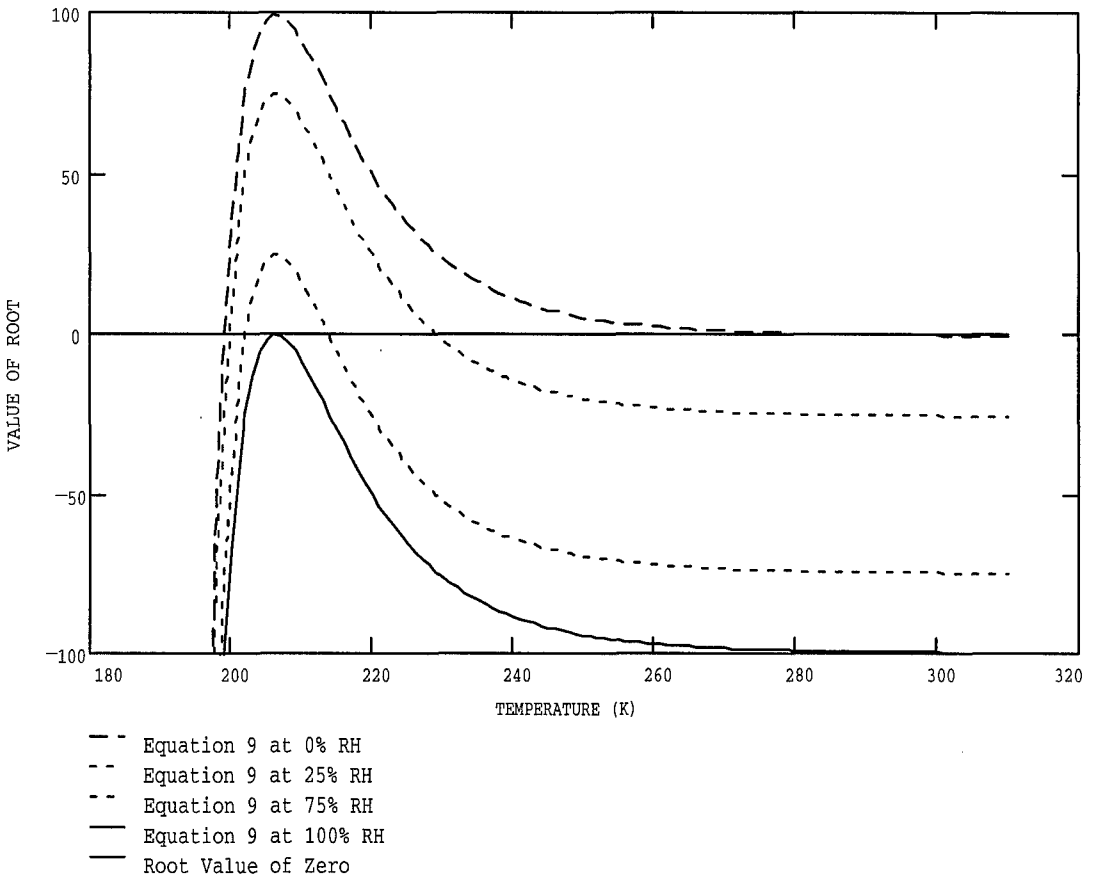

FIG 11: Eq. 9 Non-Linear Behavior Plotted as a Function of Temperature, RH.

Figure 11 shows how Eq. 9 converges to a single root when RH increases toward 100%. The critical temperature of 206 K at 100% RH for Eq. 9 and Fig. 12 is the same as the critical temperature for the 85 kft trace of Eq. 8 and Fig. 10.

3.6.4 Multiple Roots. Although Eq. 9 has two mathematically correct roots, only one of the roots is physically meaningful. In order to determine the physical meaning of each set of roots, both sets of roots are solved and plotted against critical temperatures.

Figures 12 and 13 show a set of critical temperatures at 0% RH computed for an array of pressure altitudes from the surface to 80 kft. Figure 12 uses an initial critical temperature guess of 215 K and while Fig. 13B uses 280 K.

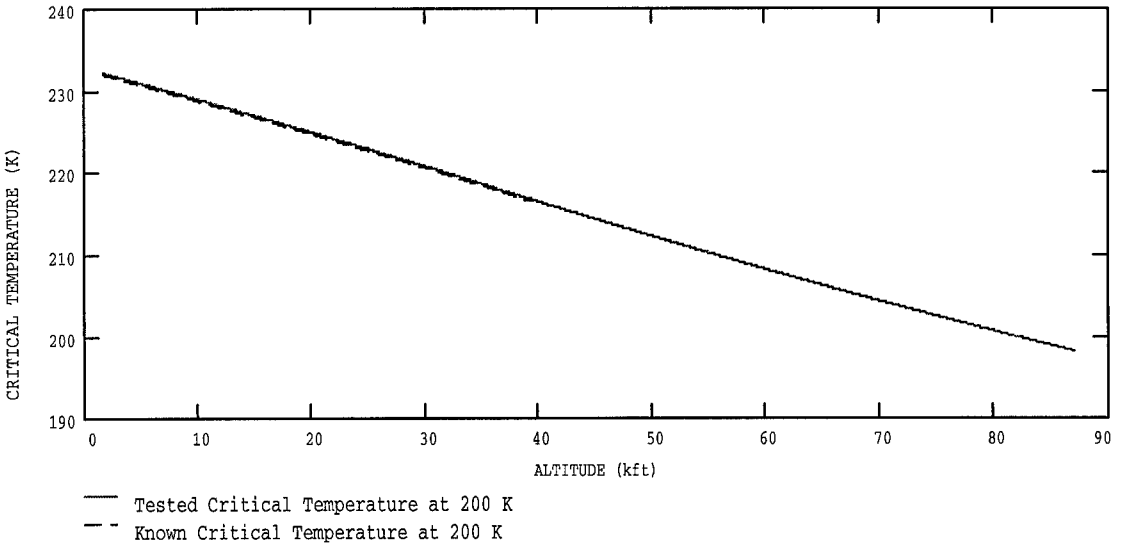

FIG 12: Eq. 9 Critical Temperatures Using an Initial Guess of 215 K.

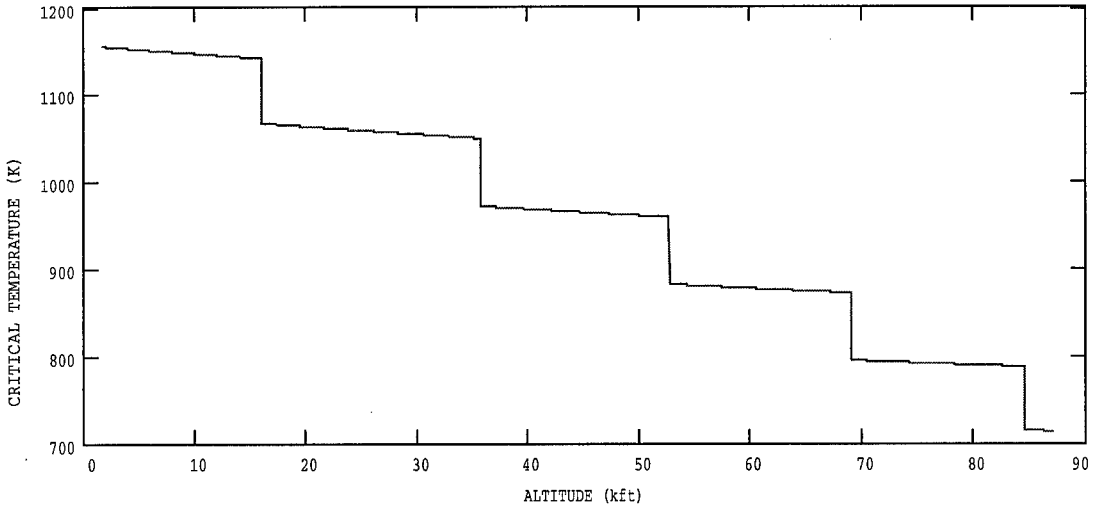

FIG 13: Eq. 9 Critical Temperatures Using an Initial Guess of 280 K.

Figure 12 shows critical temperatures which converged to the lower-valued roots shown in Fig. 10. Figure 13 shows critical temperatures which converged to an upper-valued root beyond those shown in Fig. 10. From these plots, it can be seen the critical temperatures derived from the lower roots (Fig. 12) provides a critical temperature which smoothly decreases with height. This is consistent with the Appleman nomogram and theory (Appleman, 1953). For the critical temperatures derived from the upper roots (Fig. 13), however, the critical temperature is well outside the temperatures of the earth's atmosphere. This is inconsistent with the Appleman (1953) theory and provides physically unmeaningful temperatures, therefore all upper-valued are non-physical and must be avoided when solving Eqs. 8 and 9.

To chose an initial guess which eliminated the upper-valued roots, a value to below the lowest trace's peak was chosen (see Fig. 10). The lowest trace peak was always the highest altitude trace. If a selection between the traces' peaks was selected as the initial critical temperature, the solution would not converge for the array of altitudes.

IV. Results

4.1 Overview

This chapter presents and analyzes the results derived from the RH Profile and Lapse Rate programs. It begins by describing the similarities between the contrail curves of the AFGWC (Schrader, 1994) and Saatzer (1995) algorithms, then presents the different sets of forecast contrail bases each produced using various RH profiles. A series of scatterplots, numerical summaries, and correlations are then drawn to explore and compare the impacts of different RH profiles on each set of forecast bases. Next, verification measures and inferential tests are conducted to measure the accuracy, bias, and relative difference between each set of forecast bases. After the forecast bases are analyzed, tests are conducted to observe the combined affect of RH and lapse rate on a forecast base. Each case is analyzed for its lapse rate, general relationships are drawn, and uncertainty in forecast bases due to RH and lapse rate are described. Finally, a summary of the results highlights key findings.

4.2 Contrail Curve Comparison

Two types of contrail curve comparisons were performed in this section: a comparison between the AFGWC and Saatzer algorithm curves and an initial comparison

of the output from the RH Profile Program to values attained by Schrader (1994) for the AFGWC algorithm.

First, a comparison was drawn between the AFGWC and Saatzer curves, shown in Fig. 14. No differences of more than 0.7°C are observed between any two curves for RH values of 0%, 40%, 70%, and 100%. These similarities were expected, since both the General Electric equations forming the Saatzer algorithm and the AFGWC algorithm are based on the Appleman theory (Schrader, 1994; Saatzer, 1995). As a result, both algorithms produce similar forecast bases throughout the results.

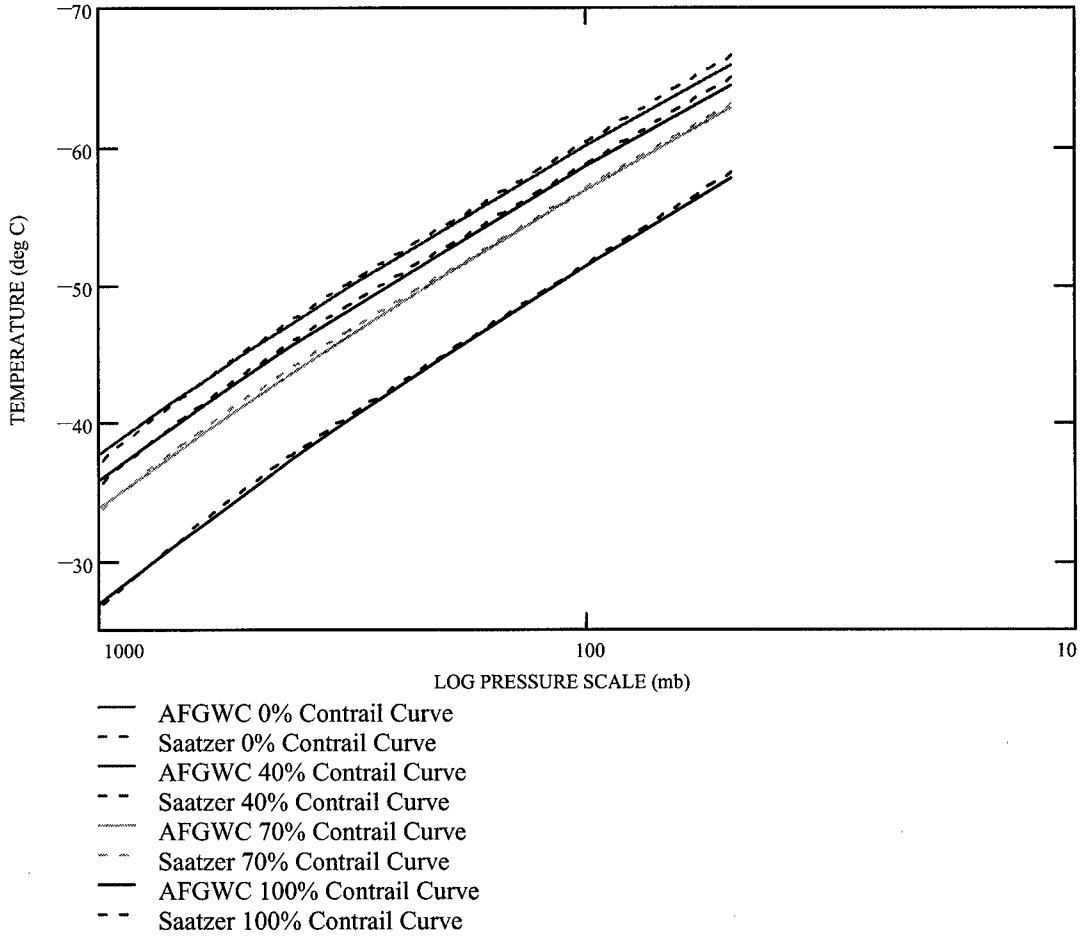

FIG 14: Comparison of AFGWC and Saatzer Contrail Curves

Next, the critical temperatures of the RH Profile Program are compared to those published by Schrader (1994). Overall, Table 3b demonstrates general agreement between the two methods. Differences less than 1.2°C were noted at 70% RH. These differences were attributed to different tolerance limits used by the RH Profile program and Schrader in the solution of Eq. 9. As the function approaches high RH values (Fig. 11), its slope near the root becomes much smaller, and thus is influenced more and more by tolerance selection. A difference in critical temperature on the order of 1-2°C can be attributed to differences in tolerances of 10^{-5}.

Table 3b: Critical Temperature Difference between Program and Schrader Values

Pressure (mb)		Critical Temperature Differences (degrees Celsius)				
		RH=0	RH=10	RH=40	RH=70	RH=100
50		0.001	0.005	0.178	0.867	-0.068
100		0.004	-0.002	0.194	0.93	-0.068
200		0.002	-0.002	0.204	0.997	-0.069
300		0.004	0.003	0.22	1.038	-0.079
400		-0.004	-0.004	0.22	1.064	-0.076
500		-0.002	-0.003	0.231	1.091	-0.079
600		0.002	-0.002	0.237	1.115	-0.077
700		-0.004	-0.002	0.24	1.131	-0.08
800		-0.003	0.005	0.236	1.146	-0.076
1000		0.002	-0.001	0.244	1.175	-0.077

4.3 Forecast Bases and Error Tables

All the forecast base data are shown in Tables 4a and 4b. These tables present the forecasted contrail bases for each of the 42 cases, grouped by RH profile, and listed by date and data set. Tables 5a and 5b then present a direct measure of forecast error by subtracting the reported base from the forecast base for each case. They also show the forecasted bases using profile 1A were always low, while 1B was always too high. Other profiles generated mostly high bases and similar forecast errors between profiles are observed for many of the cases.

TABLE 4a: AFGWC FORECASTS AND REPORTED CONTRAIL BASE TABLE								
	Profile 1A	Profile 1B	Profile 2A	Profile 2B	Profile 2C	Profile 3	Profile 4	Reported BASES
Success								
16-Apr	28.01	32.22	31.22	30.68	31.45	31.66	32.01	32.00
20-Apr	26.03	30.28	29.35	29.05	29.60	29.75	30.10	27.00
26-Apr	30.57	35.20	34.37	34.19	34.75	34.49	34.96	35.00
4-May	29.60	34.12	33.55	33.37	33.80	33.45	33.91	34.00
Wright Patterson								
2-Oct	29.88	35.69	35.56	35.49	35.56	34.52	35.10	34.00
3-Oct	29.61	33.96	33.82	33.82	33.90	33.24	33.53	34.00
4-Oct	29.88	34.27	33.57	33.33	33.71	33.45	33.80	32.00
5-Oct	29.73	34.62	34.04	33.95	34.16	33.85	34.04	34.00
7-Oct	29.99	35.91	35.69	35.69	35.76	34.47	34.89	36.00
11-Oct	29.11	34.05	32.91	32.84	33.52	32.76	32.91	32.00
16-Oct	29.14	33.46	33.11	33.02	33.11	31.91	32.93	32.00
17-Oct	30.32	36.39	34.35	34.35	36.24	33.99	34.22	34.00
Northrop								
3-Sep	34.13	38.64	37.27	37.27	37.27	37.27	37.27	35.84
9-Sep	33.54	39.27	38.64	38.27	38.64	38.27	39.27	37.06
1-Oct	34.13	41.26	38.64	38.64	40.26	38.64	40.26	38.84
6-Oct	32.66	41.38	40.38	40.38	40.38	40.38	40.38	35.51
8-Oct	32.78	36.58	35.73	35.73	35.73	35.73	36.58	33.98
13-Oct	33.73	38.64	38.46	38.46	38.46	38.46	38.46	37.31
15-Oct	33.61	37.40	36.40	36.40	36.40	36.40	37.40	35.23
29-Oct	33.25	38.02	37.02	37.02	37.02	37.02	37.02	34.78
2-Nov	33.77	37.54	36.55	36.55	37.54	37.54	37.54	35.76
6-Nov	33.71	37.51	36.51	36.51	36.51	36.51	36.51	36.21
9-Nov	30.21	33.62	32.61	32.61	33.21	33.21	33.21	32.76
20-Nov	31.45	36.25	35.40	35.40	36.25	35.40	35.40	34.06
23-Nov	31.75	37.52	36.52	36.52	37.52	36.52	36.52	35.73
1-Dec	32.73	38.46	38.46	38.46	38.46	37.46	38.46	35.81
10-Dec	31.23	35.20	35.20	35.20	35.20	34.21	35.20	33.26
15-Dec	30.74	47.43	46.41	46.41	46.41	37.47	46.41	34.21
5-Jan	29.86	34.13	33.75	33.75	33.75	33.75	33.75	31.31
12-Jan	29.81	33.83	33.83	32.82	33.83	32.82	33.83	31.76
19-Jan	28.34	32.66	32.38	32.38	32.66	32.38	32.38	30.43
21-Jan	29.31	34.13	33.31	33.31	33.31	33.31	34.13	33.06
26-Jan	29.47	34.50	32.49	32.49	33.49	33.49	33.49	31.09
28-Jan	28.71	33.75	32.74	32.74	32.74	32.74	32.74	30.54
4-Feb	32.24	42.93	41.92	41.42	41.92	42.93	42.93	34.49
11-Feb	28.84	32.90	31.88	31.88	32.90	31.88	31.88	30.93
16-Feb	28.09	33.13	32.12	32.12	33.13	33.13	33.13	31.04
24-Feb	26.67	53.52	53.33	46.86	53.33	53.52	53.52	30.39
25-Feb	28.32	32.39	31.37	31.37	31.37	31.37	32.39	29.34
26-Feb	25.39	30.53	29.49	29.49	30.21	29.49	30.21	29.84
2-Mar	30.21	45.18	44.17	44.17	44.62	33.49	44.62	33.56
4-Mar	28.60	32.26	31.65	31.65	31.65	31.65	31.65	31.23

TABLE 4b: SAATZER FORECASTS AND REPORTED CONTRAIL BASE TABLE								
	Profile 1A	Profile 1B	Profile 2A	Profile 2B	Profile 2C	Profile 3	Profile 4	Reported BASES
Success								
16-Apr	28.20	32.34	31.42	30.88	31.66	31.86	32.11	32.00
20-Apr	26.13	30.51	29.50	29.21	29.79	29.90	30.20	27.00
26-Apr	30.76	35.39	34.66	34.37	34.90	34.76	35.10	35.00
4-May	29.73	34.36	33.80	33.55	33.94	33.72	34.01	34.00
Wright Patterson								
2-Oct	30.00	35.87	35.69	35.69	35.69	34.84	35.36	34.00
3-Oct	29.73	34.19	33.96	33.96	33.96	33.46	33.67	34.00
4-Oct	29.99	34.51	33.71	33.57	33.91	33.71	33.91	32.00
5-Oct	29.73	34.73	34.16	34.16	34.28	33.95	34.16	34.00
7-Oct	30.14	36.13	35.91	35.76	35.98	34.68	35.62	36.00
11-Oct	29.27	34.28	33.60	32.98	33.83	32.84	33.52	32.00
16-Oct	29.29	33.54	33.21	33.11	33.29	32.04	33.11	32.00
17-Oct	30.55	36.47	36.31	36.31	36.39	33.99	34.22	34.00
Northrop								
3-Sep	34.13	38.64	37.27	37.27	37.27	37.27	37.27	35.84
9-Sep	33.54	39.27	38.64	38.27	38.64	38.27	38.64	37.06
1-Oct	34.13	41.26	38.64	38.27	39.27	38.27	40.26	38.84
6-Oct	32.66	41.38	40.38	39.38	40.38	39.38	40.38	35.51
8-Oct	32.78	36.58	35.73	35.73	35.73	35.73	36.58	33.98
13-Oct	33.73	38.64	38.46	38.46	38.46	38.46	38.46	37.31
15-Oct	33.61	37.40	36.40	36.40	36.40	36.40	36.40	35.23
29-Oct	33.25	38.02	37.02	37.02	37.02	37.02	37.02	34.78
2-Nov	33.77	37.54	36.55	36.55	36.55	36.55	37.54	35.76
6-Nov	33.71	37.51	36.51	36.51	36.51	36.51	36.51	36.21
9-Nov	30.21	33.62	32.61	32.61	33.21	33.21	33.21	32.76
20-Nov	31.45	36.25	35.40	35.40	35.40	35.40	35.40	34.06
23-Nov	31.75	37.52	36.52	36.52	36.52	36.52	36.52	35.73
1-Dec	32.73	38.46	38.46	37.46	38.46	37.46	38.46	35.81
10-Dec	31.23	35.20	35.20	34.21	35.20	34.21	35.20	33.26
15-Dec	30.74	47.43	46.41	37.73	46.41	37.47	46.41	34.21
5-Jan	29.86	34.13	33.75	33.75	33.75	33.75	33.75	31.31
12-Jan	29.81	33.83	33.83	32.82	33.83	32.82	33.83	31.76
19-Jan	28.34	32.66	32.38	32.38	32.38	32.38	32.38	30.43
21-Jan	29.31	34.13	33.31	33.31	33.31	33.31	34.13	33.06
26-Jan	29.47	34.50	32.49	32.49	33.49	33.49	33.49	31.09
28-Jan	28.71	33.75	32.74	32.74	32.74	32.74	32.74	30.54
4-Feb	32.24	42.93	41.42	41.42	41.92	42.93	41.92	34.49
11-Feb	28.84	32.90	31.88	31.88	31.88	31.88	31.88	30.93
16-Feb	28.09	33.13	32.12	32.12	33.13	32.12	33.13	31.04
24-Feb	26.67	53.52	46.86	46.86	53.33	53.52	53.52	30.39
25-Feb	28.32	32.39	31.37	31.37	31.37	31.37	32.39	29.34
26-Feb	25.39	30.53	29.49	29.49	30.21	29.49	30.21	29.84
2-Mar	30.21	45.18	44.17	44.17	44.17	33.49	44.62	33.56
4-Mar	28.60	32.26	31.65	31.65	31.65	31.65	31.65	31.23
NOTE: All forecast and reported bases are listed in kft								

TABLE 5a: AFGWC FORECAST BASE ERRORS: Forecast Bases - Reported Bases								
Case #		Profile 1A	Profile 1B	Profile 2A	Profile 2B	Profile 2C	Profile 3	Profile 4
	Success							
1	16-Apr	-3.99	0.22	-0.78	-1.32	-0.55	-0.34	0.01
2	20-Apr	-0.97	3.28	2.35	2.05	2.60	2.75	3.10
3	26-Apr	-4.43	0.20	-0.63	-0.81	-0.25	-0.51	-0.04
4	4-May	-4.40	0.12	-0.45	-0.63	-0.20	-0.55	-0.09
	Wright Patterson							
5	2-Oct	-4.12	1.69	1.56	1.49	1.56	0.52	1.10
6	3-Oct	-4.39	0.04	-0.18	-0.18	-0.10	-0.76	-0.47
7	4-Oct	-2.12	2.27	1.57	1.33	1.71	1.45	1.80
8	5-Oct	-4.27	0.62	0.04	-0.05	0.16	-0.15	0.04
9	7-Oct	-6.01	0.09	-0.31	-0.31	-0.24	-1.53	-1.11
10	11-Oct	-2.89	2.05	0.91	0.84	1.52	0.76	0.91
11	16-Oct	-2.86	1.46	1.11	1.02	1.11	-0.09	0.93
12	17-Oct	-3.68	2.39	0.35	0.35	2.24	-0.01	0.22
	Northrop							
13	3-Sep	-1.71	2.80	1.43	1.43	1.43	1.43	1.43
14	9-Sep	-3.52	2.21	1.58	1.21	1.58	1.21	2.21
15	1-Oct	-4.71	2.42	-0.20	-0.20	1.42	-0.20	1.42
16	6-Oct	-2.85	5.87	4.87	4.87	4.87	4.87	4.87
17	8-Oct	-1.20	2.60	1.75	1.75	1.75	1.75	2.60
18	13-Oct	-3.58	1.33	1.15	1.15	1.15	1.15	1.15
19	15-Oct	-1.62	2.17	1.17	1.17	1.17	1.17	2.17
20	29-Oct	-1.53	3.24	2.24	2.24	2.24	2.24	2.24
21	2-Nov	-1.99	1.78	0.79	0.79	1.78	1.78	1.78
22	6-Nov	-2.50	1.30	0.30	0.30	0.30	0.30	0.30
23	9-Nov	-2.55	0.86	-0.15	-0.15	0.45	0.45	0.45
24	20-Nov	-2.61	2.19	1.34	1.34	2.19	1.34	1.34
25	23-Nov	-3.98	1.79	0.79	0.79	1.79	0.79	0.79
26	1-Dec	-3.08	2.65	2.65	2.65	2.65	1.65	2.65
27	10-Dec	-2.03	1.94	1.94	1.94	1.94	0.95	1.94
28	15-Dec	-3.47	13.22	12.20	12.20	12.20	3.26	12.20
29	5-Jan	-1.45	2.82	2.44	2.44	2.44	2.44	2.44
30	12-Jan	-1.95	2.07	2.07	1.06	2.07	1.06	2.07
31	19-Jan	-2.09	2.23	1.95	1.95	2.23	1.95	1.95
32	21-Jan	-3.75	1.07	0.25	0.25	0.25	0.25	1.07
33	26-Jan	-1.62	3.41	1.40	1.40	2.40	2.40	2.40
34	28-Jan	-1.83	3.21	2.20	2.20	2.20	2.20	2.20
35	4-Feb	-2.25	8.44	7.43	6.93	7.43	8.44	8.44
36	11-Feb	-2.09	1.97	0.95	0.95	1.97	0.95	0.95
37	16-Feb	-2.95	2.09	1.08	1.08	2.09	2.09	2.09
38	24-Feb	-3.72	23.13	22.94	16.47	22.94	23.13	23.13
39	25-Feb	-1.02	3.05	2.03	2.03	2.03	2.03	3.05
40	26-Feb	-4.45	0.69	-0.35	-0.35	0.37	-0.35	0.37
41	2-Mar	-3.35	11.62	10.61	10.61	11.06	-0.07	11.06
42	4-Mar	-2.63	1.03	0.42	0.42	0.42	0.42	0.42
NOTE: All differences are in kft. Negative values indicate forecast base is below reported base								

TABLE 5b: SAATZER FORECAST BASE ERRORS: Forecast Bases - Reported Bases								
Case #		Profile 1A	Profile 1B	Profile 2A	Profile 2B	Profile 2C	Profile 3	Profile 4
	Success							
1	16-Apr	-3.80	0.34	-0.58	-1.12	-0.34	-0.14	0.11
2	20-Apr	-0.87	3.51	2.50	2.21	2.79	2.90	3.20
3	26-Apr	-4.24	0.39	-0.34	-0.63	-0.10	-0.24	0.10
4	4-May	-4.27	0.36	-0.20	-0.45	-0.06	-0.28	0.01
	Wright Patterson							
5	2-Oct	-4.00	1.87	1.69	1.69	1.69	0.84	1.36
6	3-Oct	-4.27	0.19	0.16	-0.04	-0.04	-0.54	-0.33
7	4-Oct	-2.01	2.51	1.71	1.57	1.91	1.71	1.91
8	5-Oct	-4.27	0.73	0.16	0.16	0.28	-0.05	0.16
9	7-Oct	-5.86	0.13	-0.09	-0.24	-0.02	-1.32	-0.38
10	11-Oct	-2.73	2.28	1.60	0.98	1.83	0.84	1.52
11	16-Oct	-2.71	1.54	1.21	1.11	1.29	0.04	1.11
12	17-Oct	-3.45	2.47	2.31	2.31	2.39	-0.01	0.22
	Northrop							
13	3-Sep	-1.71	2.80	1.43	1.43	1.43	1.43	1.43
14	9-Sep	-3.52	2.21	1.58	1.21	1.58	1.21	1.58
15	1-Oct	-4.71	2.42	-0.20	-0.57	0.43	-0.57	1.42
16	6-Oct	-2.85	5.87	4.87	3.87	4.87	3.87	4.87
17	8-Oct	-1.20	2.60	1.75	1.75	1.75	1.75	2.60
18	13-Oct	-3.58	1.33	1.15	1.15	1.15	1.15	1.15
19	15-Oct	-1.62	2.17	1.17	1.17	1.17	1.17	1.17
20	29-Oct	-1.53	3.24	2.24	2.24	2.24	2.24	2.24
21	2-Nov	-1.99	1.78	0.79	0.79	0.79	0.79	1.78
22	6-Nov	-2.50	1.30	0.30	0.30	0.30	0.30	0.30
23	9-Nov	-2.55	0.86	-0.15	-0.15	0.45	0.45	0.45
24	20-Nov	-2.61	2.19	1.34	1.34	1.34	1.34	1.34
25	23-Nov	-3.98	1.79	0.79	0.79	0.79	0.79	0.79
26	1-Dec	-3.08	2.65	2.65	1.65	2.65	1.65	2.65
27	10-Dec	-2.03	1.94	1.94	0.95	1.94	0.95	1.94
28	15-Dec	-3.47	13.22	12.20	3.52	12.20	3.26	12.20
29	5-Jan	-1.45	2.82	2.44	2.44	2.44	2.44	2.44
30	12-Jan	-1.95	2.07	2.07	1.06	2.07	1.06	2.07
31	19-Jan	-2.09	2.23	1.95	1.95	1.95	1.95	1.95
32	21-Jan	-3.75	1.07	0.25	0.25	0.25	0.25	1.07
33	26-Jan	-1.62	3.41	1.40	1.40	2.40	2.40	2.40
34	28-Jan	-1.83	3.21	2.20	2.20	2.20	2.20	2.20
35	4-Feb	-2.25	8.44	6.93	6.93	7.43	8.44	7.43
36	11-Feb	-2.09	1.97	0.95	0.95	0.95	0.95	0.95
37	16-Feb	-2.95	2.09	1.08	1.08	2.09	1.08	2.09
38	24-Feb	-3.72	23.13	16.47	16.47	22.94	23.13	23.13
39	25-Feb	-1.02	3.05	2.03	2.03	2.03	2.03	3.05
40	26-Feb	-4.45	0.69	-0.35	-0.35	0.37	-0.35	0.37
41	2-Mar	-3.35	11.62	10.61	10.61	10.61	-0.07	11.06
42	4-Mar	-2.63	1.03	0.42	0.42	0.42	0.42	0.42
NOTE: All differences are in kft. Negative values indicate forecast base is below reported base								

4.4 Exploratory Data Analysis

The exploratory data analysis was accomplished to gain insight into the natural processes underlying the generation of each set of forecast bases (Wilks, 1995). To compress and summarize the forecast bases shown in Tables 4 and 5, two graphical methods and numerical summaries were computed. The graphical methods included scatterplots and box-and whisker plots, while the summaries computed included forecast base means, variances, and ranges. Lastly, each set of forecast bases was correlated to the set of reported bases.

4.4.1 Scatterplots. There are four series of scatterplots, which compare forecast bases generated from profiles: 2A, 3 and 4; 2A, 2B and 2C; 1A, 1B and reported bases; and all seven sets of bases from each profile.

(1) Figures 15a and 15b show little difference between the sets of forecast bases generated by profiles 2A, 3, and 4. In all but four of the cases, little more than 1 000 ft separated each set of forecast bases. These similarities were surprising, since profile 3's RH values were generally 40% or 70% at typical contrail altitudes while profile 4 varied from 5% - 25%. Neither deviated significantly from the control group of bases generated by profile 2A. Both the AFGWC and Saatzer algorithms produced similar forecasts.

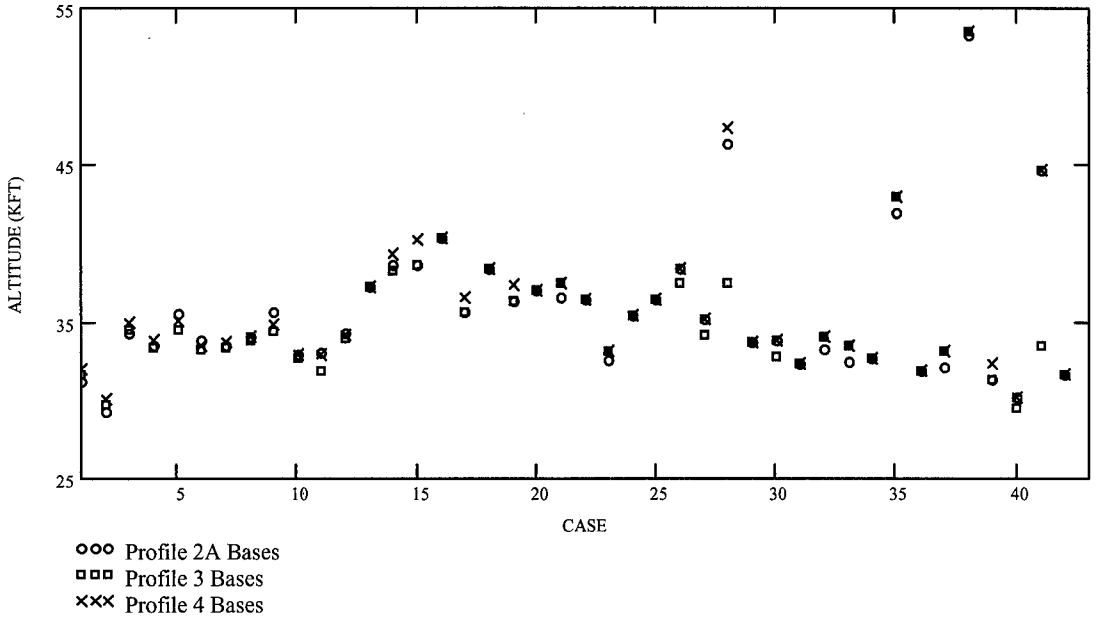

FIG. 15A: Comparison of AFGWC Algorithm Bases Generated By Profiles 2A, 3, and 4.

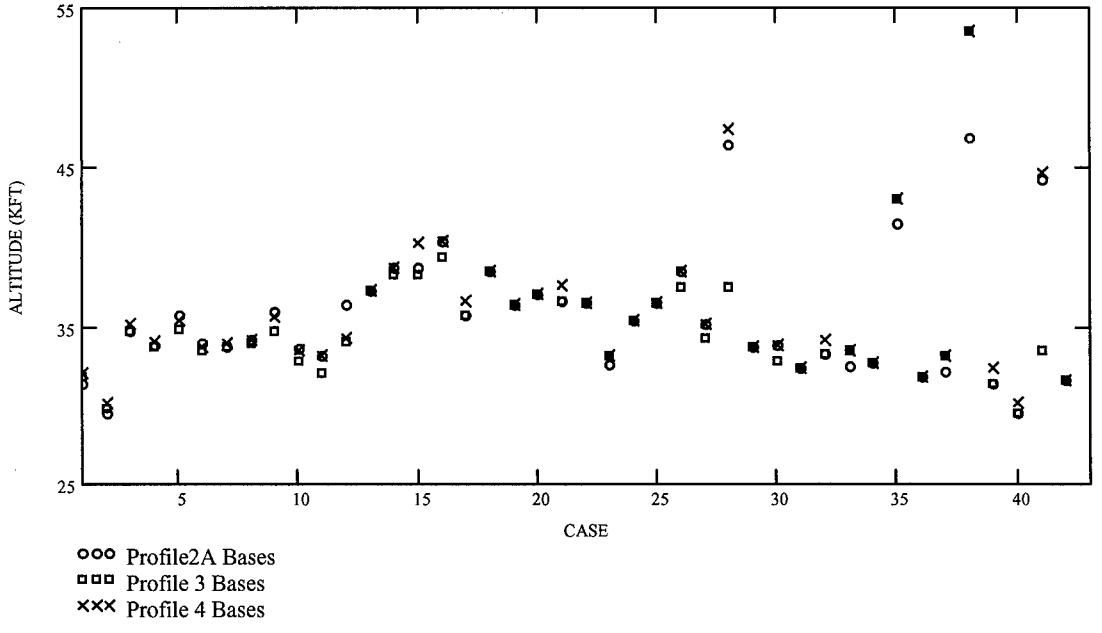

FIG. 15B: Comparison of Saatzer Algorithm Bases Generated By Profiles 2A, 3, and 4.

(2) Figures 16a and 16b demonstrate the impact of a 20% moist and dry bias on the forecast bases. These graphs present a comparison between profiles 2A, 2B, and 2C. Again, the forecast bases are similar to the comparisons drawn in Figs. 15a and 15b for profiles 2A, 3, and 4. Even when comparing the sets of bases generated by profiles 2B and 2C, which differed by an RH of 40%, only a four cases show a difference of more than 1,000 ft in forecast bases.

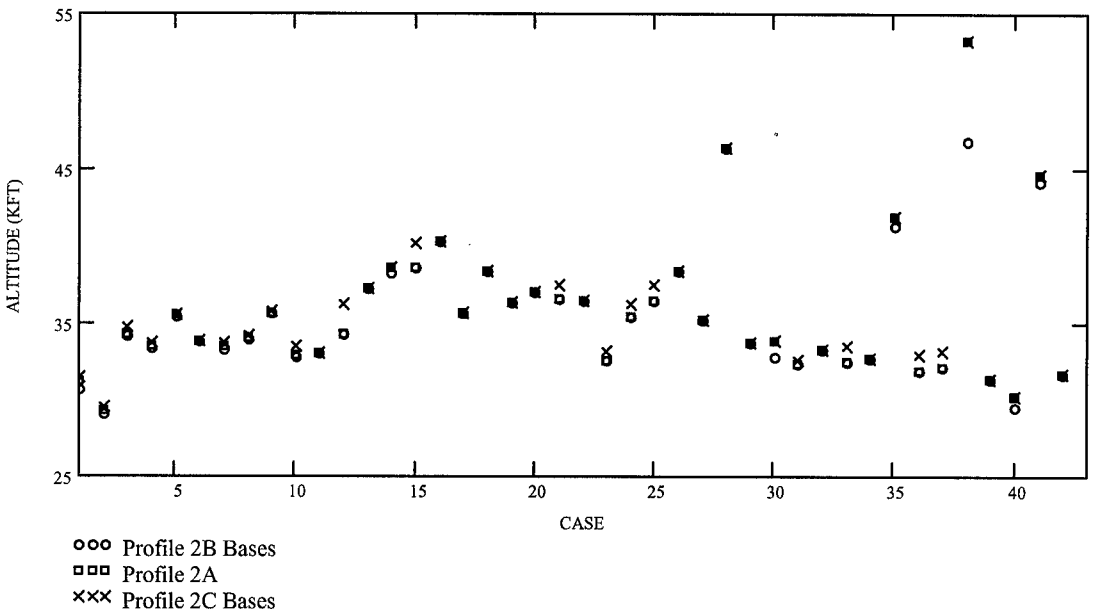

FIG. 16A:Comparison of AFGWC Algorithm Bases Generated By Profile 2A, 2B, and 2C.

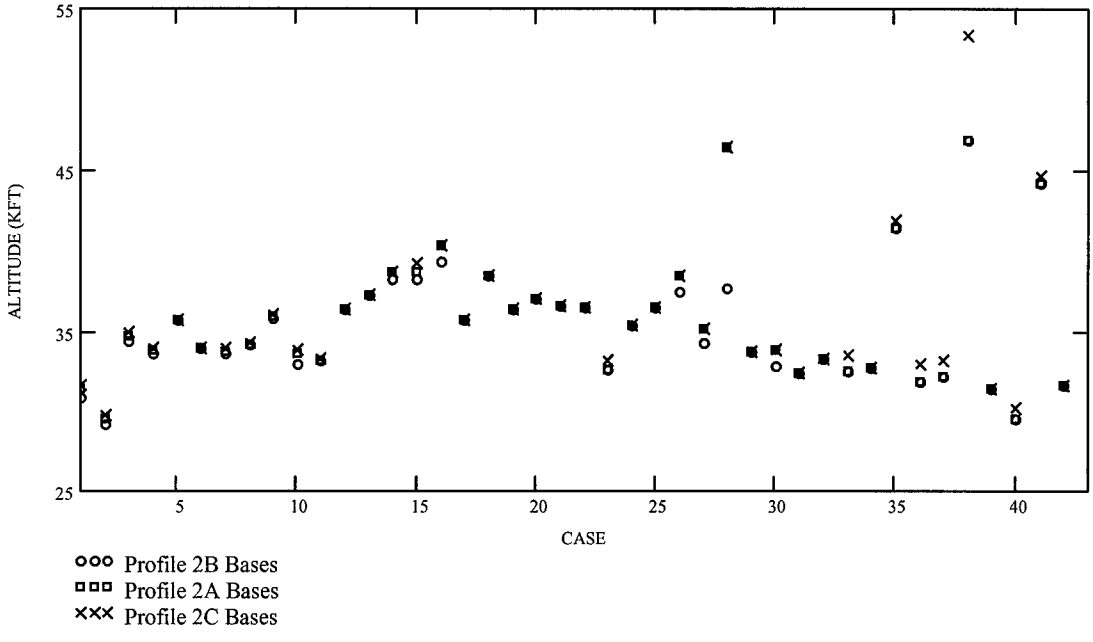

FIG. 16B: Comparison of Saatzer Algorithm Bases Generated By Profile 2A, 2B, and 2C.

(3) Figures 17a and 17b compared the bases generated by 100% RH (profile 1A) and 0% RH (profile 1B). In addition, the set of reported bases are depicted on the graphs with a solid line. In all 42 cases, the reported base falls between the bases generated by the 0% and 100% RH profile, as would be expected since the atmospheric falls between 0-100%. This set of bases, generated by 100% and 0% RH, shows the greatest possible separation between any two forecast bases for each case. Four of the 42 cases were again unusually far from the main group. These departures are referred to as "outliers". The outliers revealed unusually large separations between forecast bases using profiles 1A and 1B in all four instances.

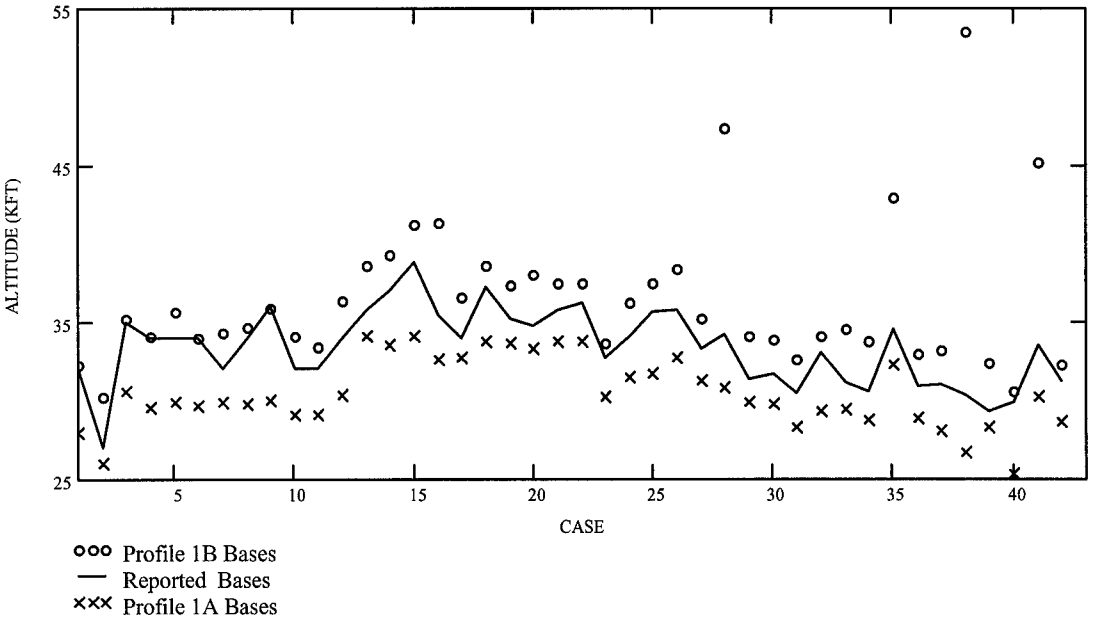

FIG. 17A: AFGWC Algorithm Bases Generated By Profiles 1A and 1B Compared to Reported Bases.

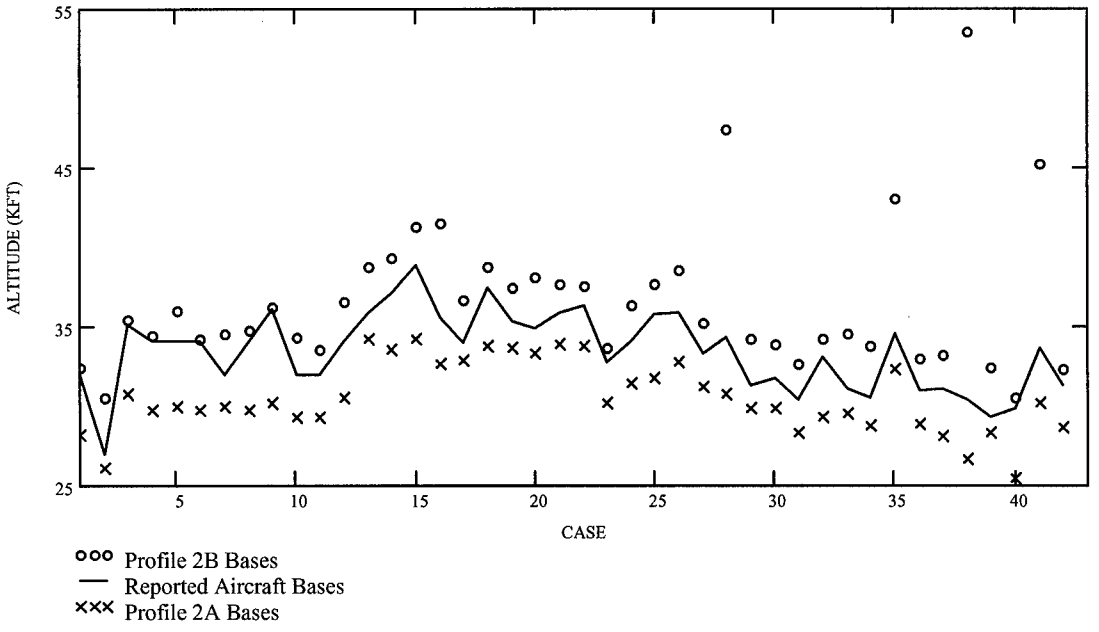

FIG 17B: Saatzer Algorithm Bases Generated By Profiles 1A and 1B Compared to Reported Bases.

(4) Figure 18 shows all seven sets of bases generated by all the profiles. The reported contrail altitudes are shown as a solid line. All the forecast bases, except those generated by profile 1A, appeared tightly grouped for most of the cases. The set of reported contrail bases are typically lower than this grouping, and above the forecast bases of profile 1A which produced the lowest forecast base for each case.

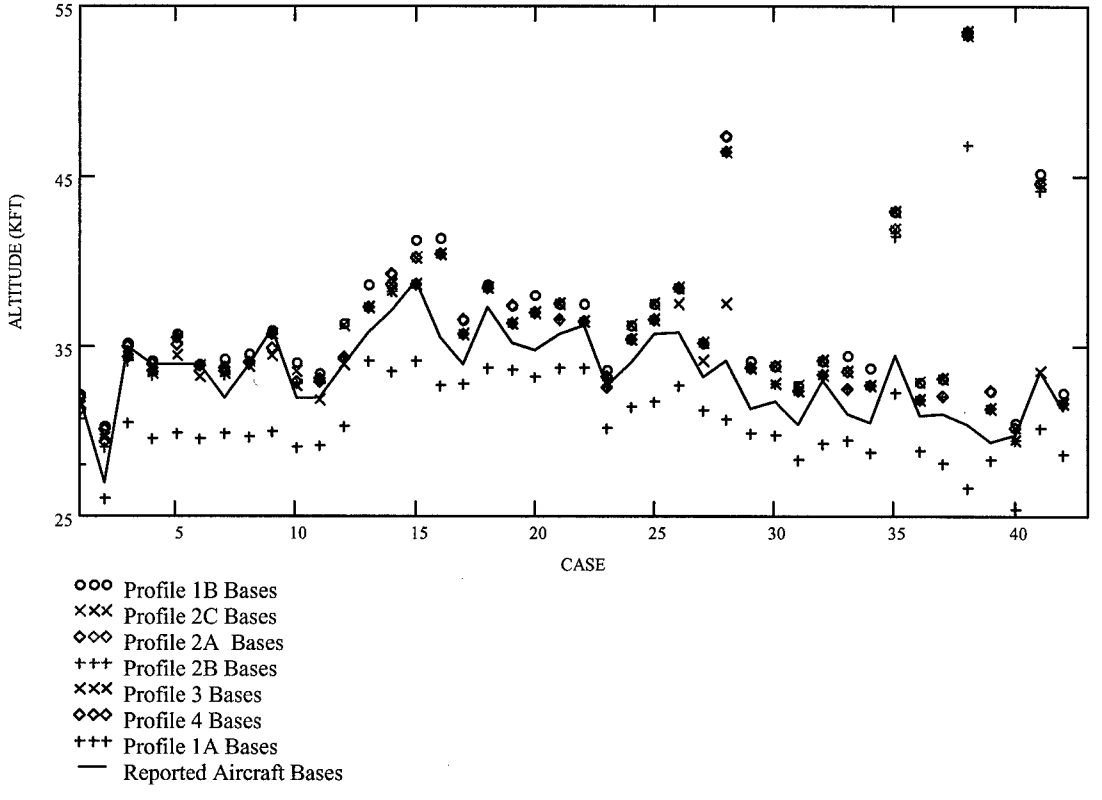

FIG. 18: AFGWC Algorithm Bases Generated By All Seven RH Profiles and Compared to Reported Bases.

4.4.2 Box and Whisker Plots (Boxplots). The box-and-whisker plots grouped each set of forecast bases by the RH profile and algorithm and illustrates their (1) center, (2) spread, (3) extent and nature of any departure from symmetry, and (4) identification of "outliers" or forecast bases that lie unusually far from the main body of forecasts (Devore, 1995; Wilks, 1995). Figure 19 shows a plot for each set of forecast bases and

one for the reported base set. The boxes in the middle are bounded by an upper and lower quartile, locating the central 50% of the forecast bases. The bar inside the box locates the median forecast base. The whiskers extend from the box to the lowest and highest bases, within $1.5*f_S$, where f_S is the fourth spread. The fourth spread is a measure of the individual forecast bases spread from the lower and upper quartiles, similar to a sample standard deviations' measure of observations location from the mean. Forecast bases outside the $1.5*f_S$ range but within $3*f_S$ are mild outliers. The mild outliers are denoted by asterisks on the plots. Those bases outside $3*f_S$ are denoted by open circles and are referred as extreme outliers (Devore, 1995; Wilks, 1995).

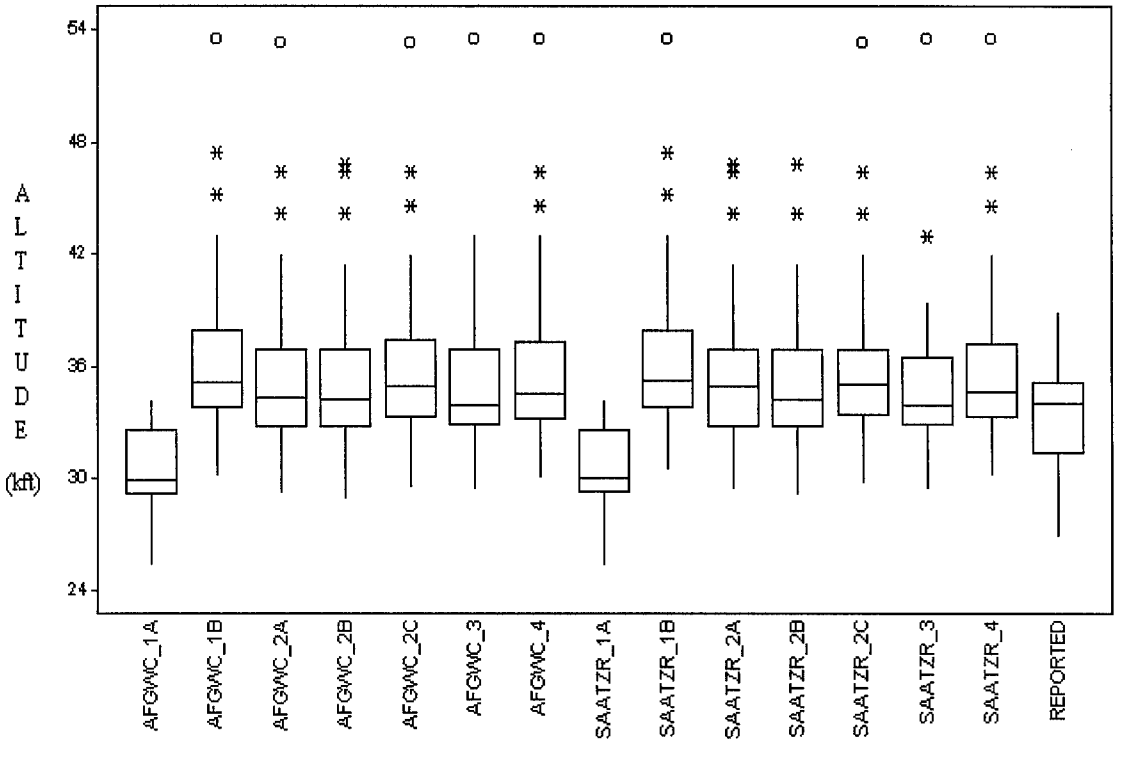

FIG. 19: Box-and-Whisker Plot. There are 14 plots representing sets of forecast bases generated from the seven different RH profiles and two algorithms. The last plot illustrates the set of reported aircraft bases.

Two of the median values are lower than the rest. Both of these were produced by profile 1A and indicate the lowest sample medians, whiskers which disproportionally extend farther down than up, and the absence of any outliers. Therefore, the forecast bases for this profile were positively skewed toward lower altitudes which were centered near 30 kft. Comparing the box plots associated with profiles 3 and 4, both show similar medians and quartiles, with those of profile 4 slightly higher. The plots associated with profile 4 are also more symmetrically centered about the median than those of profile 3, as indicated by their upper and lower quartiles. The reported bases' box plot is negatively skewed toward higher altitudes centered about 34 kft and indicates no outliers.

4.4.3 Numerical Summary. To describe each set of forecast bases average altitudes, variability, and range, Table 6 provides their means, variances, and minimum and maximum altitudes. This table shows profile 1A produced the lowest mean forecast base, near 30 kft, while 1B produced the highest, over 36 kft. Profile 1A also produced the smallest range of forecast bases differing only by less 9 kft. Profile 3, however, caused the largest range of forecast bases, exceeding 24 kft. The means of both profile 3 and 4's bases were very close, only separated by 0.61 kft (610 ft) for the AFGWC algorithm, while the variances of these profile's bases were separated by over 4 kft. When using the AFGWC algorithm, Table 6 shows profiles 1B and 2A produced the highest variances and thus most variation in the forecast bases. Lastly, the table shows the reported bases mean of 33 kft and an average variation of 6 kft.

Table 6: Numerical Summary Table of Forecast Bases. Each set of forecast bases is grouped by algorithm and RH profile used in generating it.

Algorithm	Profile	MEAN	VARIANCE	MINIMUM	MAXIMUM	RANGE
AFGWC	1A	30.46	5.06	25.39	34.13	8.74
	1B	36.45	20.59	30.28	53.52	23.24
	2A	35.62	20.61	29.35	53.33	23.98
	2B	35.38	16.20	29.05	46.86	17.81
	2C	35.95	20.08	29.60	53.33	23.73
	3	35.10	16.28	29.49	53.52	24.03
	4	35.93	20.57	30.10	53.52	23.42
Saatzer	1A	30.50	4.98	25.39	34.13	8.74
	1B	36.50	20.35	30.51	53.52	23.01
	2A	35.56	15.61	29.49	46.86	17.37
	2B	35.19	12.76	29.21	46.86	17.65
	2C	35.86	19.61	29.79	53.33	23.54
	3	35.07	15.83	29.49	53.52	24.03
	4	35.93	19.87	30.20	53.52	23.32
REPORTED BASES		33.37	5.99	27.00	38.84	11.84
	Note: All table values are listed in kft					

4.4.4 Reported Bases Frequency Distribution. The distribution in reported bases is shown in Fig. 20. This diagram illustrates the relative frequency of each reported base and clearly shows a unimodal distribution centered near 34 kft. It also illustrates a set of bases somewhat negatively skewed, agreeing with the boxplot indications in Fig. 19.

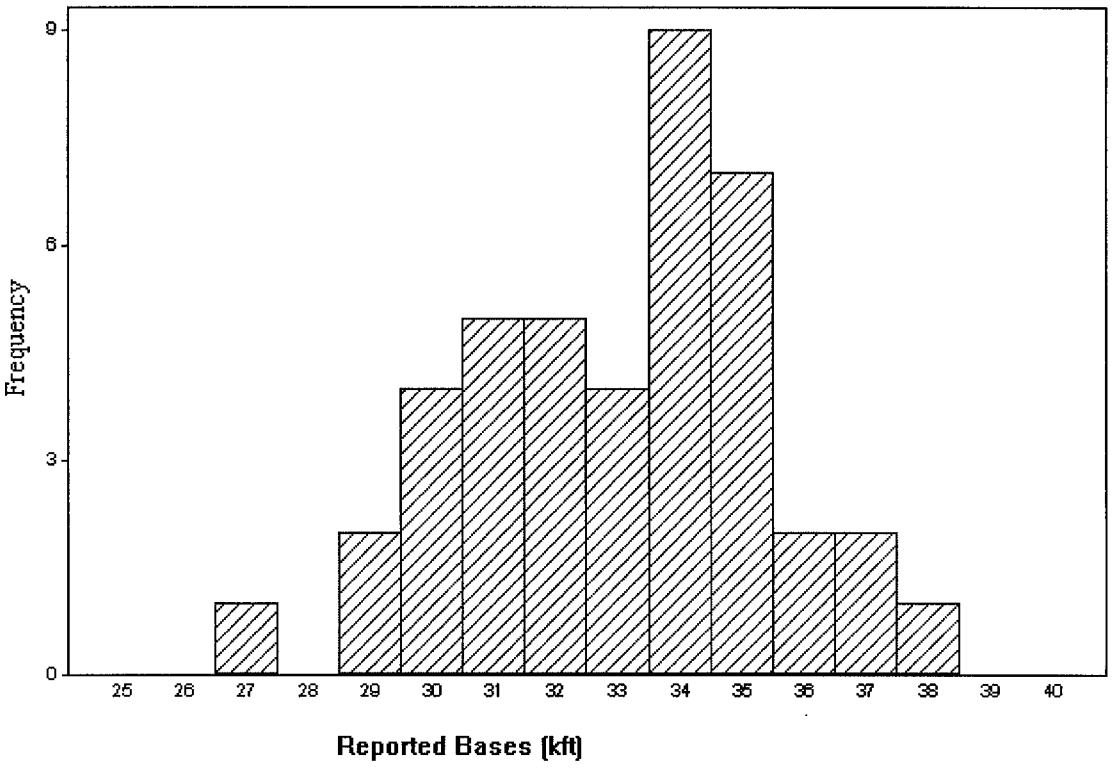

FIG 20: Frequency Histogram of Reported Bases.

4.4.5 Sample Correlation Coefficients. Sample correlation coefficients were calculated between the forecast bases using each RH profile and the reported bases. High correlations, greater than 0.70, indicate a strong joint behavior between the forecast bases and observed bases (Devore, 1995). In other words, the forecast base trends can represent reported base trends. Table 7a, however, shows weak correlation coefficients, below 0.50 (Devore, 1995).

To explain these low correlations, the plotted data in Fig. 18 was reexamined. Since Fig. 18 seemed to indicate high correlations should exist for all the cases except the four outliers, the correlation coefficients were redrawn in Table 7b without the four outliers.

The revised correlations were all above 0.876 which indeed demonstrated high correlations between the forecast bases and reported bases.

Table 7a: Sample Correlation Coefficients using All 42 cases.

RH	Algorithm	
Profile	AFGWC	Saatzer
1A	0.879	0.884
1B	0.418	0.418
2A	0.398	0.511
2B	0.508	0.535
2C	0.415	0.394
3	0.406	0.396
4	0.394	0.39

Table 7b: Sample Correlation Coefficients removing four Outliers

RH	Algorithm	
Profile	AFGWC	Saatzer
1A	0.876	0.882
1B	0.898	0.902
2A	0.902	0.905
2B	0.9	0.915
2C	0.91	0.908
3	0.884	0.9
4	0.893	0.903

4.5 Verification Measures

This section of the results computes forecast verification measures to compare the accuracy and bias of the forecast bases for each RH profile. Before computing accuracy tables and associating bias values for each set of bases, an extensive series of tests were computed to use scalar measures for continuous predictands.

The scalar measures were based on Categorical Forecasts of Continuous Predictands (Wilks, 1995). However, to use Categorical Forecast Techniques, the joint distribution of the forecast bases and reported bases had to be assumed bivariate normal (Wilks, 1995). Since there is no completely satisfactory way to verify this type of distribution, only a partial check was conducted (Devore, 1995). To perform a partial check, separate normal probability plots were constructed for each set of forecast bases and the reported bases.

4.5.1 Normal Probability Plots. Figures 21a through 21k demonstrate a reasonable normality assumption for the joint bivariate distribution, since none of the plots deviate substantially from the straight-line pattern (Devore, 1995). Additionally, the Pearson Correlation Coefficients show high correlations to the ideal normal distributions. Each set of base's had a coefficients above 0.88.

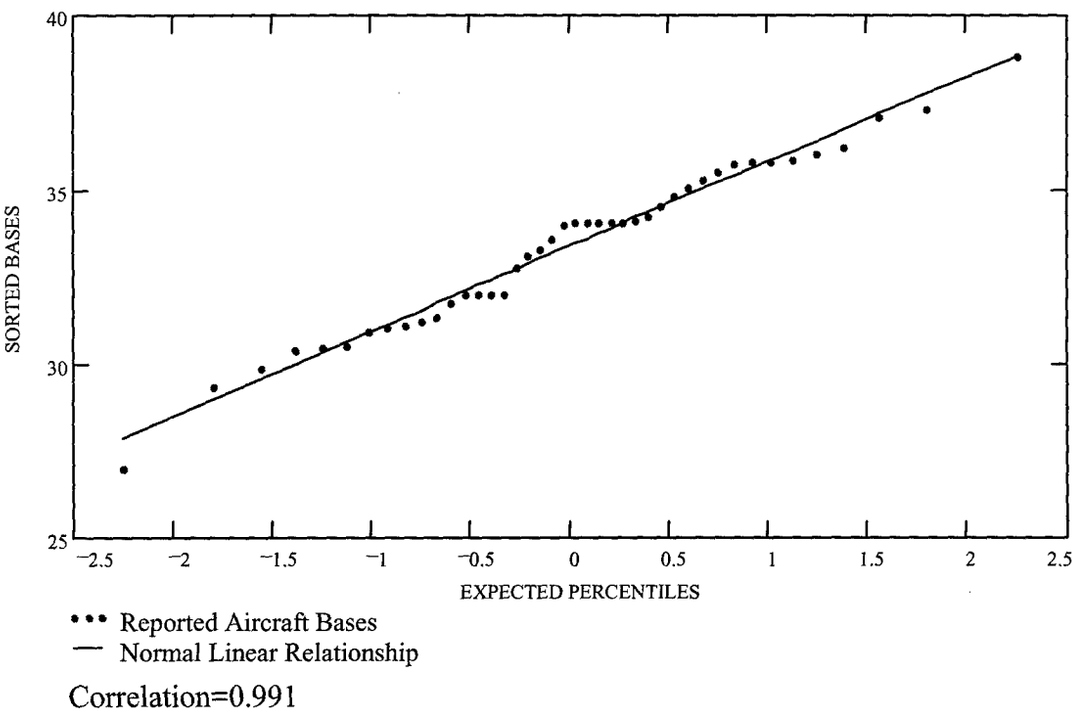

FIG. 21A: Reported Bases Normal Probability Plot.

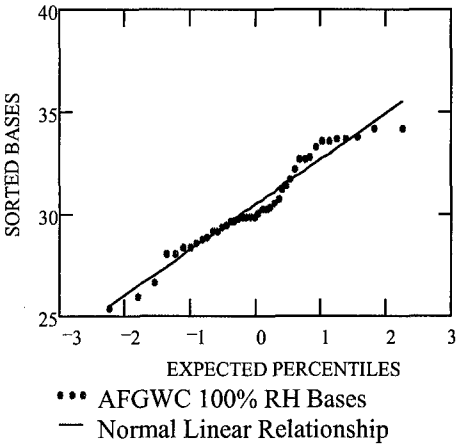

Correlation=0.98

FIG. 21B: Bases of Profile 1A Normal Probability Plot for AFGWC Algorithm.

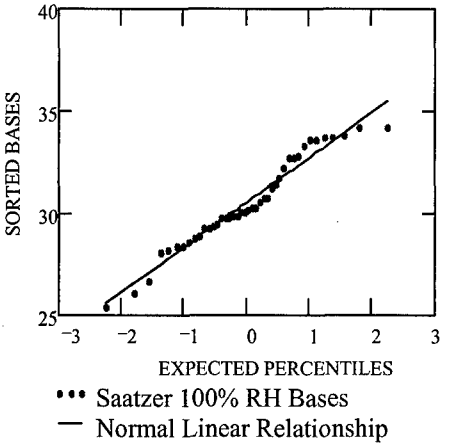

Correlation=0.981

FIG. 21C: Bases of Profile 1A Normal Probability Plot for Saatzer Algorithm.

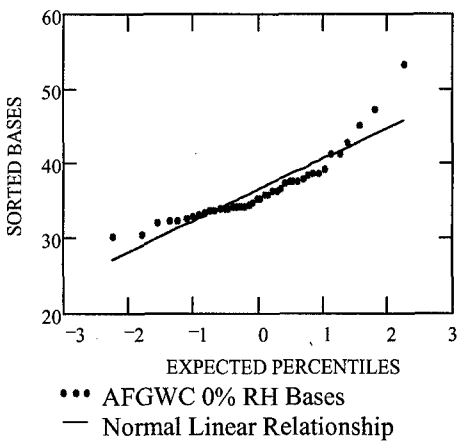

Correlation=0.918

FIG. 21D: Bases of Profile 1B Normal Probability Plot for AFGWC Algorithm.

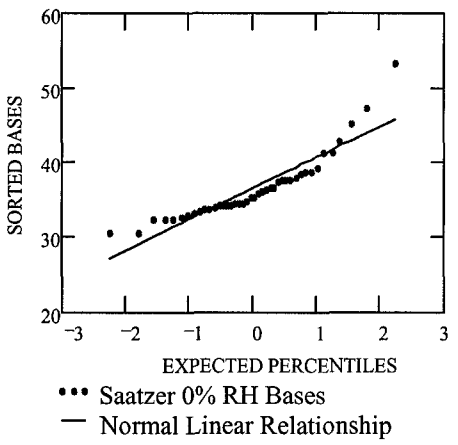

Correlation=0.918

FIG. 21E: Bases of Profile 1B Normal Probability Plot for Saatzer Algorithm.

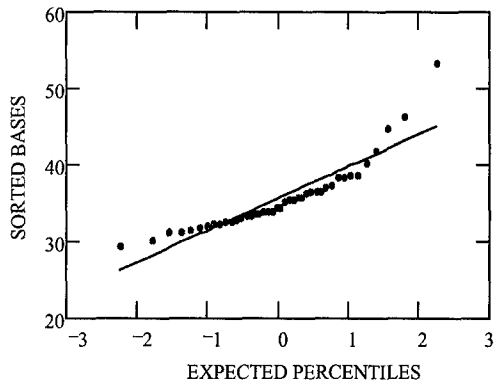

Correlation=0.913

FIG. 21F: Bases of Profile 2A Normal Probability Plot for AFGWC Algorithm.

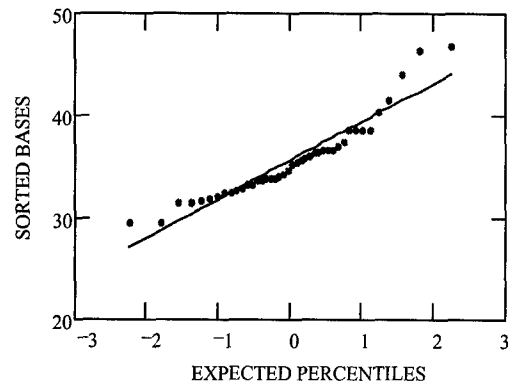

Correlation=0.953

FIG. 21G: Bases of Profile 2A Normal Probability Plot for Saatzer Algorithm.

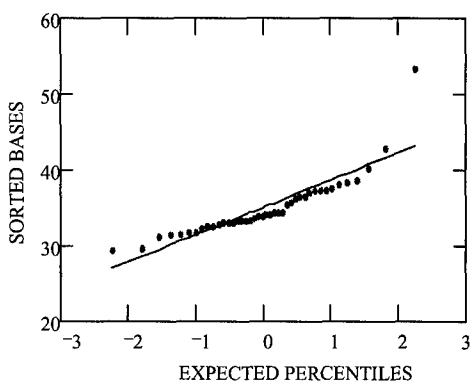

Correlation=0.883

FIG. 21H: Bases of Profile 3 Normal Probability Plot for AFGWC Algorithm.

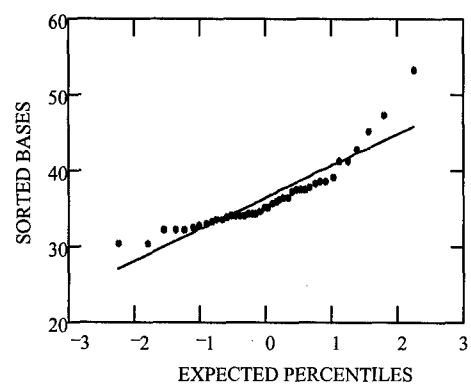

Correlation=0.876

FIG. 21I: Bases of Profile 3 Normal Probability Plot for Saatzer Algorithm.

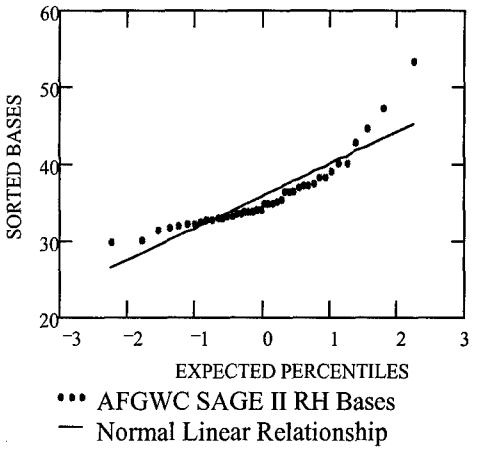

Correlation=0.908

FIG. 21J: Bases of Profile 4 Normal Probability Plot for AFGWC Algorithm.

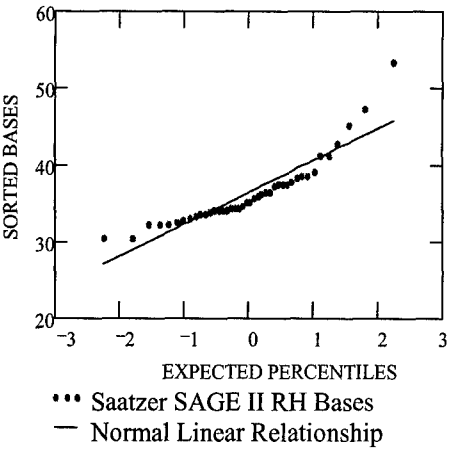

Correlation=0.905

FIG. 21K: Bases of Profile 4 Normal Probability Plot for Saatzer Algorithm.

4.5.2 Accuracy Tables. There were three types of measures used to determine each RH profile's impact on improving forecast base accuracy. They were Mean Absolute Error (MAE), Mean Squared Error (MSE), and Root Mean Squared Error (RMSE). Table 8a, MAE, describes the typical magnitude of error as less than 3 kft for all the forecast base sets. MSE was computed to show which profiles produced large individual forecast base errors, since MSE is more sensitive these type of errors than MAE (Wilks, 1995). Table 8b shows profiles 1B and 4 generated the largest individual forecast base errors and profiles 1A, 2B, and 3 the smallest. This indicated profiles with higher RH values provided smaller individual forecast base errors.

Table 8a: Mean Absolute Error (MAE) Values for each set of forecasted bases.

MAE TABLE (values in kft)		
RH	**Algorithm**	
Profile	**AFGWC**	**Saatzer**
1A	2.91	2.87
1B	3.09	3.12
2A	2.41	2.29
2B	2.21	1.99
2C	2.64	2.56
3	1.97	1.90
4	2.67	2.64

Table 8b: Mean Squared Error (MSE) Values for each set of forecasted bases.

MSE TABLE (values in kft)		
RH	**Algorithm**	
Profile	**AFGWC**	**Saatzer**
1A	9.81	9.52
1B	26.38	26.51
2A	22.55	16.27
2B	15.95	12.49
2C	23.24	23.07
3	16.93	16.66
4	24.49	24.41

Table 8c and Figure 22, RMSE, provides a comparison of relative magnitudes of the errors shown in Table 8b. The values in Table 8c indicate the bases produced by profile 1A are accurate within 3.14 kft while those of profile 1B are within 5.14 kft for the AFGWC algorithm. Table 8c also shows the bases produced by profiles 3 and 4 (AFGWC algorithm) only differ in accuracy by 0.78 kft.

Table 8c: Root Mean Squared Error (RMSE) Values for each set of forecasted bases.

RMSE TABLE (values in kft)		
RH	**Algorithm**	
Profile	**AFGWC**	**Saatzer**
1A	3.13	3.09
1B	5.14	5.15
2A	4.72	4.03
2B	3.99	3.53
2C	4.82	4.77
3	4.11	4.07
4	4.89	4.84

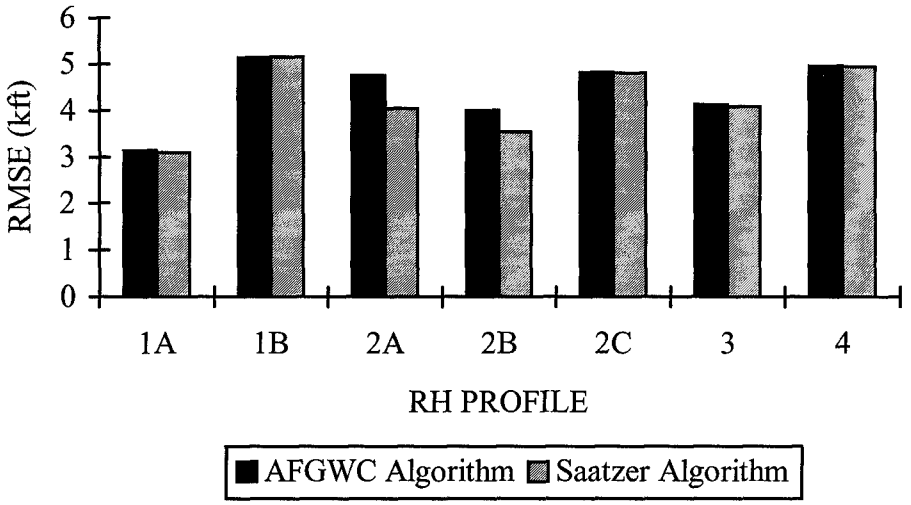

FIG. 22: Root Mean Squared Error (RMSE) Graph for All Sets of Forecast Bases.

4.5.3 Bias Measurements. To assess each profile's forecast bias, the Mean Error (ME) was computed on the seven sets of forecast bases. Table 9 and Fig. 23 show all the profiles produce forecast bases which are too high, except for profile 1A. Profile 3's forecast bases, although too high, has a slightly lower bias of 1.73 kft than does profile's 4 bias of 2.56 kft. Again, the difference between these was less than 1 kft. The bias between forecast bases, of profiles 1A and 1B, varied over 5 kft. This was expected since profile 1A, with RH values of 100%, always produced the lowest forecast bases and 1B, with RH values of 0%, always produced the highest forecast bases.

The ME also showed a bias was produced by profile 2A. Since profile 2A's measurements most accurately approximated RH values encountered by the aircraft, the forecast bases produced by this profile should exhibit little to no bias. However, Table 9

indicates these set of forecast bases were 2.2 kft too high. This implies both the AFGWC and Saatzer algorithms are biased toward forecast bases which are too high.

Table 9: Mean Error (ME) Values for each set of forecasted bases.

ME TABLE (values in kft)		
RH	**Algorithm**	
Profile	**AFGWC**	**Saatzer**
1A	-2.91	-2.87
1B	3.08	3.13
2A	2.26	2.2
2B	2.02	1.82
2C	2.58	2.5
3	1.73	1.7
4	2.56	2.56

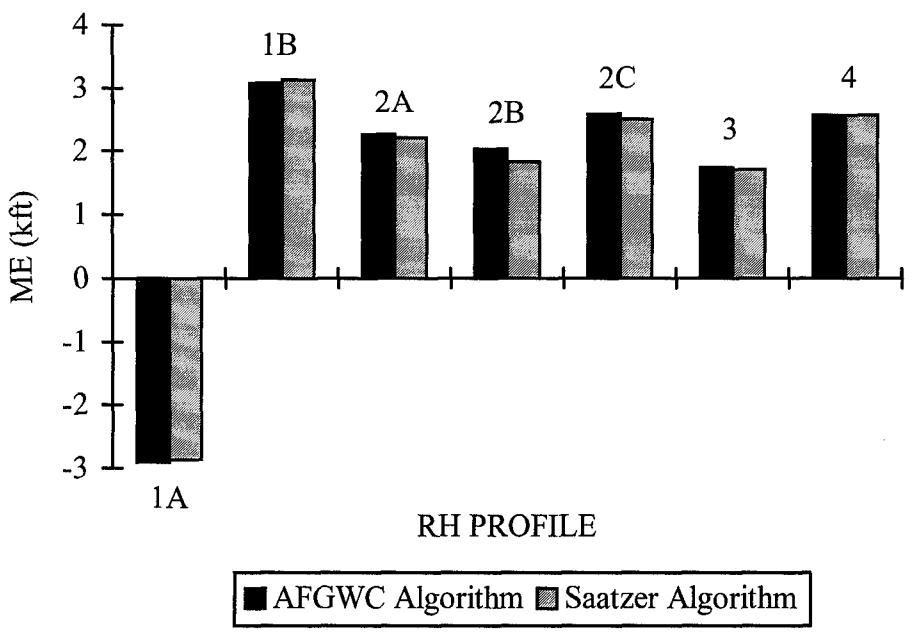

FIG. 23: Mean Error (ME) Graph for All Sets of Forecast Bases.

4.6 Inferential Tests

To further compare the bases produced by each profile, two hypothesis test were conducted, a two-tailed t-test and a randomized block Analysis of Variance (ANOVA). Both tests test whether the true averages between sets of forecast bases were different and assumed the sets were paired and bivariate normally distributed. The bivariate normal distribution was validated in section 4.5.1.

4.6.1 Two-Tailed t-Test. This test indicates the bases produced by the AFGWC's empirical RH profile (profile 3) and the SAGE II's (profile 4) were not statistically different. This is shown on Fig. 24a, by observing the test statistic values for both algorithms, 0.405 kft and 0.976 kft, falls within the critical test bounds of $\pm$ 2.02 kft. Similarly, the bases using profiles 2A and 3 are shown not to be different in Fig. 24b. Appendix D provides a full description of the tests.

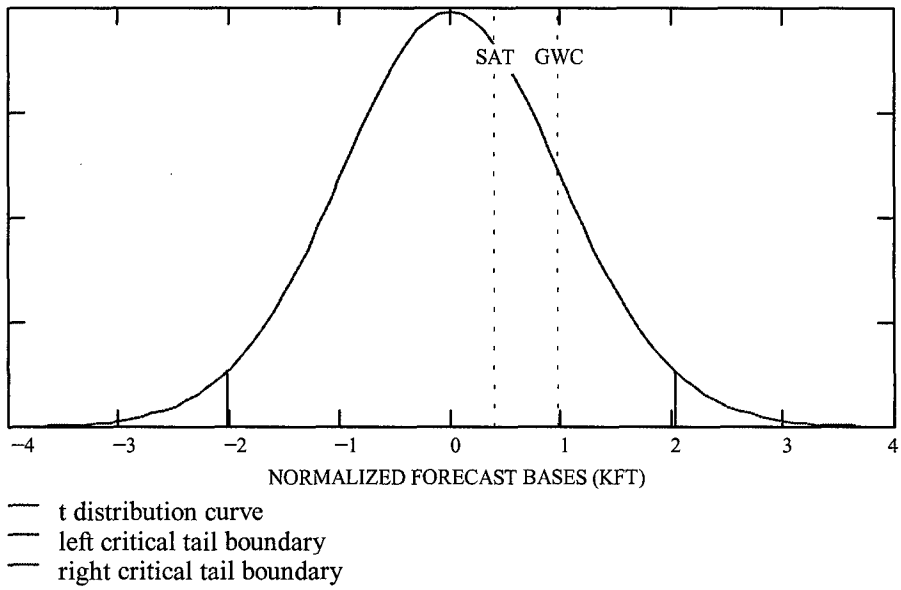

FIG. 24A: t-Test of Forecast Base Means using Profiles 3 and 4. t-Distribution curve for probability density function. "GWC" indicates the t-Test statistic for the AFGWC algorithm and "Sat" the Saatzer algorithm.

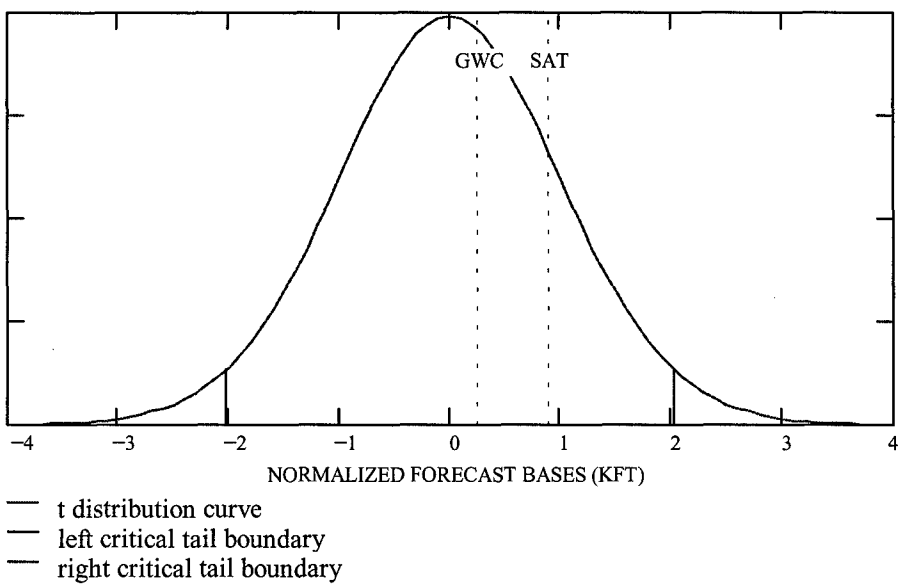

FIG 24B: t-Test of Forecast Base Means using Profiles 2A and 3. t-Distribution curve for probability density function. "GWC" indicates the t-Test statistic for the AFGWC algorithm and "Sat" the Saatzer algorithm.

4.6.2 Randomized Block Analysis of Variance (ANOVA). A randomized block ANOVA test, commonly referred to as a repeated measures exam, was conducted on forecast bases generated by the seven different RH profiles using the AFGWC algorithm. This exam proved which profiles produced statistically different bases. Figure 25 shows the normal distributions of all seven sets of forecast bases. This diagram shows the forecast bases using profile 1A were different from the other six sets of forecast bases.

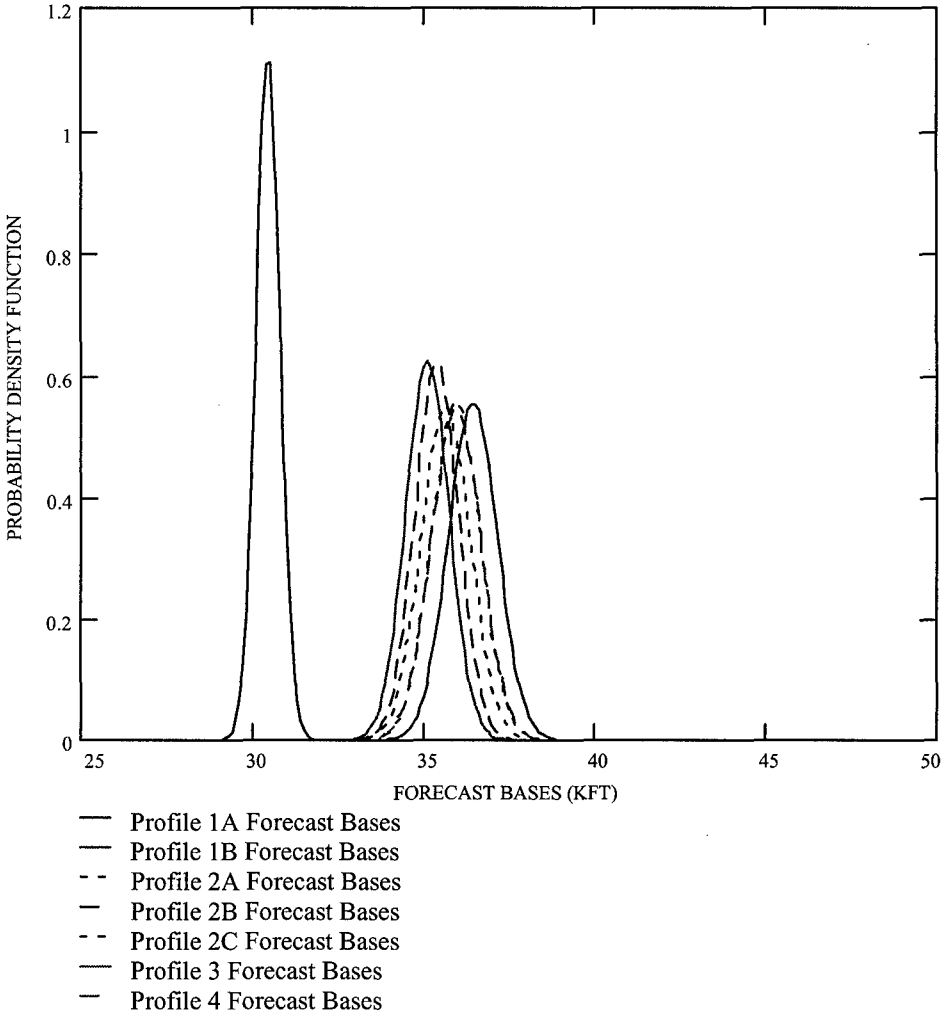

FIG. 25: Normal Distributions for Each Set of Forecast Bases.

The exam verified the bases of profile 1A were statistically different from the others and also indicated the bases of profile 1B were different from the bases produced by profiles 2A and 3. More importantly this test showed the bases of profiles 2A, 2B, 2C, 3, and 4 were *not* statistically different. With a Tukey "w" value of 1.06 kft, profile 1B just fell beyond the range to differ with several sets of bases. Appendix E provides a full description of this test.

4.7 Forecast Base Comparison using Profiles 2A and 3

This section analyses the forecast bases generated by profiles 2A and 3 in cases where both profiles produced different forecasts. Table 10 summarizes the 42 cases by describing which of the two profiles produced more accurate bases and then lists the days from each data set when this occurred.

Table 10: Forecast Base Comparison Using Profiles 2A and 3.

More Accurate Profile	**Cases/Total per Data Set**			
	Wright-Pat	Success	Northrop	Total
Profile 2A	0/8	2/4	5/30	7/42
Profile 3	0/8	2/4	6/30	8/42
Neither Profile More Accurate (both profiles produced the forecast base altitude)	8/8	0/4	19/30	27/42

Days where Profile 2A was more accurate:

Data Set	**Day**
Wright-Pat	None
Success	20 Apr 96; 4 May 96
Northrop	2 and 9 Nov 92; 4, 16, and 24 Feb 93

Days where Profile 3 was more accurate:

Data Set	**Day**
Wright-Pat	None
Success	16 and 26 Apr 96
Northrop	9 Sep 92; 1, 10 and 15 Dec 92; 12 Jan 93; 2 Mar 93

Profile 2A was expected to produce the most accurate results in all cases, since it had the most representative RH values experienced by the aircraft during contrail reports. However, Table 10 shows there were 27 cases where both profiles produced the same forecast and 8 of 42 cases where SAGE RH values (profile 3) produced more accurate bases than the observed RH values (profile 2A).

Table 11 provides an in-depth analysis for these eight cases. Vertical profile extracts from the RH Profile Program are shown in this table describing the altitude, both profiles RH values at that altitude, and the ΔT (critical temperature minus ambient temperature) using each of the RH profiles at that altitude. The first altitude where ΔT became negative, ascending through the profile, was defined as the forecast base.

	TABLE 11: RH PROFILE PROGRAM EXTRACTS for 8 CASES						
	Altitude (kft)	Profile 2A RH (%)	Profile 3 RH (%)		Profile 2A ΔT (deg C)	Profile 3 ΔT (deg C)	Reported Bases (kft)
Success							
16-Apr	31.15	60	40		0.023	1.154	
	31.18	60	40		0.037	1.168	
	31.22	60	40		-0.046	1.085	
	31.25	60	40		-0.132	0.998	
	31.61	60	40		-1.068	0.060	
	31.66	60	40		-1.147	-0.019	
	31.69	60	40		-1.233	-0.105	
	31.95	59	40		-1.647	-0.586	
	31.97	59	40		-1.740	-0.679	
	32.01	59	40		-1.822	-0.761	32.00
26-Apr	34.34	42	40		0.082	0.180	
	34.37	42	40		-0.007	0.091	
	34.39	42	40		0.005	0.103	
	34.43	42	40		0.020	0.118	
	34.46	42	40		-0.064	0.034	
	34.49	42	40		-0.152	-0.054	
	34.51	42	40		-0.141	-0.043	
	34.55	42	40		-0.225	-0.127	35.00
Northrop							
9-Sep	36.31	34	40		2.866	2.596	37.06
	37.29	34	40		1.499	1.230	
	38.27	34	40		0.234	-0.034	
	38.64	34	40		-0.406	-0.673	
	39.27	34	40		-1.430	-1.696	
	40.28	34	40		-3.290	-3.555	
	41.29	34	40		-4.648	-4.911	
1-Dec	35.64	25	40		4.282	3.636	35.81
	36.47	25	40		1.913	1.270	
	37.46	25	40		0.247	-0.393	
	38.46	26	40		-1.855	-2.453	
	38.64	26	40		-2.276	-2.873	
	38.83	26	40		-2.593	-3.190	

Note: All "Extracts" are from days where bases generated by Profile 3 were more accurate than bases of Profile 2A.

	TABLE 11 (cont): RH PROFILE PROGRAM EXTRACTS for 8 CASES						
	Altitude	Profile 2A	Profile 3		Profile 2A	Profile 3	Reported
	(kft)	RH (%)	RH (%)		ΔT (deg C)	ΔT (deg C)	Bases (kft)
Northrop							
10-Dec	33.21	32	40		2.821	2.459	33.26
	34.13	33	40		0.482	0.165	
	34.21	33	40		0.315	-0.002	
	35.20	33	40		-1.844	-2.160	
	36.21	33	40		-4.200	-4.514	
	37.07	33	40		-6.052	-6.365	
	37.73	33	70		-7.161	-9.226	
	38.09	33	70		-6.102	-8.163	
15-Dec	36.49	33	40		1.490	1.177	34.21
	37.47	32	70		0.667	-1.443	
	37.73	32	70		0.382	-1.726	
	38.46	32	70		0.802	-1.298	
	38.64	32	70		0.880	-1.219	
	39.45	32	10		2.735	3.563	
	40.18	31	10		2.596	3.379	
12-Jan	30.81	33	40		5.231	4.908	31.76
	31.81	34	40		2.522	2.245	
	32.82	35	40		0.217	-0.014	
	33.83	36	70		-2.185	-4.159	
	33.93	36	70		-2.340	-4.313	
	34.13	36	70		-2.151	-4.122	
	34.83	35	70		1.302	-0.707	
	35.81	34	10		2.281	3.211	
2-Mar	32.49	38	40		2.538	2.444	
	33.49	38	70		0.676	-1.209	33.56
	33.60	38	70		0.522	-1.363	
	34.13	38	70		1.658	-0.222	
	34.49	37	70		1.260	-0.662	
	35.47	36	10		3.042	4.062	
	36.30	35	10		4.117	5.088	
Note: All "Extracts" are from days where bases generated by Profile 3 were more accurate than bases of Profile 2A.							
Note: On 15 Dec and 2 Mar, the forecast bases of profile 2A where seperated by too large of difference from the bases of profile 3 to make a representative data extraction.							

Overall, profiles 2A and 3 produced forecast bases which differed by 120 ft to 11 100 ft. In two of eight cases, 16 April 1996 and 26 April 1996 (Success Data), both profiles forecast bases below the reported base altitudes; however, they differed only by 0.44 and 0.12 kft, respectively. One of the eight cases, 2 March 1993 (Northrop Data), produced a slightly low forecast base while profile 2A's forecast base was more than 10 kft above the reported base. In the remaining five cases, both profiles produced forecast bases above the reported bases.

In the six cases where profile 2A erred above the reported base, its RH values were 2 - 38% lower than profile 3's. This enabled profile 3 to produce a lower ΔT at similar altitudes, and thus a lower and more accurate forecast base. Only two of six cases, however, demonstrated a difference in forecast bases over 1 kft. On 15 December 1992 and 2 March 1993 (Northrop Data), an increase of RH from 40% to 70% for profile 3 created a difference in RH between the two profiles of 38% and 32%, respectively. The sudden increase in RH from 40% to 70% was due to the tropopause designation. This RH difference of 38% created large forecast base differences of 8.93 kft and 11.1 kft between the two sets of forecast bases. These two cases were largely responsible for skewing the mean and variances of Table 6 as well as the verification accuracy tables (MAE, MSE, and RMSE) and bias (ME) of Tables 8a through 8c and Table 9.

When these two cases, along with the two other outliers, 6 November 1992 and 4 February 1992 (Northrop Data), were removed from the RMSE and ME computations, the difference in profile 2A's and 3's accuracy and bias became much smaller. RMSE values for the forecast base sets of profiles 2A and 3 decreased from 4.72 and 4.11 kft (Table 8c) to 1.58 and 1.57 kft with the outliers removed. This meant the difference was

decreased from 0.61 to 0.01 kft by removing the outliers. Similarly, bias values changed from 2.26 and 1.73 kft (Table 9) to 1.11 and 1.02 kft, creating a change in differences from 0.53 to 0.09 kft.

4.8 Lapse Rate Comparisons

This section of the results discusses the dependence of forecast bases on a combination of lapse rate and RH.

4.8.1 Case-by-Case Depth and Lapse Rate Computations. For each of the 42 cases, Table 12 shows the lapse rates and altitude differences (depths) between the bases produced by profile 1A (100% RH) and 1B (0% RH). Overall, the cases' lapse rates varied from 2.5 °C km^{-1} (24 February 1993) to 9.3 °C km^{-1} (6 November 1992) with an average of 7.477 °C km^{-1}. Corresponding depths for these rates were 26.85 kft, 3.79 kft, and 6.00 kft. These corresponding depths illustrated the smallest lapse rates produced the greatest depths. Similarly, as lapse rates became larger, depths decreased.

The four outlier cases (15 December 1993; 4 and 24 February, and 2 March 1993), case #28, #35, #38, and #41 in Figs. 15 through 18, had the smallest lapse rates between 2.5 and 4.5 °C km^{-1}. These small lapse rates produced depths greater than 10 kft.

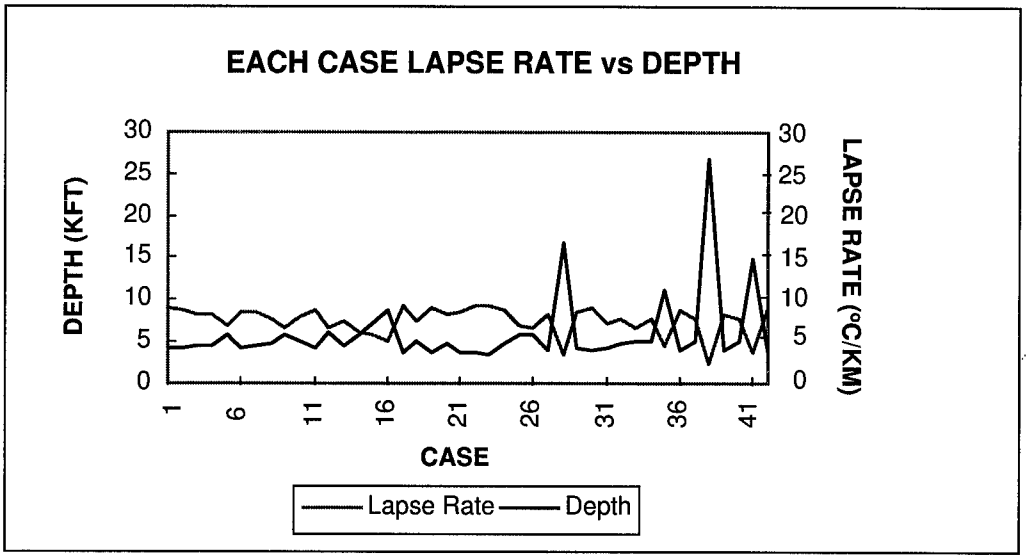

FIG. 25B: Case-by-Case Comparison of Lapse Rate vs Depth. Average lapse rate between case's forecast bases produced by profile 1A and 1B is compared to the altitudes of those bases.

4.8.2 General Relationship of Lapse Rate to Forecast Bases. Figures 26 and 27 show normalized the forecast bases from Figs. 7 and 8. These normalized depths show relative altitude changes between the reference level and the forecast bases using 0% RH.

Table 12: CASE-By-CASE LAPSE RATE and DEPTH					
Data Set		**Lapse**		**Avg Lapse**	**Avg**
		Rate	**Depth**	**Rate**	**Depth**
		(deg C/km)	**(kft)**	**(deg C/km)**	**(kft)**
Success				8.546	4.48
	16-Apr	9.030	4.21		
	20-Apr	8.778	4.24		
	26-Apr	8.184	4.63		
	4-May	8.324	4.52		
Wright-Pat				7.748	5.09
	2-Oct	6.886	5.81		
	3-Oct	8.597	4.35		
	4-Oct	8.595	4.39		
	5-Oct	7.792	4.88		
	7-Oct	6.703	5.92		
	11-Oct	7.842	4.94		
	16-Oct	8.816	4.32		
	17-Oct	6.751	6.07		
Northrop				7.258	6.46
	3-Sep	7.348	4.51		
	9-Sep	6.009	5.73		
	1-Oct	5.839	7.13		
	6-Oct	5.002	8.72		
	8-Oct	9.236	3.80		
	13-Oct	7.477	4.91		
	15-Oct	9.000	3.79		
	29-Oct	8.109	4.77		
	2-Nov	8.437	3.77		
	6-Nov	9.338	3.79		
	9-Nov	9.241	3.41		
	20-Nov	8.819	4.80		
	23-Nov	6.941	5.77		
	1-Dec	6.701	5.73		
	10-Dec	8.331	3.98		
	15-Dec	3.340	16.69		
	5-Jan	8.531	4.27		
	12-Jan	8.993	4.01		
	19-Jan	7.130	4.32		
	21-Jan	7.691	4.82		
	26-Jan	6.721	5.03		
	28-Jan	7.672	5.05		
	4-Feb	4.479	11.21		
	11-Feb	8.725	4.06		
	16-Feb	7.677	5.04		
	24-Feb	2.480	26.85		
	25-Feb	8.227	4.07		
	26-Feb	7.669	5.13		
	2-Mar	3.616	14.97		
	4-Mar	8.960	3.66		
All Cases Combined				7.477	6.00
Note: Combined cases does not recognize different contrail factors between Northrop and the other two data sets.					

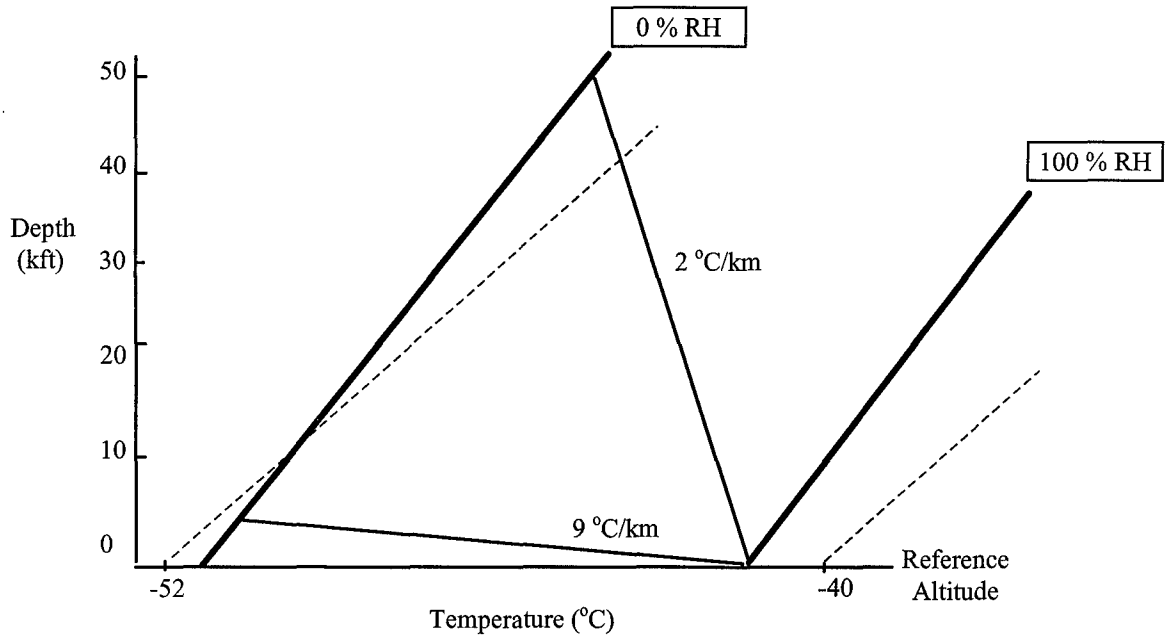

FIG. 26: Normalized Lapse Rates Showing Depth on Skew-T, Log-P Diagram (representation).

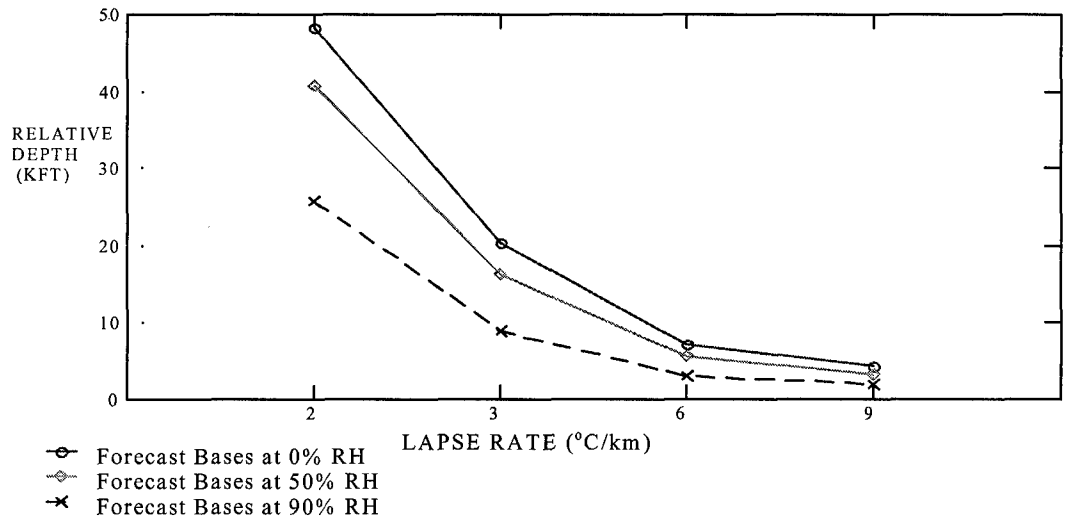

FIG. 27: Normalized Depth Chart. The zero ordinate indicates the reference altitude.

Besides showing the difference (depth) for the forecast bases using 100% and 0% RH, Fig. 27 shows depths for forecast bases using 50% and 90% RH. The 50% curve demonstrates the non-linear affect of RH on forecast bases. Although the 50% RH value is the median for values of RH from 0 - 100%, it does not locate the central forecast base depth or difference produced by these RH values. Figure 27, however, shows the 50% curve is closer to the 0% curve, instead of centered between the 100% and 0% curves. This is due to the non-linear relationship of RH with critical temperature at each pressure level. It was visualized on Fig. 1 by the non-linear separation between each RH curve of the Appleman Nomogram. Consequently, the 90% RH curve approximates the mid-way point between the depth from the 100% and 0% RH bases. This value, however, changed for different lapse rates. Table 13, shows mid-way RH values ranging from about 91% to 79% for the four tested lapse rates.

Table 13: Depth Computations for Forecast Bases of Different Lapse Rates.

Lapse Rate (deg C/km)		Depth 100-0% (kft)	Depth 100-50% (kft)	Depth 50-0% (kft)		Mid-Way RH (%)
	High-Bypass Contrail Factor					
2		48.216	40.672	7.544		91.197
3		20.336	16.072	4.264		85.323
6		7.216	5.576	1.64		82.286
9		4.264	3.28	0.984		79.438
7.477		5.248	4.264	0.984		
	Low-Bypass Contrail Factor					
2		45.264	38.048	7.216		
3		19.352	15.416	3.936		
6		6.888	5.248	1.64		
9		4.264	3.28	0.984		
7.477		5.248	4.264	0.984		

The difference in mid-way RH values was again due to the non-linear behavior of RH. Similar to RH's non-linear change with depth, RH also behaves non-linearly for different altitudes and thus for different lapse rates. This is a direct result of the non-linear behavior of critical temperature with pressure and was visualized on Fig 5, by the nearly linear RH contrail curves drawn on log-pressure coordinates.

Table 13 also compares depths for the four lapse rates between high and low bypass contrail factors. Little to no change occurred when the contrail factor was changed.

Overall, different lapse rates were used to show how they combined with RH to affect the forecast base. For each lapse rate, RH was shown to vary in a non-linear way with depth (Fig. 27). Since depth is the height above a reference altitude (forecast base using 100% RH), then RH was also shown to vary non-linearly with forecast bases. The non-linear relationship of RH with forecast bases implies forecast base uncertainty not only depends on the magnitude of the error in RH but also on the values of RH and lapse rate of the atmosphere.

4.8.3 Forecast Base Uncertainty with RH and Lapse Rate. This section shows the incremental changes in RH within a depth for the two lapse rates, 7.477 °C km^{-1} and 2 °C km^{-1}, displayed in Fig 26. Figures 27a and 27b show the slope (ΔDepth/ΔRH) becomes increasingly smaller as RH decreases from 100% to 0%.

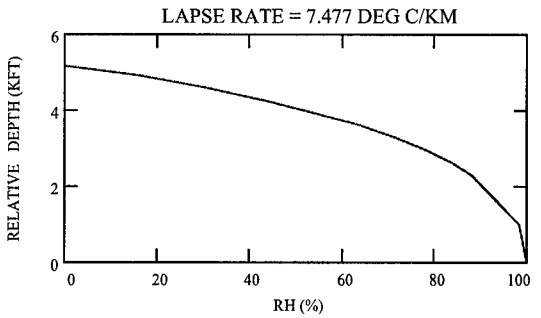

FIG. 28A: Forecast Base Uncertainty Curve for 7.477 °C/km.

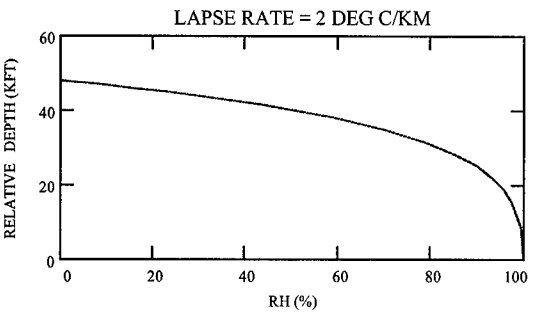

FIG. 28B: Forecast Base Uncertainty Curve for 2 °C/km.

The incremental change in depth, ΔDepth, can be thought of as the uncertainty in forecasting a contrail base for an incremental change in RH. Thus, the slopes of the curves in Figs. 28a and 28b show the uncertainty in a forecast base for a range of RH

values. When this interpretation is applied to Fig 28a, RH values between 0-40% provide an uncertainty in forecast bases of less than 1 kft. For a particular RH value between 0 - 40%, the uncertainty can be expressed in terms of the average slope, $\Delta Depth/\Delta RH = (5.1\text{-}4.3 \text{ kft})/(40\text{-}0\%) = 0.02$ kft per %RH. In other words, for the cases' average lapse rate, 7.477°C/km, an average uncertainty of 0.02 kft per each %RH exists for RH values between 0-40%. Table 14 summarizes the typical uncertainties, for three ranges of RH between 0% and 100%.

Table 14: Forecast Base Uncertainty Computations.

Lapse Rate	RH	ΔDepth/ΔRH	Depth Range
(deg C/km)	Range (%)	(kft / %RH)	(kft)
7.477	0-40	0.02	<1
	40-70	0.03	~1
	70-100	0.11	3
2	0-40	0.15	5.8
	40-70	0.23	7
	70-100	1.17	35

4.9 Chapter Summary

During the exploratory data analysis, all seven RH profiles appeared to produce similar forecast bases for each case. Scatterplots showed similarities between bases produced by profiles 2A, 3, and 4 and profiles 2A, 2B, and 2C. Four of the 42 cases were shown to be outliers, producing unusually large separations between the forecast bases of profiles 1A and 1B. The aircraft's reported bases were then shown to fall between the

forecast bases of profiles 1A and 1B. Profiles 1A and 1B were also shown to produce the lowest and highest forecast bases for each case, however, only those of profile 1A were consistently below the reported bases. Boxplots and numerical summaries showed bases of profile 1A had the lowest mean (30 kft), smallest range (8.7 kft), and were positively skewed toward lower altitudes. Bases of profiles 3 and 4 had similar means, 35.1 and 35.9 kft, and were positively skewed, but had variances which differed by over 5 kft. Each set of forecast bases also demonstrated high positive correlation with the reported bases, suggesting the major physical processes which affected the reported bases were reflected in these forecasts.

Accuracy and bias measurements were shown next, demonstrating each profile produced similar forecast bases. MAE values were all within 3 kft, MSE values indicated profiles 1B and 4 generated bases with slightly more error, and RMSE showed bases of profiles 3 and 4 to be within 0.78 kft. ME showed forecast bases of profiles 3 and 4 had biases within 0.83 kft. ME also showed profile 1A was the only profile to produce forecast bases with negative bias. Surprisingly, bases of profile 2A showed a higher positive bias than those of profile 3.

To compare the significance of the different accuracy and bias measurements, two t-tests and a Randomized Block ANOVA test compared the forecast bases of each profile. Using a test level of 0.05 (95% Confidence), only two of the seven profiles, 1A and 1B, produced a statistically different set of forecast bases. However, to explain why profile 3 produced more accurate bases than profile 2A in 8 of the 42 cases, those eight cases were closely examined. Only two of these eight cases indicated profile 3 produced a significantly better forecast base, greater than 1 kft. Both cases were outliers and when

removed from the accuracy computations brought the RMSE values to within 0.01 kft of each other.

The last section of this chapter analyzed the affect of lapse rate on forecast bases. Lapse rate accounted for the large separation between forecast bases of profiles 1A and 1B in the four outlier cases and a case-by-case analysis for all 42 showed smaller lapse rates produced larger separations or depths. The four outliers were shown to have the smallest lapse rates, 2.5-4.5°C/km, and the largest depths, 11-26 kft. Changes in forecast bases were then shown to be related non-linearly to changes in RH and lapse rate. Curves for specific lapse rates demonstrated the incremental uncertainty in forecast bases as a function of RH. This uncertainty of forecast bases, as a function of RH and lapse rate, summed the results and analysis and provided some concrete evidence as to the affect of RH on forecast bases.

V. Conclusions and Recommendations

5.1 Conclusion

This thesis, for the first time, validated the altitudes at which contrails first form (contrail bases). The results summarized in Chapter IV show: (1) AFGWC can not improve its contrail base forecasts by using more climatologically accurate RH values, such as SAGE II, (2) the AFGWC contrail algorithm has an inherent high forecast base bias, and (3) the degree to which forecast bases are affected by RH greatly depends on atmospheric lapse rate.

The first result surprisingly showed no significant improvements could be made to forecast contrail bases by replacing current empirical RH estimates with the more accurate SAGE II values. Although SAGE II RH values (profile 4) are presumably more accurate (McCormick, 1994) than empirical values (profile 3), they were shown to produce forecast bases 0.78 kft less accurate (RMSE) and had a 0.83 kft higher positive bias (ME) than those of profile 3. However, a two tailed t-test indicated neither profile produced significantly different bases, while numerical summaries noted the means were only separated by 0.61 kft. Since the AFGWC algorithm only forecasts in 1 kft increments, this difference may not even exceed the algorithm's forecast resolution. The reason for higher accuracy and smaller bias for individual cases (Table 5a) was due to profile 3's climatologically high RH bias of 70% near the tropopause (Jiusto and Pilie, 1964; Chu et al., 1993; Chiou et al., 1993; Larsen et al., 1993; McCormick and Chiou,

1994). SAGE II values at typical tropopause altitudes, 10-12 km, were only 12-24% (McCormick and Chiou, 1994) while the empirical values were 40% or 70%. Since a majority of the reported bases occurred near these altitudes, profile 3's RH values were 16-58% higher allowing it to produce lower, more accurate forecast bases with less positive bias.

The second significant result of the thesis showed a positive forecast base bias using profile 2A (in-situ RH values). In-situ measurements should have produced a set of forecast bases with little to no bias, since these RH values most closely approximated the conditions encountered by the aircraft during contrail formation. This bias was not attributed to the RH instrument error. At an average case lapse rate of 7.477 ^{o}C km^{-1} and a rawinsonde RH error of 3%, an RMSE of 4.75 kft does not correspond to the smaller forecast base uncertainties described in Fig. 28a. Even when the in-situ RH values were increased by 20% (profile 2B), they still exhibited a positive bias of 2.02 kft and an RMSE of 3.99 kft, indicating a gross RH error of 20%, still could not fully account for the positive bias and error. A comparison of forecast base accuracies presented in Table 5a shows 13 cases where the forecast bases were lowered and made more accurate by the increase in RH of 20%. However, only 1 of 13 cases made a significant forecast base improvement, over 1 kft. The Saatzer algorithm showed similar results for both of these profiles as well. These results indicate the AFGWC algorithm and Saatzer algorithm have a tendency to forecast bases too high. In order to lower forecast bases and compensate for this high forecast base bias, three algorithm parameters can be adjusted: artificially raise RH values, artificially raise contrail factor, or artificially lower ambient temperatures.

Lastly, this thesis showed the contrail forecast algorithms are dependent on a combination of RH and lapse rate. First, profiles 1A and 1B showed the largest difference between any two forecast bases by using RH values of 0% and 100%. Differences (depths) of nearly 20 kft (Table 6) were shown for the four outlier cases which had the smallest lapse rates, 2.5 to 4.5 ^{o}C km^{-1}. For the 42 cases, smaller lapse rates were shown to produce the largest depths while larger lapse rates produced the smallest depths (Table 12). These observations were then generalized by the construction of four artificial lapse rates and corresponding depths (Figs. 26 and 27). The set of RH curves in Fig. 27 demonstrated the non-linear relationship between RH and lapse rate with forecast bases. Since each curve produced a non-linear decrease with increasing lapse rate, RH affected forecast bases differently depending on lapse rate. Similarly, a particular range of RH values affected forecast bases differently since the separation between the curves was shown to be non-linear. Finally, these non-linear relationships were summarized by the forecast base uncertainty curves of Figs. 28a and 28b. These curves demonstrated the insignificance of RH accuracy at low RH values. They also showed RH accuracy may not affect forecast bases when its value is high if the lapse rate is large. For example, with an average lapse rate of 7.477 ^{o}C km^{-1}, the difference in forecast bases when using 100% vice 0% was shown to vary by only 5.248 kft, 4.264 kft of this variation coming from RH values of 50-100% while the remaining 0.984 kft from RH values between 0-50% (Table 13). Therefore, even a high RH value (>50%), in error by as much as 50%, would only affect the forecast base by 4 kft. For the several cases where lapse rates of 9^{o}C/km were observed, any RH value between 0 - 100% could have been used to forecast a base within 5 kft. In fact, if the atmosphere were assumed to have

the average lapse rate of the cases tested and an RH between 0-70% at contrail altitude, any RH value between 0-70% will produce a forecast base within 1 kft of each other (Table 14). These results suggest several key applications for forecasting contrail bases.

5.2 Applications

Two applications to forecasting contrail bases are suggested by relating forecast bases to RH and lapse rate in Figs. 7 and 27. The first application involves a quick look at a rawinsonde trace on a Skew-T Log-P diagram with the Appleman nomogram (RH curves) predrawn. Skew-T's with the Appleman 0, 60, 90, and 100% RH curves are already available from the Defense Mapping Agency or can be generated on a computerized Skew-T program available from the 88th Weather Squadron (Weaver, 1996). If the quick look shows an atmospheric trace with a large lapse rate, above the average mid-tropospheric rate of 6.5 ^{o}C km^{-1} (Wallace and Hobbs, 1977), use the 60% RH curve as the forecast base (Fig. 7). The detailed method is described by Appleman (1957). The 60% RH curve divides forecast base uncertainty for RH values from 0 - 90% (Fig. 27), a range of RH values encountered by the majority of the cases tested (Saatzer, 1995). The entire forecast process will take about 30 seconds and produce a forecast base accurate within 1 - 2 kft (Table 14).

The second application involves using the Normalized Depth Chart (fig 27) in a limited data situation to make contrail forecasts based on persistence. First, modify Fig. 27 to include RH curves drawn every 20% (Fig. 29). Figure 29 is then used with the

current reported base, lapse rate, and RH and forecast lapse rate and RH to produce a forecast base.

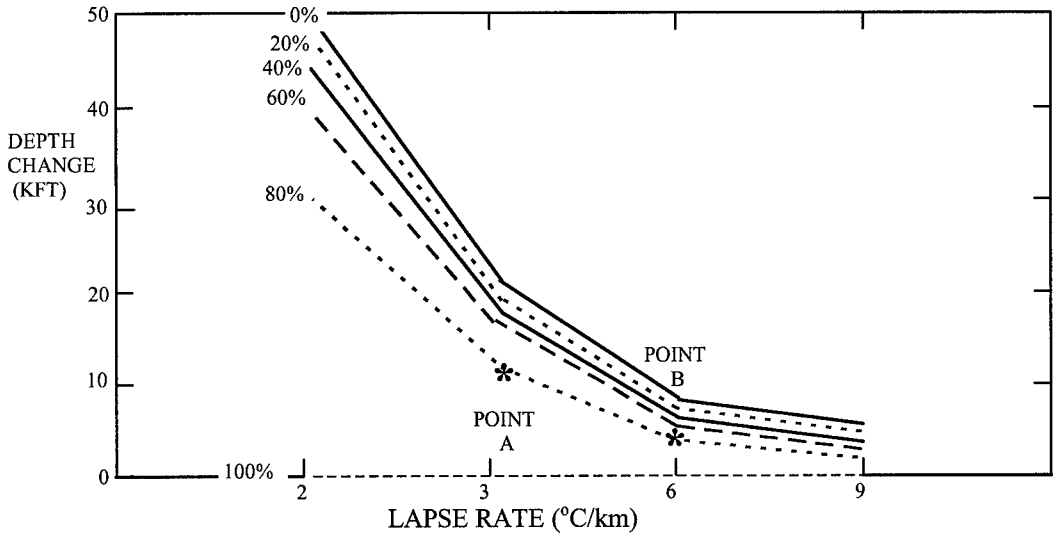

FIG 29: Modified Depth Chart. Each RH curve shows how forecast base changes as a function of RH and lapse rate.

Enter Fig. 29 with the current lapse rate and ambient RH of the reported base altitude. This is the starting point. For example, point A represents the starting point for a current lapse rate of 3°C/km and RH of 80%. Next, forecast a new lapse rate and RH for the time a contrail forecast base is needed and draw that point on the figure. This point represents the final point. Point B is a forecasted lapse rate of 6°C/km and RH of 60%. The change in depth between the starting point and final point represents the change in altitude between the current reported base and forecast base. For this example, the forecast base will decrease by 6 kft, the difference between point B (5 kft) and point A (11 kft). Therefore, if the reported base altitude was 35 kft, the forecast base altitude will be 29 kft.

This method can be applied to situations where only satellite information and current observations are known for specific points, such as deployed operations, and lapse rate and RH can be forecasted.

5.3 Recommendations

AFGWC should keep the empirical RH profile, vice SAGE II values, for its algorithm. Although SAGE II has been proven to be climatologically more accurate than empirical estimates (Chu et al., 1993; Larsen et al., 1993; Chiou et al., 1993), its low average RH values near the tropopause create large forecast base errors when the observed RH value is much above 24% (Table 11) and the lapse rate small. SAGE II gains in RH accuracy are made where atmospheric conditions are dry and cloud free (McCormick and Chiou, 1994). Therefore the gains in SAGE II RH accuracies were not realized by AFGWC forecasts since the algorithm is quite insensitive to low RH values. Alternately, the empirical RH values better estimated those outlier cases with an RH of 40% or 70%, reducing forecast error by over 8 kft (Tables 5a and 11). Additionally, since the algorithm has a positive RH bias, the frequently high RH value of 70% in the tropopause artificially lowered the bases, making them more accurate.

Future research should focus on three areas: climatological study, probability and general forecast guidance, and further investigation into the Appleman theory bias. More data needs to be analyzed to determine typical ranges of RH values at contrail altitudes. By doing this, a particular RH can be used to accurately divide forecast base uncertainty and simplify programming and deployed forecast methods. Next, conditional probability

forecasts can be generated and tested using different lapse rate and RH value combinations. Instead of measuring these conditional forecasts against climatolgical tables (Wilks, 1995), they can be measured against the Modified Depth Chart (Fig. 29) for a relative comparison and subsequent probability forecast. By using the conditional distributions of a maximum forecast base, one can compute the probability the forecast base is at or below some critical altitude required for flying operations. Figure 29 can also be used to develop generalized forecast guidance based on typical lapse rate and humidity changes for synoptically driven patterns. Therefore, a forecast can be made based on synoptic scale changes. Finally, more research into the physics of the Appleman theory needs to account for the AFGWC algorithm's positive forecast base bias.

Bibliography

Air Weather Service (AWS), 1979: The Use of the Skew-T, Log-P Diagram in Analysis and Forecasting, , Air Weather Service Tech. Rep. AWS/TR-79/006, HQ Air Weather Service, 140 pp.

Air Weather Service (AWS), 1981: Forecasting Aircraft Condensation Trails, Air Weather Service Tech. Rep. AWS/TR-81/006, HQ Air Weather Service, 46 pp.

Appleman, Herbert S., 1953: The Formation of Exhaust Condensation Trails by Jet Aircraft, *Bull. Amer. Meteor. Soc.*, **34**, 14-20.

Appleman, Herbert S., 1957: Derivation of Jet-Aircraft Contrail-Formation Curves, Air Weather Service Tech. Rep. AWS TR 105-145, HQ Air Weather Service, 46 pp.

Atmospheric Instrument Research (AIR), 1996: A New Gas Rawinsonde System, AIR Inc.

Bjornson, B. M., 1992: SAC Contrail Formation Study, USAF Environmental Technical Applications Center Project Rep. USAFETAC/PR-92/003, 48 pp.

Buck, A. L., 1981: New Equations for Capturing Vapor Pressure and Enhancement Factor, *J. of Appl. Meteor.*, **20**, 1527-1532.

Chiou, E.W., et al., 1996: Proposed Reference Model for Middle Atmosphere Water Vapor, *Adv. Space Res.*, **18**, 59-89.

Chu, W. P., et al., 1993: Algorithms and Sensitivity Analyses for Stratospheric Aerosol and Gas Experiment II Water Vapor Retrieval, *J. Geophy. Res.*, **98**, D3, 4857-4866.

Coleman, Rich F., 1996: A New Formulation for the Critical Temperature for Contrail Formation, *J. Appl. Meteor.*, **35**, 2270-2282.

Devore, Jay L., 1995: *Probability and Statistics for the Engineering and Sciences*, 4th Edition, Duxbury Press, 467 pp.

Duffield, G. F., and G. D. Nastrom, 1983: Equations and Algorithms for Meteorological Applications in Air Weather Service, Air Weather Service Tech. Rep. AWS/TR-83/001, HQ Air Weather Service, 58 pp.

Federal Aviation Regulations (FAR), 1996, Jeppesen Sanderson, Englewood, CO.

Fleagle, R. G., and J. A. Businger, 1980: *An Introduction to Atmospheric Physics*, Second Edition, Academic Press, 432 pp.

Jiutso, James E., 1961: Prediction of Aircraft Condensation Trails, PROJECT CONTRAILS, CAL Report No,VC-1055-P-5, Cornell Aeronautical Laboratory, 26 pp.

Jiusto, J. E., and R. J. Pilie, 1958: A Laboratory Study of Contrails, *J. Meteor.*, **15**, 149-154.

Jiutso, J. E., and R. J. Pilie, 1964: Contrail Forecasting, CAL Report No. VC-1660-P-3, Cornell Aeronautical Laboratory, 36 pp.

Larsen, J.C., et al., 1993: A Comparison of the Stratospheric Aerosol and Gas Experiment II Tropospheric Water Vapor to Radiosonde Measurements, *J. Geophys. Res.*, **98**, D3, 4897-4917.

List, R. J., 1984: *Smithsonian Meteorological Tables*, Sixth Revised Edition, Smithsonian Institution Press, 527 pp.

MathSoft Applications, 1995: User's Guide, MATHCAD 6.0/MATHCAD PLUS 6.0, MathSoft Inc.

McCormick, M. P., 1987: SAGE II: An Overview, *Adv. Space Res.*, **7**, 219-226.

McCormick, M. P., and E. W. Chiou, 1994: Climatology of Water Vapor in the Upper Troposphere and Lower Stratosphere Determined from SAGE II Observations, *Fifth Symposium on Global Change Studies*, Nashville, TE.

Miller, W. F., 1990: SAC Contrail Forecasting Algorithm Validation Study, USAF Environmental Technical Applications Center Project Rep. USAFETAC/PR-90/003, 28 pp.

NASA, Ames Research Center, 1996: Subsonic Aircraft: Contrail and Cloud Effects Special Study (Success), Mission Plan, Ames Research Center, 99 pp.

Peters, J. L., 1993: New Techniques for Contrail Forecasting, Air Weather Service Tech. Rep. AWS/TR-93/001, HQ Air Weather Service, 35 pp.

Polander, J., Aeronautical Systems Meteorologist, 1996: Personal Correspondence, 88th Weather Squadron, Wright-Patterson AFB, OH.

Rind, D., et al., 1993: Overview of Stratospheric Aerosol and Gas Experiment II Water Vapor Observations: Method, Validation, and Data Characteristics, *J. Geophys. Res.*, **98**, D3, 4857-4866.

Saatzer, P., 1995: Pilot Alert System Flight Test Final Report, Final Technical Report for Period November 1988 - May 1993, Northrop Grumman Corporation, 241 pp.

Schrader, Mark L., 1994: Calculations of Critical Temperature of Contrail Formation for Different Engine Types (Draft), HQ Air Weather Service, Scott AFB, IL.

Speltz, David J., 1995: Validation of the Appleman Contrail Forecasting Scheme Using Engine Specific Aircraft Data. *Cloud Impacts on DOD Operations and Systems 1995 Conference (CIDOS-95)*, Hanscom AFB, MA.

Taylor, J. R., 1982: *An Introduction to Error Analysis*, University Science Books.

Vaisala Promotional Package, 1996: RS-80 Description, Vaisala Inc.

Wallace, J. M., and P. V. Hobbs, 1977: *Atmospheric Science: An Introductory Survey*, Academic Press, 71-97.

Weaver, S., Chief Aeronautical Systems Meteorologist, 1996: Personal Correspondence, 88th Weather Squadron, Wright-Patterson AFB, OH.

Wilks, Daniel S., 1995: *Statistical Methods in the Atmospheric Sciences*, Academic Press.

Flow Chart for Profile Comparison Proram

Appendix A

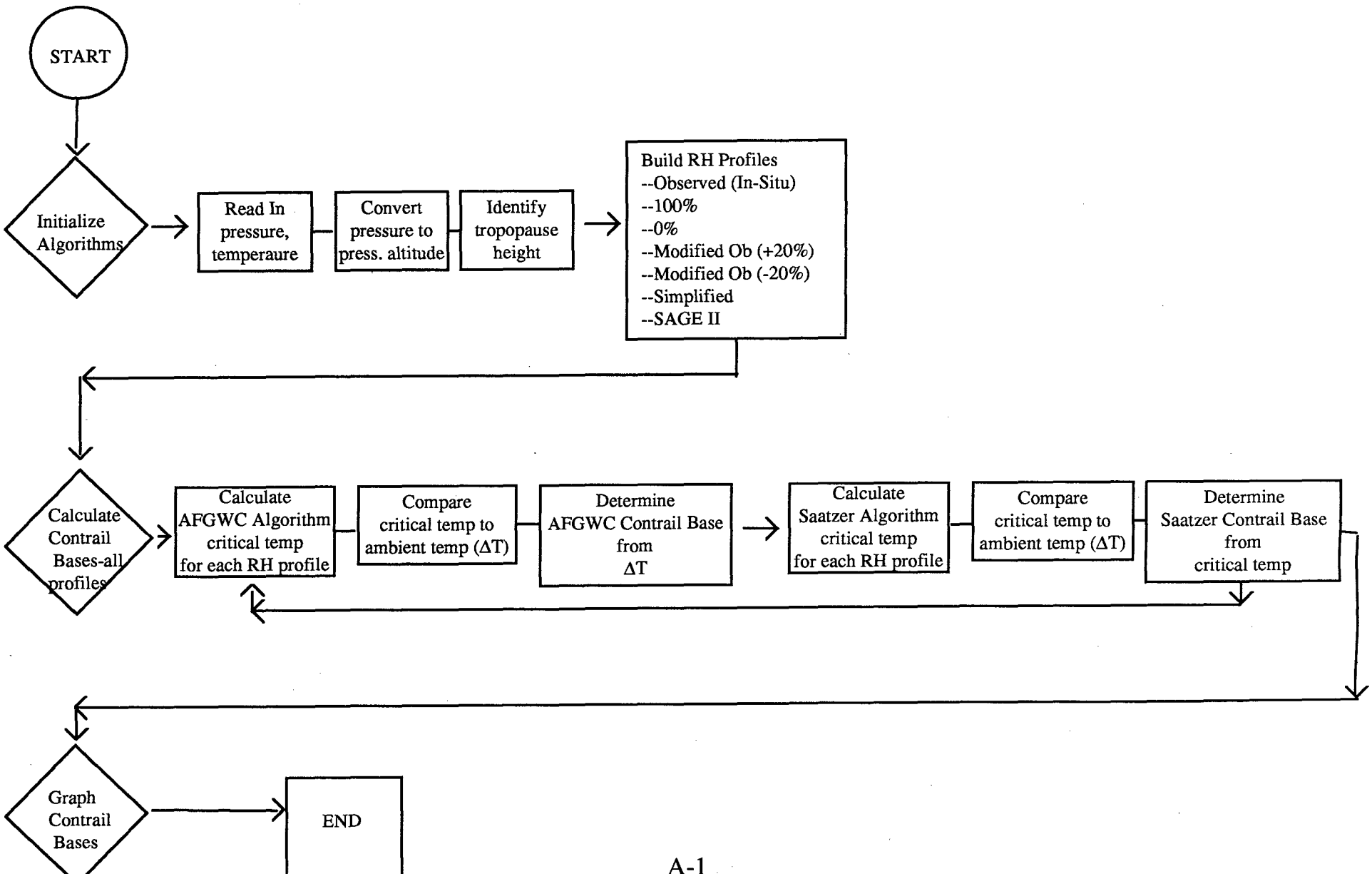

Appendix B: RH Profile Program

Appendix B Table of Contents

I. Variable Declarations and Conversions. Before the program calculates the specific algorithms, it will read in the raw data, label the columns of data with varaibles such as p for pressure, etc., and derive any other parameters (i.e. pressure altitudes) from the raw data.

ORIGIN ≡ 1

```
data := READPRN(s2117)
```

* READPRN reads in 4 columns of data (pressures, temperatures, dewpoints, and relative humidities).
* i defines the number of rows in each column.
* p and temp are varaible names given to the different columns of data

```
i := 1.. rows(data)
p := data<1>
temp := data<2>
```

*tempK converts temperatures from Celcius to Kelvin

```
tempK := temp + 273.15
```

```
CF := 0.039
```

* CF is a constant contrail factor defined for a high-bypass engine (Schrader, 1994).

Altitude Conversions: To convert the pressure levels (p) to pressure altitudes (alt), the following relationships are derived from the ideal gas law and hypsomertric equation (List, 1984).

At or below 11,000 m altitude (226.19mb)

$$\frac{p_s}{1013.25} = \left(\frac{288 - 0.0065 \cdot z}{288}\right)^{5.256}$$

Above 11,000 m altitude (226.19mb)

$$\frac{z - 11000}{14600} = \log\left(\frac{226.19}{ps}\right)$$

$$\text{ConvertAlt}(p) := \begin{cases} 44307.69 - 11874.50 \cdot (p)^{0.19} & \text{if } p \geq 226.19 \\ 11000.0 + 6340.70 \cdot \ln\left(\frac{226.19}{p}\right) & \text{if } p < 226.19 \end{cases}$$

$$altm_i := \text{ConvertAlt}(p_i)$$

$$altkm_i := \frac{\text{ConvertAlt}(p_i)}{1000}$$

$$altft_i := \text{ConvertAlt}(p_i) \cdot 3.28$$

$$altkft_i := \frac{\text{ConvertAlt}(p_i) \cdot 3.28}{1000}$$

altm is the converted pressure altitude in meters. Also listed are altitude conversions for km, ft, and kft.

Tropopause Definition: The program will define the tropopause on the rawinsonde. To define the tropopause level, it must first find the lowest height in the atmosphere where the rawinsonde's lapse rate, change of temperature with height, decreases to an average lapse rate 2 °C/km for a 2 km depth. Once this height is found, it is identified as the "conventional tropopause" (AWS, 1979).

Define Incremental Temperature Change over 50 levels or approximately 2 km depth at 200 mb.

$$j := 1 .. \text{rows}(data) - 50$$

$$\begin{aligned} dT_j := {} & \left(temp_j - temp_{j+1}\right) + \left(temp_{j+1} - temp_{j+2}\right) + \left(temp_{j+2} - temp_{j+3}\right) \cdots \\ & + \left(temp_{j+3} - temp_{j+4}\right) + \left(temp_{j+4} - temp_{j+5}\right) + \left(temp_{j+5} - temp_{j+6}\right) \cdots \\ & + \left(temp_{j+6} - temp_{j+7}\right) + \left(temp_{j+7} - temp_{j+8}\right) + \left(temp_{j+8} - temp_{j+9}\right) \cdots \\ & + \left(temp_{j+9} - temp_{j+10}\right) + \left(temp_{j+10} - temp_{j+11}\right) \cdots \\ & + \left(temp_{j+11} - temp_{j+12}\right) + \left(temp_{j+12} - temp_{j+13}\right) + \left(temp_{j+13} - temp_{j+14}\right) + \left(temp_{j+14} - temp_{j+15}\right) \cdots \\ & + \left(temp_{j+15} - temp_{j+16}\right) + \left(temp_{j+16} - temp_{j+17}\right) + \left(temp_{j+17} - temp_{j+18}\right) + \left(temp_{j+18} - temp_{j+19}\right) \cdots \\ & + \left(temp_{j+19} - temp_{j+20}\right) + \left(temp_{j+20} - temp_{j+21}\right) + \left(temp_{j+21} - temp_{j+22}\right) + \left(temp_{j+22} - temp_{j+23}\right) \cdots \\ & + \left(temp_{j+23} - temp_{j+24}\right) + \left(temp_{j+24} - temp_{j+25}\right) \cdots \\ & + \left(temp_{j+25} - temp_{j+26}\right) + \left(temp_{j+26} - temp_{j+27}\right) + \left(temp_{j+27} - temp_{j+28}\right) \cdots \\ & + \left(temp_{j+28} - temp_{j+29}\right) + \left(temp_{j+29} - temp_{j+30}\right) + \left(temp_{j+30} - temp_{j+31}\right) \cdots \\ & + \left(temp_{j+31} - temp_{j+32}\right) + \left(temp_{j+32} - temp_{j+33}\right) + \left(temp_{j+33} - temp_{j+34}\right) \cdots \\ & + \left(temp_{j+34} - temp_{j+35}\right) + \left(temp_{j+35} - temp_{j+36}\right) \cdots \\ & + \left(temp_{j+36} - temp_{j+37}\right) + \left(temp_{j+37} - temp_{j+38}\right) + \left(temp_{j+38} - temp_{j+39}\right) + \left(temp_{j+39} - temp_{j+40}\right) \cdots \\ & + \left(temp_{j+40} - temp_{j+41}\right) + \left(temp_{j+41} - temp_{j+42}\right) + \left(temp_{j+42} - temp_{j+43}\right) + \left(temp_{j+43} - temp_{j+44}\right) \cdots \\ & + \left(temp_{j+44} - temp_{j+45}\right) + \left(temp_{j+45} - temp_{j+46}\right) + \left(temp_{j+46} - temp_{j+47}\right) + \left(temp_{j+47} - temp_{j+48}\right) \cdots \\ & + \left(temp_{j+48} - temp_{j+49}\right) + \left(temp_{j+49} - temp_{j+50}\right) \end{aligned}$$

$dZ_j := altkm_{j+50} - altkm_j$ Define Altitude change over those same 50 levels.

$lapse_j := \frac{dT_j}{dZ_j}$ Define Lapse Rate in °C per km over those 50 levels, with a base at each j.

Starting above 350 mb, look for lapse rate to decrease to 2 °C/km and define the base of this layer as the tropopause (AWS, 1979).

findp(p) :=
n ← 1
while $p_n > 350$
  n ← n + 1
n

trop(lapse, thres) :=
j ← findp(p)
while $lapse_j > thres$
  j ← j + 1
j

$tropp := p_{trop(lapse, 2.0)}$ tropp = 198.6 Trop defined in mb.

$tropopause := altm_{trop(lapse, 2.0)}$ $tropopause = 1.182 \cdot 10^4$ Trop defined in meters.

II. Relative Humidity (RH) Profile Options. Before the program enters the specific algorithms, it will define the three primary profiles: 2A, 3, 4. It will then modify profile 2A by addding and subtracting 20% of its value to each level. Each of these profiles will be computed seperately on different program executions.

A. Profiles 2A, 2B, 2C: These profiles uses relative humidities gathered from the rawinsondes. Each level has an observed relative humidity.

Profile 2A:

$rh_O := data^{<4>}$ rh_o is the varaible name given to the column of data with relative humidity values.

Profile 2B (+20%):

$rh_{20plus} := rh_O + rh_O \cdot 0.20$

$rh_{Oa_i} :=$
0 if $rh_{20plus_i} \le 0$
100 if $rh_{20plus_i} \ge 100$
rh_{20plus_i} otherwise

Profile 2C (-20%)

$rh_{20minus} := rh_O - rh_O \cdot 0.20$

$rh_{Ob_i} :=$
0 if $rh_{20minus_i} \le 0$
100 if $rh_{20minus_i} \ge 100$
$rh_{20minus_i}$ otherwise

B. Profile 3 (Empirical): This profile uses empirically based averages (Appleman, 1953) to divide the atmosphere into three large layers; troposphere, tropopause, and stratosphere. Relative Humidities of 40% are assigned to the troposphere, 70% within 300 meters of the tropopause, and 10% to the stratosphere.

$$rh_{S_i} := \begin{cases} 10 & \text{if } altm_i > tropopause + 300 \\ 40 & \text{if } altm_i < tropopause - 300 \\ 70 & \text{otherwise} \end{cases}$$

$RH_S := rh_S$

rh_{rhS} compares each altitude measures by the rawinsonde to the tropopause level and assigns a simplified relative humidity value to each of those altitudes based on whether they are above (10%), below (40%) or within 300m of the tropopause (70%).

C. Profile 4 (SAGE II): This profile uses relative humidities from a climatological table (McCormick, 1994) based on latitude and season. All four seasons were used but only Spring for the 20-40°N abnd is listed as an example.

$$rh_{II.sp_i} := \begin{cases} 30 & \text{if } altkm_i < 6.5 \\ 17.8 & \text{if } 6.5 \le altkm_i < 7.5 \\ 19.9 & \text{if } 7.5 \le altkm_i < 8.5 \\ 21.6 & \text{if } 8.5 \le altkm_i < 9.5 \\ 23.1 & \text{if } 9.5 \le altkm_i < 10.5 \\ 22.3 & \text{if } 10.5 \le altkm_i < 11.5 \\ 16.6 & \text{if } 11.5 \le altkm_i < 12.5 \\ 12.4 & \text{if } 12.5 \le altkm_i < 13.5 \\ 9.25 & \text{if } 13.5 \le altkm_i < 14.5 \\ 17.1 & \text{if } 14.5 \le altkm_i < 15.5 \\ 6.17 & \text{if } 15.5 \le altkm_i < 16.5 \\ 6.62 & \text{if } 16.5 \le altkm_i < 17.5 \\ 5 & \text{if } 17.5 \le altkm_i \end{cases}$$

$RH_{II} := rh_{II.sp}$

III. AFGWC Contrail Algorithm. The AFGWC algorithm uses a modified Appleman technique, Schrader equations and formulae (Schrader, 1994), for calculating critical temperatures. It then compares these temperatures to the ambient temperature. A contrail at that level is said to exist if the ambient temperature is less than or equal to the critical temperature. This process is computed for each level and consecutive contrail levels are combined to form one large layer. The base and top of this layer is provided as the contrail forecast.

III. AFGWC Contrail Algorithm. The AFGWC algorithm uses a modified Appleman technique, Schrader equations and formulae (Schrader, 1994), for calculating critical temperatures. It then compares these temperatures to the ambient temperature. A contrail at that level is said to exist if the ambient temperature is less than or equal to the critical temperature. This process is computed for each level and consecutive contrail levels are combined to form one large layer. The base and top of this layer is provided as the contrail forecast.

The Schrader formulae are composed of four steps. First, define a critical slope for each layer based on the contrail factor. This slope represents an average and constant amount of moisture/heat ratio added by the aircraft engine at a specific pressure and is described as a contrail factor. Secondly, this slope is set equal to a theoretical derivative, Goff-Gratch equation, describing saturation vapor pressure as a function of temperature. The temperature where this equality holds is defined as the temperaturation needed for saturation, given this engine type at some specific pressure. Since this temperature ocurrs at saturation, the RH is assumed to be 100%. The third step is to use the calculatins from the previous two steps to solve for a critical temperature at some specific RH instead of 100%. Lastly, this critical temperature is compared to the ambient temperature for that level and if the ambient temperature <= critical temperature that level is labeled as a contrail level.

A. STEP 1: Find Critical Slope for each layer, where p is pressure in mb. This slope is tangent to the saturation curve (on an e-T graph) at some critical temperature.

$$crit\_slope_i := \frac{p_i}{622} \cdot CF$$

B. STEP 2: To find $T_{c.100}$, set Goff-Gratch Derivitive equal to critical slope for each level. This provides a critical temp at 100% relative humidity. In other words, the derivitive is defined on an e-T graph for the saturation curve (100%) at a critical temperature ($T_{c.100}$) corresponding to the vapor pressure (e). The internal method used by MATHCAD to find the root is a series of successive approximations to the root. This evaluation uses the "Secant Method" to converge to the root. As a starting point for this evaluation process, I provide a guess value for the root of T=300 K (MathSoft, 1996)

Goff-Gratch Equation (List, 1984).

$$Goff(T) := 10^{\left(23.832241 - 5.02808 \cdot \frac{\ln(T)}{\ln(10)} - 1.3816 \cdot 10^{-7} \cdot 10^{11.334 - 0.0303998 \cdot T} + 8.1328 \cdot 10^{-3} \cdot 10^{3.49149 - \frac{1302.8844}{T}} - \frac{2949.076}{T}\right)}$$

Goff-Gratch Derivative

$$\text{GoffDer}(T) := 10^{\left[\begin{array}{l} 23.832241 - 5.02808\cdot\frac{\ln(T)}{\ln(10)} \ldots \\ +-1.3816\cdot10^{-7}\cdot10^{11.334 - 3.03998\cdot10^{-2}\cdot T} \ldots \\ +8.1328\cdot10^{-3}\cdot10^{3.49149 - \frac{1302.8844}{T}} \ldots \\ +\frac{-2949.076}{T} \end{array}\right]} \cdot \left[\begin{array}{l} \frac{-5.02808}{T\cdot\ln(10)} \ldots \\ +4.200036368\cdot10^{-9}\cdot10^{\left(11.334 - 3.03998\cdot10^{-2}\cdot T\right)}\cdot\ln(10) \ldots \\ +10.59609824832\cdot\frac{10^{\left(3.49149 - \frac{1302.8844}{T}\right)}}{T^2}\cdot\ln(10) \ldots \\ +\frac{2949.076}{T^2} \end{array}\right]\cdot\ln(10)$$

To solve the Goff Gratch derivative ($d(e_s)/dt$) for each level, the program will set it equal to the critical slope of that level. MATHCAD will then find the root of this function, $f(T_{c.100})$, solving for $T_{c.100}$. To help MATHCAD solve for the root function, a reasonable estimate is entered as a starting point for MATHCAD's secant convergence. Once the converged value is within a tolerable error of margin, MATHCAD designates that value as a solution for that level and proceeds to solve the next level. The reasonable temperature used for this root function is T:=300 K. Also remember, critical slopes at each level have been determined in step I.

$$T_{c.100} := 300$$

$$f(T_{c.100}) := \text{GoffDer}(T_{c.100}) - \text{crit\_slope}_i$$

$$T_{c.100_i} := \text{root}(f(T_{c.100}), T_{c.100})$$

C. STEP 3: Find the Critcal Temperature for any relative humidity value. To do this, the equation below is solved for $T_{c.RH}$.

$$\frac{e_{s.100} - (T_{c.100} - T_{c.RH})\cdot\text{crit\_slope}}{e_{s.RH}}\cdot 100 = RH$$

where RH = specific value of relative humidity defined at each level (different for each profile), $e_{s.100}$ = Goff Gratch value at $T_{c.100}$, $T_{c.100}$ = critical temperature for saturation at a specific pressure level for a specific contrail factor, and $T_{c.RH}$ is the unknown critical temperature for the value of relative humidity set on the right hand side.

To solve above equation for $T_{c.RH}$, the program must first define the other variables in the equation in terms of $T_{c.RH}$. By doing so, the program can substitute those variable expressions into the equation and solve for the root.

1. Define $e_{s.100}$ at each $T_{c.100}$ using the Goff Gratch equation (not the derivative).

$$e_{s.100_i} := Goff\left(T_{c.100_i}\right)$$

For MATHCAD to iteratively solve the left hand side of this equation in terms of T_c, the program will make an intial guess of 200 K. Special care must be taken to select a representative first guess for all values of the array or MATHCAD will not converge to the proper root.

Profile 2A

$$T_c := 200$$

$$f\left(T_c, rh_O\right) := \frac{e_{s.100_i} - \left(T_{c.100_i} - T_c\right)\cdot\left(crit\_slope_i\right)}{Goff\left(T_c\right)}\cdot 100 - rh_{O_i}$$

$$T_{c.O_i} := root\left(f\left(T_c, rh_O\right), T_c\right)$$

Profile 2B

$$T_c := 200$$

$$f\left(T_c, rh_{Oa}\right) := \frac{e_{s.100_i} - \left(T_{c.100_i} - T_c\right)\cdot\left(crit\_slope_i\right)}{Goff\left(T_c\right)}\cdot 100 - rh_{Oa_i}$$

$$T_{c.Oa_i} := root\left(f\left(T_c, rh_{Oa}\right), T_c\right)$$

Profile 2C

$$T_c := 200$$

$$f\left(T_c, rh_{Ob}\right) := \frac{e_{s.100_i} - \left(T_{c.100_i} - T_c\right)\cdot\left(crit\_slope_i\right)}{Goff\left(T_c\right)}\cdot 100 - rh_{Ob_i}$$

$$T_{c.Ob_i} := root\left(f\left(T_c, rh_{Ob}\right), T_c\right)$$

Profile 3

$T_c := 200$

$$f(T_c, rh_S) := \frac{e_{s.100_i} - \left(T_{c.100_i} - T_c\right) \cdot \left(crit\_slope_i\right)}{Goff(T_c)} \cdot 100 - rh_{S_i}$$

$$T_{c.S_i} := root\left(f(T_c, rh_S), T_c\right)$$

Profile 4

$T_c := 200$

$$f(T_c, RH_{II}) := \frac{e_{s.100_i} - \left(T_{c.100_i} - T_c\right) \cdot \left(crit\_slope_i\right)}{Goff(T_c)} \cdot 100 - RH_{II_i}$$

$$T_{c.II_i} := root\left(f(T_c, RH_{II}), T_c\right)$$

D. STEP 4: Compare critical temperatures for each profile to observed temperatures of rawinsonde data (ambient temperatures). If ambient temperature is equal to or colder than the critical temperature a contrail will form. If the program compares the difference between the two temperatures is zero or negative then a contrail layer exists for that level.

$\Delta GWC_O := tempK - T_{c.O}$

$\Delta GWC_{Oa} := tempK - T_{c.Oa}$

$\Delta GWC_{Ob} := tempK - T_{c.Ob}$

$\Delta GWC_S := tempK - T_{c.S}$

$\Delta GWC_{II} := tempK - T_{c.II}$

IV. Saatzer Contrail Algorithm. This algorithm uses two sets of formulae. The first set is curve fit for RH's <= 90%, while the second is for RH's > 90%.

A. STEP 1: Define numerical procedures for calculating onset temperature (ref: Saatzer, p.6-10) using a curve fit equations between altitudes of 25 - 50 kft and RH <= 90%.

$$A_0 := -117.445 + 6487.20 \cdot CF - 182454.5 \cdot CF^2 + 1772719 \cdot CF^3$$

$$A_1 := 0.332437 - 60.6166 \cdot CF + 1552.4 \cdot CF^2 - 13265.5 \cdot CF^3$$

$$A_2 := -0.0055724 + 0.42889 \cdot CF - 10.1451 \cdot CF^2 + 76.2117 \cdot CF^3$$

$$T_{d\_alt_i} := A_0 + A_1 \cdot altkft_i + A_2 \cdot \left(altkft_i\right)^2$$

Profile 2A

$$\Delta T_{O_i} := 4.466 \cdot 10^{-2} \cdot rh_{O_i} - 3.944 \cdot 10^{-4} \cdot \left(rh_{O_i}\right)^2 + 6.4815 \cdot 10^{-6} \cdot \left(rh_{O_i}\right)^3$$

$$T_{co.O_i} := T_{d\_alt_i} + \Delta T_{O_i}$$

$$\Delta sat_O := temp - T_{co.O}$$

Profile 2B

$$\Delta T_{Oa_i} := 4.466 \cdot 10^{-2} \cdot rh_{Oa_i} - 3.944 \cdot 10^{-4} \cdot \left(rh_{Oa_i}\right)^2 + 6.4815 \cdot 10^{-6} \cdot \left(rh_{Oa_i}\right)^3$$

$$T_{co.Oa_i} := T_{d\_alt_i} + \Delta T_{Oa_i}$$

$$\Delta sat_{Oa} := temp - T_{co.Oa}$$

Profile 2C

$$\Delta T_{Ob_i} := 4.466 \cdot 10^{-2} \cdot rh_{Ob_i} - 3.944 \cdot 10^{-4} \cdot \left(rh_{Ob_i}\right)^2 + 6.4815 \cdot 10^{-6} \cdot \left(rh_{Ob_i}\right)^3$$

$$T_{co.Ob_i} := T_{d\_alt_i} + \Delta T_{Ob_i}$$

$$\Delta sat_{Ob} := temp - T_{co.Ob}$$

Profile 3

$$\Delta T_{S_i} := 4.466 \cdot 10^{-2} \cdot rh_{S_i} - 3.944 \cdot 10^{-4} \cdot \left(rh_{S_i}\right)^2 + 6.4815 \cdot 10^{-6} \cdot \left(rh_{S_i}\right)^3$$

$$T_{co.S_i} := T_{d\_alt_i} + \Delta T_{S_i}$$

$$\Delta sat_S := temp - T_{co.S}$$

Profile 4

$$\Delta T_{II_i} := 4.466 \cdot 10^{-2} \cdot RH_{II_i} - 3.944 \cdot 10^{-4} \cdot \left(RH_{II_i}\right)^2 + 6.4815 \cdot 10^{-6} \cdot \left(RH_{II_i}\right)^3$$

$$T_{co.II_i} := T_{d\_alt_i} + \Delta T_{II_i}$$

$$\Delta sat_{II} := temp - T_{co.II}$$

B. STEP 2: Define curve fit equations for RH > 90% by varying onset temperatures as a function of contrail factor an altitude of 40 kft. The onset temperature produced by this set of equations is the warmest temperature at which contrails occurr.

$$\Delta alt_i := 40 - altkft_i$$

$$\Delta T_{c40_i} := 0.032 + 0.4711 \cdot \Delta alt_i + 0.00019286 \cdot (\Delta alt_i)^2$$

$$T_{c40} := -61.27 + 581.1 \cdot CF + 4500 \cdot CF^2$$

$$Tc_i := T_{c40} + \Delta T_{c40_i}$$

$$\Delta sat_{90} := temp - Tc$$

C. STEP 3: Define which contrail onset temperature, based on relative humidity, to use for each level. Since the Simplified and SAGE profiles do not exceed 90%, the contrail onset temperature change generated from the first set of curve fit equations (<=90%) are used. An onset temperature change must then be decided for each level in profiles 2A, 2B, and 2C.

$$\Delta Sat_{O_i} := \begin{cases} \Delta sat_{O_i} & \text{if } rh_{O_i} \le 90 \\ \Delta sat_{90_i} & \text{if } rh_{O_i} > 90 \end{cases} \quad \Delta Sat_{Oa_i} := \begin{cases} \Delta sat_{Oa_i} & \text{if } rh_{Oa_i} \le 90 \\ \Delta sat_{90_i} & \text{if } rh_{Oa_i} > 90 \end{cases} \quad \Delta Sat_{Ob_i} := \begin{cases} \Delta sat_{Ob_i} & \text{if } rh_{Ob_i} \le 90 \\ \Delta sat_{90_i} & \text{if } rh_{Ob_i} > 90 \end{cases}$$

$$\Delta Sat_S := \Delta sat_S \qquad \Delta Sat_{II} := \Delta sat_{II}$$

V. Matrix for Export. The following matrix is compiled of an array, from the surface to the last rawinsonde measurement, of ambient temperatures, pressures, pressure altitudes, ambient RH values, modified ambient RH values, empirical RH values, SAGE II RH values, and ΔT's using the five profiles (computed above) for the AFGWC and Saatzer algorithms.

$RawData^{<1>} := temp$ $RawData^{<7>} := rh_S$ $RawData^{<13>} := \Delta GWC_S$ $RawData^{<19>} := \Delta Sat_S$

$RawData^{<2>} := p$ $RawData^{<8>} := RH_{II}$ $RawData^{<14>} := \Delta GWC_{II}$ $RawData^{<20>} := \Delta Sat_{II}$

$RawData^{<3>} := altkft$ $RawData^{<10>} := \Delta GWC_O$ $RawData^{<16>} := \Delta Sat_O$

$RawData^{<4>} := rh_O$ $RawData^{<11>} := \Delta GWC_{Oa}$ $RawData^{<17>} := \Delta Sat_{Oa}$

$RawData^{<5>} := rh_{Oa}$ $RawData^{<12>} := \Delta GWC_{Ob}$ $RawData^{<18>} := \Delta Sat_{Ob}$

$RawData^{<6>} := rh_{Ob}$

RawData =

	1	2	3	4	5	6	7	8	9	10	11	12	13	14	15	16
1	20.7	956.1	1.851	29	34.8	23.2	40	30	0	57.659	57.365	57.936	57.084	57.61	0	57.226
2	20.3	953.9	1.914	27	32.4	21.6	40	30	0	57.382	57.114	57.635	56.709	57.235	0	56.93
3	20.1	953	1.94	27	32.4	21.6	40	30	0	57.192	56.925	57.446	56.52	57.046	0	56.742
4	19.8	951.6	1.98	28	33.6	22.4	40	30	0	56.86	56.579	57.125	56.236	56.762	0	56.423
5	19.5	950	2.026	28	33.6	22.4	40	30	0	56.579	56.298	56.843	55.955	56.48	0	56.143
6	19.3	948.6	2.066	29	34.8	23.2	40	30	0	56.346	56.052	56.623	55.771	56.297	0	55.924
7	19.2	947.4	2.1	29	34.8	23.2	40	30	0	56.26	55.966	56.537	55.685	56.21	0	55.839
8	19	946	2.141	30	36	24	40	30	0	56.027	55.719	56.316	55.501	56.027	0	55.62
9	18.9	944.9	2.172	30	36	24	40	30	0	55.939	55.631	56.228	55.414	55.939	0	55.534
10	18.8	943.3	2.218	30	36	24	40	30	0	55.858	55.55	56.147	55.333	55.858	0	55.455
11	18.5	941.4	2.273	31	37.2	24.8	40	30	0	55.53	55.208	55.831	55.055	55.58	0	55.141
12	18.3	939.6	2.325	31	37.2	24.8	40	30	0	55.351	55.029	55.652	54.876	55.401	0	54.965
13	18.1	937.5	2.386	31	37.2	24.8	40	30	0	55.176	54.854	55.477	54.701	55.226	0	54.793
14	18	935.9	2.432	31	37.2	24.8	40	30	0	55.095	54.773	55.396	54.62	55.145	0	54.714
15	17.8	934.1	2.485	32	38.4	25.6	40	30	0	54.865	54.529	55.179	54.441	54.966	0	54.499

Appendix C: Lapse Rate Comparison Program

Appendix C Table of Contents

ORIGIN≡1 CF := 0.039 x := 400 i := 1..x

I. Altitude, Pressure, and Saturation Definitions

Altitude: Set i counter to 400 to make 400 levels of data, then define ALT as the altitude in mete making each level 100 meters apart. This means the pressure altitudes range from the surface to 40,000 m in 100 m increments.

$ALT_i := 100 \cdot i$ $\quad ALTKFT := \frac{3.28 \cdot ALT}{1000}$ $\quad altkm := \frac{ALT}{1000}$

At or Below 11,000 m $\quad$ Above 11,000 m

$$\frac{p_s}{1013.25} = \left(\frac{288 - 0.0065 \cdot z}{288}\right)^{5.256} \qquad \frac{z - 11000}{14600} = \log\left(\frac{226.19}{ps}\right)$$

Pressure: Define Standard pressure altitude conversion equations and convert the pressure altitud in meters to pressures in mb for altitudes above and below 11,000 meters.

$$ConvertPress(ALT) := \begin{cases} 1013.25 \cdot \left(1. - 2.25694 \cdot 10^{-5} \cdot ALT\right)^{5.256} & \text{if } ALT \le 11000 \\ \dfrac{226.19}{\exp\left(1.57711 \cdot 10^{-4} \cdot ALT - 1.73482\right)} & \text{if } ALT > 11000 \end{cases}$$

$p_i := \text{ConvertPress}(ALT_i)$ Set p_i as pressure array for 400 levels of data.

Saturation: Define Critical Slope and Goff-Gratch Eqn and Derivative in the same manner as defined in the RH Profile Program.

$$\text{crit\_slope}_i := \frac{p_i}{622} \cdot CF$$

$$\text{Goff}(T) := 10^{\left(23.832241 - 5.02808 \cdot \frac{\ln(T)}{\ln(10)} - 1.3816 \cdot 10^{-7} \cdot 10^{11.334 - 0.0303998 \cdot T} + 8.1328 \cdot 10^{-3} \cdot 10^{3.49149 - \frac{1302.8844}{T}} - \frac{2949.076}{T}\right)}$$

$$\text{GoffDer}(T) := 10^{\left[\begin{array}{l} 23.832241 - 5.02808 \cdot \frac{\ln(T)}{\ln(10)} \ldots \\ + -1.3816 \cdot 10^{-7} \cdot 10^{11.334 - 3.03998 \cdot 10^{-2} \cdot T} \ldots \\ + 8.1328 \cdot 10^{-3} \cdot 10^{3.49149 - \frac{1302.8844}{T}} \ldots \\ + \frac{-2949.08}{T} \end{array}\right]} \cdot \left[\begin{array}{l} \frac{-5.02808}{T \cdot \ln(10)} \ldots \\ + 4.20004 \cdot 10^{-9} \cdot 10^{\left(11.334 - 3.03998 \cdot 10^{-2} \cdot T\right)} \cdot \ln(10) \ldots \\ + 10.59609824832 \cdot \frac{10^{\left(3.49149 - \frac{1302.8844}{T}\right)}}{T^2} \cdot \ln(10) \ldots \\ + \frac{2949.08}{T^2} \end{array}\right] \cdot \ln(10)$$

Critical Temperature at 100% RH: Compute 100% RH critical temperatures and saturation vapor pressures to use for subsequent 50% and 0% contrail base computations.

$T_{c.100} := 300$

$f(T_{c.100}) := \text{GoffDer}(T_{c.100}) - \text{crit\_slope}_i$

$T_{c.100_i} := \text{root}(f(T_{c.100}), T_{c.100})$ $T_{c100_i} := T_{c.100_i} - 273.15$

Sat Vapor Press at Tc100 $e_{s.100_i} := \text{Goff}(T_{c.100_i})$

II. Construction of Lapse Rate Profiles

Define y=300 as 300 mb or 30,000 ft for the 100% RH base. 30 kft is a representative altitude for the 100% RH contrail base based on data set's results computed in the Profile Comparison Prograı This altitude will serve as a bottom bound, starting point, for constructing 4 different temperature profiles. "startlapse" defines the pressure level where pressure first decreases to 300 mb or below. A 50% and 0% RH base is then computed for each of the temperature profiles.

$y := 300$

$startlapse := \left| \begin{array}{l} k \leftarrow 1 \\ \text{while } p_k > y \\ \quad k \leftarrow k + 1 \\ k \end{array} \right.$

$startlapse = 92$

$ALTKFT_{startlapse} = 30.176$

$T_{c100_{startlapse}} = -40.504$

The 100% RH critical temperature will be defined as the starting ambient temperature for eacl of the 4 different lapse rate (temperature) profiles. By setting the 100% critical temperature equal the ambient temperature at this level, I am defining a contrail altitude at this level since the ambien temp will be defined as reaching the 100% critical saturation temperature.

N is a new counter to build the 4 unique lapse rate profiles. Since the first ambient temperatu in each profile, InitialTemp, is the 100% critical saturation temperature, the first constructed ambie temp. of the profile is a level (+1) above that temperature.

$N := startlapse + 1 .. x$ $\qquad$ $InitialTemp := T_{c100_{startlapse}}$

LapseRateKM and LapseRate100M is an example converting lapse rate from the standard convention of km/°C to 100m/°C. This conversion is needed to remain consistent with the interval between pressure levels.

$LapseRateKM := -4$ $\qquad$ $LapseRate100M := \frac{LapseRateKM}{10}$ $\qquad$ $LapseRate100M = -0.4$

4 Unique Lapse Rates are now defined and their corresponding temperature profiles constructed from 30 - 100 kft.

$lapse1 := 0.2$ $lapse2 := 0.3$

$temp1_{startlapse} := InitialTemp$ $temp2_{startlapse} := InitialTemp$

$temp1_N := temp1_{N-1} - lapse1$ $temp2_N := temp2_{N-1} - lapse2$

$lapse3 := 0.6$ $lapse4 := 0.9$

$temp3_{startlapse} := InitialTemp$ $temp4_{startlapse} := InitialTemp$

$temp3_N := temp3_{N-1} - lapse3$ $temp4_N := temp4_{N-1} - lapse4$

III. Compute Bases using Profiles 1B, 50%, and 90% RH.

Critical Temperatures at 0% RH are defined for each level in all 4 constructed lapse rate profiles. These temperatures are compared to the profiles' constructed temperature.

$$TT_{c0_N} := \left(T_{c.100_N} - \frac{e_{s.100_N}}{crit\_slope_N} \right) - 273.15$$

$\Delta T_0^{<1>} := temp1 - TT_{c0}$ $\Delta T_0^{<2>} := temp2 - TT_{c0}$ $\Delta T_0^{<3>} := temp3 - TT_{c0}$ $\Delta T_0^{<4>} := temp4 - TT_{c0}$

Compute Bases: All critical temperature comparisons are run through a program to compute cont base. When the ambient temperature decreases to the critical temp, or the ΔT becomes zero or negative, saturation has been reached a contrail base altitude is forecast.

$delta(data, col) := data^{<col>}$

$base(data, col) :=$ | $s \leftarrow (startlapse + 1)$ | while $delta(data, col)_s \geq 0$ | $s \leftarrow s + 1$ | s

$$percent0 := \begin{bmatrix} ALTKFT_{base}(\Delta T_0, 1) \\ ALTKFT_{base}(\Delta T_0, 2) \\ ALTKFT_{base}(\Delta T_0, 3) \\ ALTKFT_{base}(\Delta T_0, 4) \end{bmatrix}$$

$lap := 1..4$

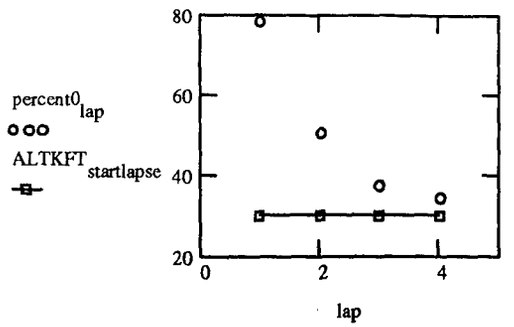

percent0 is an array of forecast bases using 0% RH and each of the 4 lapse rate.

Critical Temperatures at 50% RH are defined for each level in all 4 constructed lapse rate profiles. These temperatures are compared to the profiles' constructed temperature.

$T_c := 180$

$$f(T_c, rh) := \frac{e_{s.100_N} - (T_{c.100_N} - T_c) \cdot (crit\_slope_N)}{Goff(T_c)} \cdot 100 - rh$$

$T_{c50_N} := root(f(T_c, 50), T_c) - 273.15$

$\Delta T_{50}^{<1>} := temp1 - T_{c50}$ $\Delta T_{50}^{<2>} := temp2 - T_{c50}$ $\Delta T_{50}^{<3>} := temp3 - T_{c50}$ $\Delta T_{50}^{<4>} := temp4 - T_{c50}$

$$percent50 := \begin{bmatrix} ALTKFT_{base}(\Delta T_{50}, 1) \\ ALTKFT_{base}(\Delta T_{50}, 2) \\ ALTKFT_{base}(\Delta T_{50}, 3) \\ ALTKFT_{base}(\Delta T_{50}, 4) \end{bmatrix}$$

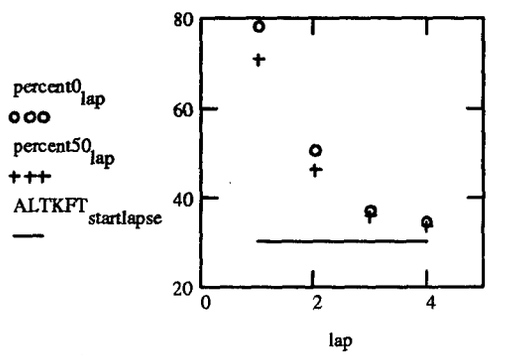

percent50 is an array of forecast bases using 50% RH and each of the 4 lapse rate.

Critical Temperatures at 90% RH are defined for each level in all 4 constructed lapse rate profiles. These temperatures are compared to the profiles' constructed temperature.

$$T_c := 180$$

$$f(T_c, rh) := \frac{e_{s.100_N} - (T_{c.100_N} - T_c) \cdot (crit\_slope_N)}{Goff(T_c)} \cdot 100 - rh$$

$$T_{c85_N} := root(f(T_c, 90), T_c) - 273.15$$

$$\Delta T_{85}^{<1>} := temp1 - T_{c85} \quad \Delta T_{85}^{<2>} := temp2 - T_{c85} \quad \Delta T_{85}^{<3>} := temp3 - T_{c85} \quad \Delta T_{85}^{<4>} := temp4 - T_{c85}$$

$$percent85 := \begin{bmatrix} ALTKFT_{base}(\Delta T_{85}, 1) \\ ALTKFT_{base}(\Delta T_{85}, 2) \\ ALTKFT_{base}(\Delta T_{85}, 3) \\ ALTKFT_{base}(\Delta T_{85}, 4) \end{bmatrix}$$

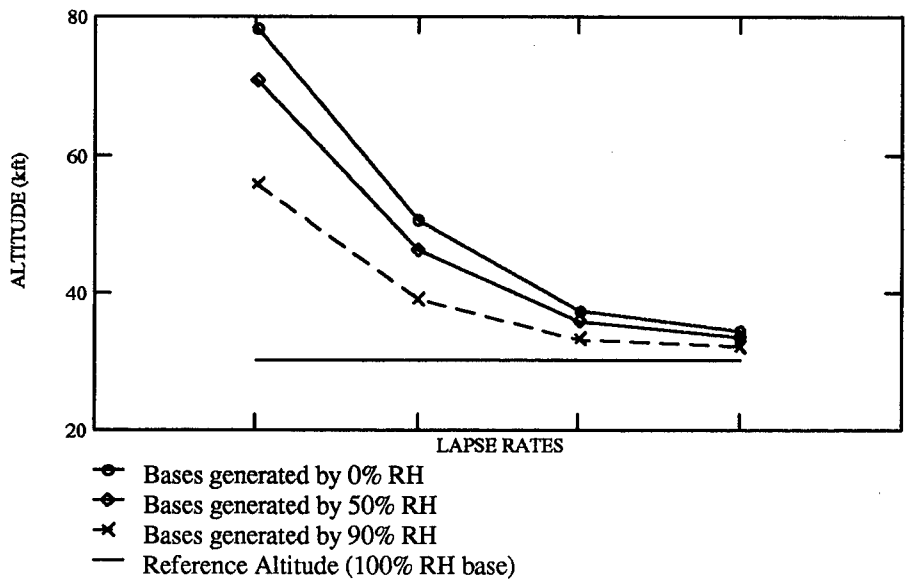

IV. RH Mid-Point Calculations

$$add100m(lapse) := \frac{ALT_{base(\Delta T_0, lapse)} - ALT_{startlapse}}{2} \qquad newlapse(lapse) := \frac{add100m(lapse) + ALT_{startlapse}}{100}$$

newlapse(1) = 165.5

newlapse(2) = 123

newlapse(3) = 103

newlapse(5) = 100

newlapse(4) = 98.5

Determine mid-level of depths so can compute correspondin RH value. Mid-level of depth is the difference from the base 100% RH (assumed starting point) and 0% RH for each laps rate.

RH MIDPOINT Calculations for Each Lapse Rate

CN := 166

crittemp := $temp1_{CN}$ + 273.15

$$\frac{e_{s.100_{CN}} - \left(T_{c.100_{CN}} - crittemp\right)\cdot\left(crit\_slope_{CN}\right)}{Goff(crittemp)}\cdot 100 = 91.197$$ 2 deg C/km = 91.197%

CN := 123

crittemp := $temp2_{CN}$ + 273.15

$$\frac{e_{s.100_{CN}} - \left(T_{c.100_{CN}} - crittemp\right)\cdot\left(crit\_slope_{CN}\right)}{Goff(crittemp)}\cdot 100 = 85.323$$ 3 deg C/km = 85.323%

CN := 103

crittemp := $temp3_{CN}$ + 273.15

$$\frac{e_{s.100_{CN}} - \left(T_{c.100_{CN}} - crittemp\right)\cdot\left(crit\_slope_{CN}\right)}{Goff(crittemp)}\cdot 100 = 82.286$$ 6 deg C/km = 82.286%

CN := 99

crittemp := $temp4_{CN}$ + 273.15

$$\frac{e_{s.100_{CN}} - \left(T_{c.100_{CN}} - crittemp\right)\cdot\left(crit\_slope_{CN}\right)}{Goff(crittemp)}\cdot 100 = 79.438$$ 9 deg C/km = 79.438%

RH Values for Relative Depth Changes for 7.4772°C/km: Computes RH values given a relative depth change.

$CN := 108$

$crittemp := temp5_{CN} + 273.15$ 10.8 km, RH = -1.523 %

$$\frac{e_{s.100_{CN}} - \left(T_{c.100_{CN}} - crittemp\right)\cdot\left(crit\_slope_{CN}\right)}{Goff(crittemp)}\cdot 100 = -1.523$$

$CN := 107$

$crittemp := temp5_{CN} + 273.15$ 10.7 km, RH = 15.745 %

$$\frac{e_{s.100_{CN}} - \left(T_{c.100_{CN}} - crittemp\right)\cdot\left(crit\_slope_{CN}\right)}{Goff(crittemp)}\cdot 100 = 15.745$$

$CN := 106$

$crittemp := temp5_{CN} + 273.15$ 10.6 km, RH = 30.649 %

$$\frac{e_{s.100_{CN}} - \left(T_{c.100_{CN}} - crittemp\right)\cdot\left(crit\_slope_{CN}\right)}{Goff(crittemp)}\cdot 100 = 30.649$$

$CN := 105$

$crittemp := temp5_{CN} + 273.15$ 10.5 km, RH = 43.459 %

$$\frac{e_{s.100_{CN}} - \left(T_{c.100_{CN}} - crittemp\right)\cdot\left(crit\_slope_{CN}\right)}{Goff(crittemp)}\cdot 100 = 43.459$$

$CN := 104$

$crittemp := temp5_{CN} + 273.15$ 10.4 km, RH = 54.416 %

$$\frac{e_{s.100_{CN}} - \left(T_{c.100_{CN}} - crittemp\right)\cdot\left(crit\_slope_{CN}\right)}{Goff(crittemp)}\cdot 100 = 54.416$$

$CN := 103$

$crittemp := temp5_{CN} + 273.15$ 10.3 km, RH = 63.735 %

$$\frac{e_{s.100_{CN}} - \left(T_{c.100_{CN}} - crittemp\right) \cdot \left(crit\_slope_{CN}\right)}{Goff(crittemp)} \cdot 100 = 63.735$$

$CN := 102$

$crittemp := temp5_{CN} + 273.15$ 10.2 km, RH = 71.605 %

$$\frac{e_{s.100_{CN}} - \left(T_{c.100_{CN}} - crittemp\right) \cdot \left(crit\_slope_{CN}\right)}{Goff(crittemp)} \cdot 100 = 71.605$$

$CN := 101$

$crittemp := temp5_{CN} + 273.15$ 10.1 km, RH = 78.195 %

$$\frac{e_{s.100_{CN}} - \left(T_{c.100_{CN}} - crittemp\right) \cdot \left(crit\_slope_{CN}\right)}{Goff(crittemp)} \cdot 100 = 78.195$$

$CN := 100$

$crittemp := temp5_{CN} + 273.15$ 10.0 km, RH = 83.657 %

$$\frac{e_{s.100_{CN}} - \left(T_{c.100_{CN}} - crittemp\right) \cdot \left(crit\_slope_{CN}\right)}{Goff(crittemp)} \cdot 100 = 83.657$$

$CN := 99$

$crittemp := temp5_{CN} + 273.15$ 9.9 km, RH = 88.123 %

$$\frac{e_{s.100_{CN}} - \left(T_{c.100_{CN}} - crittemp\right) \cdot \left(crit\_slope_{CN}\right)}{Goff(crittemp)} \cdot 100 = 88.123$$

$CN := 95$

$crittemp := temp5_{CN} + 273.15$ 9.5 km, RH = 98.219 %

$$\frac{e_{s.100_{CN}} - \left(T_{c.100_{CN}} - crittemp\right) \cdot \left(crit\_slope_{CN}\right)}{Goff(crittemp)} \cdot 100 = 98.219$$

$CN := 92$

$crittemp := temp5_{CN} + 273.15$ 9.2 km, RH = 100 %

$$\frac{e_{s.100_{CN}} - \left(T_{c.100_{CN}} - crittemp\right) \cdot \left(crit\_slope_{CN}\right)}{Goff(crittemp)} \cdot 100 = 100$$

RH Values for Relative Depth Changes for 2°C/km:

$CN := 239$

$crittemp := temp1_{CN} + 273.15$ 23.9 km, RH = -0.2 %

$$\frac{e_{s.100_{CN}} - \left(T_{c.100_{CN}} - crittemp\right) \cdot \left(crit\_slope_{CN}\right)}{Goff(crittemp)} \cdot 100 = -0.2$$

$CN := 236$

$crittemp := temp1_{CN} + 273.15$ 23.6 km, RH = 8.3 %

$$\frac{e_{s.100_{CN}} - \left(T_{c.100_{CN}} - crittemp\right) \cdot \left(crit\_slope_{CN}\right)}{Goff(crittemp)} \cdot 100 = 8.3$$

$CN := 233$

$crittemp := temp1_{CN} + 273.15$ 23.3 km, RH = 16.118 %

$$\frac{e_{s.100_{CN}} - \left(T_{c.100_{CN}} - crittemp\right) \cdot \left(crit\_slope_{CN}\right)}{Goff(crittemp)} \cdot 100 = 16.118$$

$CN := 230$

$crittemp := temp1_{CN} + 273.15$ 23.0 km, RH = 23.31 %

$$\frac{e_{s.100_{CN}} - \left(T_{c.100_{CN}} - crittemp\right) \cdot \left(crit\_slope_{CN}\right)}{Goff(crittemp)} \cdot 100 = 23.31$$

$CN := 220$

$crittemp := temp1_{CN} + 273.15$ 22.0 km, RH = 43.373 %

$$\frac{e_{s.100_{CN}} - \left(T_{c.100_{CN}} - crittemp\right) \cdot \left(crit\_slope_{CN}\right)}{Goff(crittemp)} \cdot 100 = 43.373$$

$CN := 210$

$crittemp := temp1_{CN} + 273.15$ 21.0 km, RH = 58.539 %

$$\frac{e_{s.100_{CN}} - \left(T_{c.100_{CN}} - crittemp\right) \cdot \left(crit\_slope_{CN}\right)}{Goff(crittemp)} \cdot 100 = 58.539$$

$CN := 200$

$crittemp := temp1_{CN} + 273.15$ 20.0 km, RH = 69.973 %

$$\frac{e_{s.100_{CN}} - \left(T_{c.100_{CN}} - crittemp\right) \cdot \left(crit\_slope_{CN}\right)}{Goff(crittemp)} \cdot 100 = 69.973$$

$CN := 190$

$crittemp := temp1_{CN} + 273.15$ 19.0 km, RH = 78.554 %

$$\frac{e_{s.100_{CN}} - \left(T_{c.100_{CN}} - crittemp\right) \cdot \left(crit\_slope_{CN}\right)}{Goff(crittemp)} \cdot 100 = 78.554$$

$CN := 180$

$crittemp := temp1_{CN} + 273.15$ 18.0 km, RH = 84.954 %

$$\frac{e_{s.100_{CN}} - \left(T_{c.100_{CN}} - crittemp\right) \cdot \left(crit\_slope_{CN}\right)}{Goff(crittemp)} \cdot 100 = 84.954$$

$CN := 170$

$crittemp := temp1_{CN} + 273.15$ 17.0 km, RH = 89.682 %

$$\frac{e_{s.100_{CN}} - \left(T_{c.100_{CN}} - crittemp\right) \cdot \left(crit\_slope_{CN}\right)}{Goff(crittemp)} \cdot 100 = 89.682$$

$CN := 160$

$crittemp := temp1_{CN} + 273.15$

16.0 km, RH = 93.132 %

$$\frac{e_{s.100_{CN}} - \left(T_{c.100_{CN}} - crittemp\right) \cdot \left(crit\_slope_{CN}\right)}{Goff(crittemp)} \cdot 100 = 93.132$$

$CN := 150$

$crittemp := temp1_{CN} + 273.15$

15.0 km, RH = 95.607 %

$$\frac{e_{s.100_{CN}} - \left(T_{c.100_{CN}} - crittemp\right) \cdot \left(crit\_slope_{CN}\right)}{Goff(crittemp)} \cdot 100 = 95.607$$

$CN := 140$

$crittemp := temp1_{CN} + 273.15$

14.0 km, RH = 97.34 %

$$\frac{e_{s.100_{CN}} - \left(T_{c.100_{CN}} - crittemp\right) \cdot \left(crit\_slope_{CN}\right)}{Goff(crittemp)} \cdot 100 = 97.34$$

$CN := 120$

$crittemp := temp1_{CN} + 273.15$

12.0 km, RH = 99.268 %

$$\frac{e_{s.100_{CN}} - \left(T_{c.100_{CN}} - crittemp\right) \cdot \left(crit\_slope_{CN}\right)}{Goff(crittemp)} \cdot 100 = 99.268$$

$CN := 93$

$crittemp := temp1_{CN} + 273.15$

9.3 km, RH = 99.999 %

$$\frac{e_{s.100_{CN}} - \left(T_{c.100_{CN}} - crittemp\right) \cdot \left(crit\_slope_{CN}\right)}{Goff(crittemp)} \cdot 100 = 99.999$$

IV. Depths of Each Lapse Rate are Computed: all depths are computed in kft. Depths are taken from the forecast bases at 50% and 0% RH from the reference altitude.

$$ALTKFT_{startlapse} = 30.176 \qquad percent50 = \begin{bmatrix} 70.848 \\ 46.248 \\ 35.752 \\ 33.456 \end{bmatrix} \qquad percent0 = \begin{bmatrix} 78.392 \\ 50.512 \\ 37.392 \\ 34.44 \end{bmatrix}$$

$$percent0 - ALTKFT_{startlapse} = \begin{bmatrix} 48.216 \\ 20.336 \\ 7.216 \\ 4.264 \end{bmatrix}$$

Total Depth Computed: From forecast bases usin; 100% to 0% RH.

$$percent50 - ALTKFT_{startlapse} = \begin{bmatrix} 40.672 \\ 16.072 \\ 5.576 \\ 3.28 \end{bmatrix}$$

Depth at 50% RH Computed from forecast bases using 100% to 50% RH.

$$percent0 - percent50 = \begin{bmatrix} 7.544 \\ 4.264 \\ 1.64 \\ 0.984 \end{bmatrix}$$

Fractional Depth from 50% to 0% Computed from forecast bases using 50% to 0%. This depth is only 1/4 - 1/5 of the total depth.

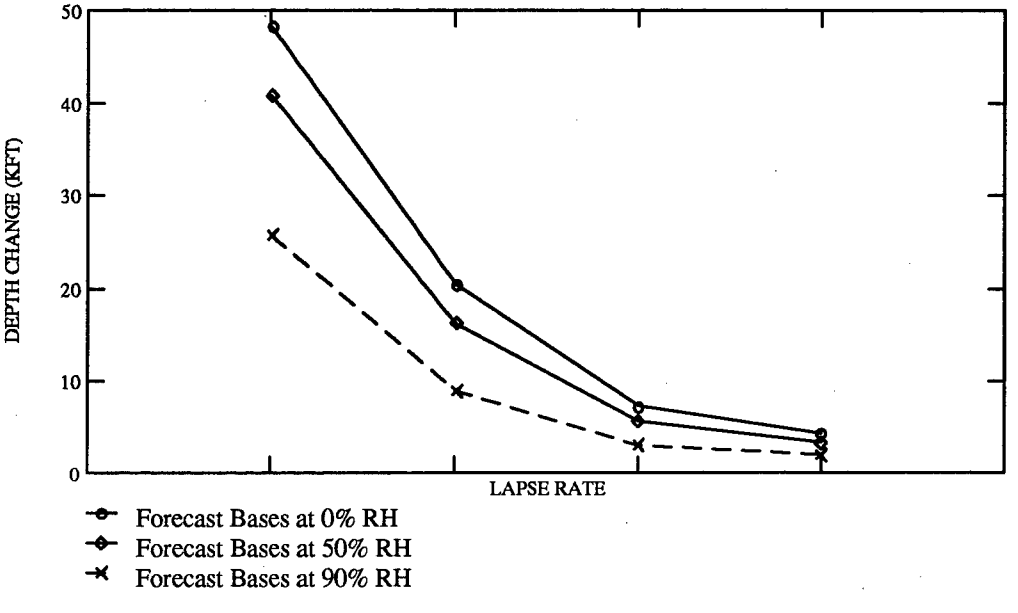

Appendix D: Two-Tailed t-Test

Two-Tailed Hypothesis Test for Algorithm Forecast Bases

Focus Question: Is the true average of differences of the forecast bases generated by Profile and 2A or Profile 3 and 4 more than 500 (0.5 kft) feet? A null, H_0, and an alternate, H_A, hypothesis are defined for a logical frame of reference to judge later tests. 500 feet is used since AFGWC forecasts bases to the nearest 1 kft altitude and a difference of 500 ft or more will create a different forecast value by 1 kft.

$\mathbf{H_0}$: $\mu 1 - \mu 2 = -0.5$

$\mathbf{H_A}$: $\mu 1 - \mu 2 \neq -0.5$

Assumptions:

1) Forecast bases are normally distributed
2) Population of differences is normally distributed
3) Joint Distribution of Forecasts is bivariate normal

Aptness Assessment: To verify the samples are normally distributed, each set of forecasts from the RH profiles was tested for normality. This also verified a bivariate normal distribution.

Test Statistic: A t-test was chosen since the joint distribution was bivariate normal and the population of differences was Gaussian as a result. Two different t-statistics were used since some of the paired forecast bases demonstrated high correlation. If the test samples are paired and have high positive correlation, the t test statistic can be modified to produce a more powerful and sensitive test (Wilks, 1994). A method explained by Wilks (1994) modifies the denominator to produce a smaller standard deviation for positively correlated samples. By making this modification, smaller differences in the numerator can be detected adding to the tests power and sensitivity. Since the paired forecasts generated by the Observed and Simplified profiles demonstrated a high correlation, the modified statistic was used, while the unmodified version was used on the Simplified, SAGE II test.

Test Statistic Computations:

Sample sizes:

$n := 42$

Means:

$m1(colA) := mean(dat1(colA))$

$m2(colB) := mean(dat2(colB))$

Standard deviations:

$$s1(colA) := stdev(dat1(colA)) \cdot \sqrt{\frac{n}{n-1}}$$

$$s2(colB) := stdev(dat1(colB)) \cdot \sqrt{\frac{n}{n-1}}$$

Pearson Correlation Coefficient

$$Correlation(colA, colB) := corr(dat1(colA), dat2(colB))$$

Degrees of freedom:

$$df := n - 1 \qquad df = 41$$

Standard error of the difference of means:

Unmodified Standard Error

$$sd(colA, colB) := \sqrt{s1(colA)^2 + s2(colB)^2}$$

Modified Standard Error

$$s(colA, colB) := \sqrt{\frac{(s1(colA))^2 + (s2(colB))^2 - 2 \cdot Correlation(colA, colB) \cdot s1(colA) \cdot s2(colB)}{n}}$$

Test statistic (t):

Unmodified Test Statistic

$$td(colA, colB) := \frac{|m1(colA) - m2(colB)| - 0.5}{sd(colA, colB)}$$

Modified Test Statistic

$$t(colA, colB) := \frac{|m1(colA) - m2(colB)| - 0.5}{s(colA, colB)}$$

Test Level: The test level defines the improbable region under the null distribution. It is a probability boundary used to describe a range of ordinary values under the null distribution (Wilks, 1995). Commonly, a test level value of 0.05 is chosen.

Test Level:

$$\alpha := 0.05$$

Critical Value: The critical value is the test statistic's bounded values associated with the test level and null distribution. The test statistic must fall within these bounds, for the null hypothesis to be accepted.

Critical Value:

$$t_{crit} := qt\left(1 - \frac{\alpha}{2}, df\right) \qquad t_{crit} = 2.02 \qquad -t_{crit} = -2.02$$

TABLE OF HYPOTHESIS TEST RESULTS:

Algorithm	RH Profiles	
	Profile 2A and 3	*Profile 3 and 4*
AFGWC:		
correlation	Correlation(3,6) = 0.973	Correlation(7,6) = 0.345
standard error	s(3,6) = 0.172	sd(7,6) = 5.054
test statistic	t(3,6) = 0.26	td(7,6) = 0.976
critical value	$t_{crit} = 2.02$	$-t_{crit} = -2.02$
Saatzer:		
correlation	Correlation(10,13) = 0.933	Correlation(14,13) = 0.394
standard error	s(10,13) = 0.264	sd(14,13) = 5.085
test statistic	t(10,13) = 0.912	td(14,13) = 0.405
critical value	$t_{crit} = 2.02$	$-t_{crit} = -2.02$

KNOWLEDGE CLAIM: H_o is not rejected for either set of tests on the algorithms, since t (or td) <= t_{crit} for all tests for each test.

VALUE CLAIM: For this set of 42 cases, forecast bases, generated by Profiles 2A and 3 or 3 and 4, do not differ by more than 500 feet.

Appendix E: Randomized Block Analysis of Variance (ANOVA) Test

ANOVA For Forecast Bases using Seven RH Profiles on Each Case (AFGWC Algorithm)

Focus Question: Is the true average of differences of the forecast bases generated by any the seven RH profiles significantly different from one another?

$\mathbf{H_{0A}}$: $\mu 1=\mu 2=\mu 3=\mu 4=\mu 5=\mu 6=\mu 7$

$\mathbf{H_{aA}}$: At least two means are different due to the different RH profile used

Assumptions:

1) Each case has all seven RH profiles applied to produce seven different forecast bases
2) Forecast bases are normally distributed
3) Population of differences is normally distributed
4) Joint Distribution of Forecasts is bivariate normal

Aptness Assessment: Similar to two-tailed t-test.

Test Statistic: A F_A-test statistic is used for ANOVA comparisons for each RH profile (treatment).

Test Statistic Computations:

Sample Mean of Each Profile's Mean:

$$\text{sample}_{\text{stat}}(\text{newdata}) := \left| \begin{array}{l} \text{for } t \in 1..\text{rows}(\text{newdata}) \\ \quad \left| \begin{array}{l} \text{meanv}_t \leftarrow \text{mean}\left[\left(\text{newdata}^T\right)^{\langle t \rangle}\right] \\ n \leftarrow \text{rows}\left(\left(\text{newdata}^T\right)\right) \\ \text{stdv}_t \leftarrow \sqrt{n \cdot \dfrac{\text{var}\left[\left[\left(\text{newdata}^T\right)^{\langle t \rangle}\right]\right]}{n-1}} \end{array} \right. \\ \text{values} \leftarrow \text{augment}(\text{meanv}, \text{stdv}) \end{array} \right.$$

$$\text{sample}_{\text{stat}}(\text{newdata}) = \begin{bmatrix} 30.456 & 2.249 \\ 36.446 & 4.538 \\ 35.651 & 4.538 \\ 35.382 & 4.025 \\ 35.946 & 4.481 \\ 35.114 & 4.027 \\ 35.951 & 4.595 \end{bmatrix}$$

First column is the mean of each profile. Second column is estimated standard deviation of each profile

Sample Mean of Each Case:

$$s_{stat}(StatT) = \left| \begin{array}{l} \text{for } t \in 1..\text{rows}(StatT) \\ \quad \left| \begin{array}{l} meanv_t \leftarrow \text{mean}\left[\left(StatT^T \right)^{\langle t \rangle} \right] \\ n \leftarrow \text{rows}\left(\left(StatT^T \right) \right) \\ stdv_t \leftarrow \sqrt{n \cdot \dfrac{\text{var}\left[\left[\left(StatT^T \right)^{\langle t \rangle} \right] \right]}{n-1}} \end{array} \right. \\ values \leftarrow \text{augment}(meanv, stdv) \end{array} \right.$$

Provides a column of means and a column of estimated standard deviations for each case (similar to profile means and SD above).

Sample Mean of All Profiles Combined (xbar..):

$i := 1..7$ $\quad xbar_{i.} := sample_{stat}(newdata)^{\langle 1 \rangle}$ $\quad s_{i.} := sample_{stat}(newdata)^{\langle 2 \rangle}$

$xbar_{..} := \text{mean}(xbar_{i.})$ $\quad xbar_{j.} := s_{stat}(StatT)^{\langle 1 \rangle}$

$xbar_{..} = 34.992$

Total Sum of Squares (SST):

$$SST := \sum_{i=1}^{7} \sum_{j=1}^{42} \left(newdata_{i,j} - xbar_{..} \right)^2 \qquad SST = 5.969 \cdot 10^3$$

Error Sum of Squares (SSE):

$$SSE := \sum_{i=1}^{7} \sum_{j=1}^{42} \left(newdata_{i,j} - xbar_{i._i} - xbar_{j._j} + xbar_{..} \right)^2 \qquad SSE = 780.306$$

Treatment Sum of Squares (SSA):

$$SSA := \sum_{i=1}^{7} \sum_{j=1}^{42} \left(xbar_{i._i} - xbar_{..} \right)^2 \qquad SSA = 1.055 \cdot 10^3$$

Degrees of Freedom (ν_1, ν_2):

$\nu_1 = I - 1$

$\nu_2 = I*(J-1)$

where

I = number of Treatments (7 profiles) = 7 $I := 7$

J = number of observations (42 cases) = 42 $J := 42$

Test statistic (F_{star}):

$$F_A := \frac{\frac{SSA}{I-1}}{\left[\frac{SSE}{I\cdot(J-1)}\right]} \qquad F_A = 64.679$$

Test Level: $\alpha := 0.05$

Critical Value (Devore, 1995, Table A.7)**:**

$F_{crit} = F_{\alpha, \nu1, \nu2} = F_{\alpha, I-1, I(J-1)} = F_{0.05,6,infinity} = 2.10$

KNOWLEDGE CLAIM: Since $F_{star} >> F_{crit}$, reject Ho and claim at least two of the forecast means are different.

VALUE CLAIM: At least, one of the profiles produces significant forecast base differences as compared to the others.

Simultaneous Confidence Statements Using the Studentized Range Distribution (Tukey's Procedure)

Mean Squared Error (MSE):

$$MSE := \frac{SSE}{I\cdot(J-1)} \qquad MSE = 2.719$$

MSE in kft

Upper/Lower α Critical Tail Value for Studentized Range Distribution:

$Q_A = Q_{\alpha, I, (I-1)(J-1)} = Q_{0.05,7,6*41} = Q_{0.05,7,infinity} = 4.17$ kft $Q_A := 4.17$

Tukey Interval (in kft):

$$w := Q_A \cdot \sqrt{\frac{MSE}{J}}$$

$w = 1.061$

ProfileMeans =

Profile	Mean Base (kft)
1A	30.456
1B	36.446
2A	35.651
2B	35.382
2C	35.946
3	35.114
4	35.951

KNOWLEDGE CLAIM: At w=1.061 kft, forecast bases of profile 1A are significantly different from the other six sets. Additionally, profile 1B produces forecast bases which differ from those of profiles 2B and 3.

VALUE CLAIM: Only profiles 1A and 1B produce different forecast bases, while the forecast bases of the remaining five profiles are statistically similar.

Vita

Allen Christopher Rabayda, the son of Daniel and Patricia Rabyada, [redacted]a. He graduated from Panther Valley High School in June, 1984 then attended the Pennsylvania State University where he enrolled in the Reserve Officer Training Program. In May 1988, Allen graduated from Penn State with a Bachelor of Science Degree in Meteorology. After graduation, he completed several courses in Computer Assisted Instruction until becoming commissioned a second lieutenant in the Air Force in May 1989.

Allen's first assignment was to provide meteorological support to the Army at Fort Carson, Colorado. After arriving at Fort Carson in October, 1989, Allen was assigned as the Cadre Weather Team Officer in Charge where he developed and executed weather support for the 4th Infantry Division, a heavy mechanized armor and aviation force of over 20,000 members. While stationed at Fort Carson, Allen married the former Christine Lynn Wagner, daughter of Sandra and Paul Wagner of Reading, Pennsylvania [redacted].

On April 7, 1992, Allen was next assigned to Royal Air Force Lakenheath, England. At Lakenheath, he provided meteorological support to the 48th Fighter Wing as Wing Weather Officer. He supported the F-15 Strike Eagles of the 48th in several European contingency operations which included Operations Provide Comfort and Deny Flight.

While at Lakenheath, Allen was promoted to his current rank of captain. [redacted] Daniel Paul Rabayda was born to Allen and Christine. Shortly after, in July of 1995 Allen, Christine, and Daniel returned to the United States for their next assignment, AFIT.

In August of 1995, Allen began the Meteorology program at AFIT. He graduated from AFIT on March 25, 1997 and was then assigned to Asheville, North Carolina as a staff meteorologist for the Air Force Combat Climatology Center. He anticipates to be stationed at Asheville for 3 years.

REPORT DOCUMENTATION PAGE

Form Approved
OMB No. 0704-0188

1. AGENCY USE ONLY *(Leave blank)*	2. REPORT DATE	3. REPORT TYPE AND DATES COVERED
	MAR 97	

4. TITLE AND SUBTITLE
MOISTURE SENSITIVITY OF CONTRAIL FORECAST ALGORITHMS

5. FUNDING NUMBERS

6. AUTHOR(S)
Captain Allen C. Rabayda

7. PERFORMING ORGANIZATION NAME(S) AND ADDRESS(ES)
AFIT/ENP
Lt Col Michael Walters

8. PERFORMING ORGANIZATION REPORT NUMBER

9. SPONSORING/MONITORING AGENCY NAME(S) AND ADDRESS(ES)
88th Weather Squadron (Mr Steve Weaver)
2049 Monhan Wy,
Bldg 91, Area B
Wright Patterson AFB, OH 45433-2704

10. SPONSORING/MONITORING AGENCY REPORT NUMBER

11. SUPPLEMENTARY NOTES

12a. DISTRIBUTION/AVAILABILITY STATEMENT
For Public Release; Distribution Unlimited

12b. DISTRIBUTION CODE

13. ABSTRACT *(Maximum 200 words)*

This thesis looked at using new relative humidity (RH) climatolgies to improve the Air Force Global Weather Center's (AFGWC) contrail forecasts. To study the effect of the new RH climatolgies, the currently used empirical relative humidity (RH) profile is replaced with a more accurate climatological one, Stratospheric And Gaseous Experiment II (SAGE II). To compare the forecasted base accuracy and bias, the study examines sets of forecast bases generated by both the empirical and SAGE II profiles on 42 days. Each set of forecast bases are shown to be statistically similar with a series of hypothesis tests. Additional RH profiles with values from 0% to 100% are then tested to gage their affect on forecast bases. Again little statistical difference in forecast bases are noted between the additional profiles. In general, a high forecast base bias is shown for two algorithms derived from the Appleman theory. This thesis also reveals the dependence of forecast bases on RH and lapse rate. Lapse rates from 2°C/km to 9°C/km and forecast bases generated by RH values of 0% and 100% are used to show how RH variations of more than 30% may only vary forecasts by less than 1,000 feet.

14. SUBJECT TERMS

15. NUMBER OF PAGES
159

16. PRICE CODE

17. SECURITY CLASSIFICATION OF REPORT	18. SECURITY CLASSIFICATION OF THIS PAGE	19. SECURITY CLASSIFICATION OF ABSTRACT	20. LIMITATION OF ABSTRACT
Unclassified	Unclassified	Unclassified	